NASA Contractor Report 189620

MODELING AND ANALYSIS METHODOLOGY FOR AEROELASTICALLY TAILORED CHORDWISE DEFORMABLE WINGS

Lawrence W. Rehfield, Stephen Chang and Peter J. Zischka

University of California
Davis, California 95616

CONTRACT NAS1-18754
July 1992

National Aeronautics and Space Administration

Langley Research Center
Hampton, Virginia 23665-5225

NASA Contractor Report 189620

MODELING AND ANALYSIS METHODOLOGY FOR AEROELASTICALLY TAILORED CHORDWISE DEFORMABLE WINGS

Lawrence W. Rehfield, Stephen Chang and Peter J. Zischka

University of California
Davis, California 95616

CONTRACT NAS1-18754
July 1992

National Aeronautics and
Space Administration

Langley Research Center
Hampton, Virginia 23665-5225

CONTENTS

SUMMARY

Structural models and design analysis methodology have been created for composite primary aircraft structures that are appropriate for the preliminary or conceptual phase of design. Emphasis has been given to high aspect ratio wings and the potential of aeroelastic tailoring to enhance lift production. In contrast to previous work devoted to tailoring specific configurations to specific missions, this research focuses upon understanding, modeling, tailoring mechanisms and creating design concepts that accentuate individual behavioral characteristics. As the roles of wing bending and twisting deformations are rather well understood, attention is directed to elastically produced chordwise camber. A scientific understanding of behavior and design concepts which accentuate camber producing deformations are presented and applied to a generic transport wing.

The models are simple. Closed form expressions for all the stiffnesses and compliances permit rapid assessment of design changes and facilitate understanding of the cause-effect relationships between configuration and response. The models are useful for teaching, initial sizing in preliminary design, optimization and parametric studies, providing trend information, establishing intuitive insight into behavior and isolating and identifying independent design-controlled mechanisms. Validation of models by large-scale finite element simulation and selected experiments is conducted for the bending concept of producing favorable camber deformations.

Two primary and two secondary structural concepts have been created which produce chordwise camber deformation that results in enhanced lift. A wing box can be tailored to utilize each of these with composites. In attempting to optimize the aerodynamic benefits, we have found that there are two optimum designs that are of interest. There is a "weight" optimum which corresponds to the maximum lift per unit structural weight. There is also a "lift" optimum that corresponds to maximum absolute lift. Experience indicates that a large weight penalty accompanies the transition from weight to lift optimum designs.

It appears that lift enhancements of sufficient magnitude can be produced to render this type of wing tailoring of practical interest. If reasonable assumptions are used for angle of attack and a margin against airfoil stall is considered, section lift increases of up to fifteen percent are predicted.

INTRODUCTION

Elastic tailoring refers to the utilization of the design flexibility of composites to achieve performance goals. The goals are usually accomplished by selecting an appropriate structural concept, fiber orientation, ply stacking sequence and a blend of materials. In aeronautical applications, emphasis has been given to tailoring deformations which influence the aerodynamics of the system (ref. 1). This is called "aeroelastic tailoring." Aeroelastic instabilities may be avoided in this manner (ref. 1), as in the X-29, or performance enhancements, such as increased lift (refs. 2, 3) or maximizing lift-to-drag ratio (ref. 1), can be achieved.

Early work in aeroelastic tailoring focused on simple laminated construction of plate-like, rather low aspect ratio lifting surfaces. The design procedures are described in ref. 4 in the following manner:

> "The design for a desired static aeroelastic response was initially an iterative process performed by a structural engineer trying to satisfy a requirement for twist and camber established by an aerodynamicist."

Since that time, considerable progress has been made, including the effective use of optimization algorithms (refs. 1, 4). Emphasis, however, seems to have been given always to tailoring specific configurations to specific missions, a practice that did not foster scientific understanding or permit a firm grasp of the cause-effect relationship between configuration and response. In contrast to this approach, our research breaks with the past and focuses upon understanding, modeling, tailoring mechanisms and creating design concepts that accentuate individual behavioral characteristics.

Interest in swept forward wings, which resulted in the X-29, focused attention on wing bending and twisting deformations. As these deformation modes are understood rather well now, our research has emphasized elastically produced chordwise camber. While camber deformations have been tailored by ad hoc methods for specific configurations (ref. 4), it remained to create the basis for scientific understanding of behavior and design concepts which accentuate this deformation mode.

Structural tailoring concepts have been developed to create wings with elastically produced camber for the purpose of increasing the lift generated by the wing. Currently, the usual means of accomplishing this is with controls, the most common of which are flaps. If natural, intrinsic means are used to enhance lift, then flap requirements and their associated systems may be reduced. This will yield weight savings, acquisition cost savings and maintenance cost savings. The desired effects are presented in fig. 1.

The fundamental mechanisms that are utilized produce camber deformations in response to the usual loading of the wing such as bending moments and torque. The camber enhances the production of lift and further modifies the loads. Significant lift increases may be produced by tailoring using modern composite material systems (refs. 2, 3). An Overview of this research is given in ref. 2.

There are several concepts that have been used in our tailoring work. They are illustrated in figs. 2 and 3. The continuous filament grid stiffened structures (fig. 3) are particularly useful for tailoring response. One way to elastically tailor a structure is to orient the stiffeners suitably with respect to the primary load direction to derive the most desirable response. Grid-stiffened concepts are particularly effective for elastic tailoring a structure because stiffeners made of unidirectional material can be oriented to create a wide variation of elastic properties.

This report is organized as follows. Modeling is discussed first, followed by a presentation of concepts for producing elastic camber deformations. Design analysis methodology specifically devoted to the bending concept of producing camber is presented and applied to a transport wing. Next, the twisting concept for camber creation is treated and applied to a transport wing with the same external dimensions considered previously. Finally, experimental methodology is described which was utilized to evaluate the bending concept for a small-scale model box beam, and experimental data are presented and correlated with analysis predictions. A summary of the project accomplishments is given followed by the references.

Short, self-contained subjects are presented in appendices. Appendix A is concerned with the aerodynamics of chordwise deformable wings. Appendix B is a compilation of stiffness equations for our simple ideal tailored box model for aeroelastic tailoring studies. Appendix C contains a finite element correlation study for a small scale model box beam. Appendix D is devoted to rib concepts for chordwise deformable wings. In Appendix E, a static aeroelastic stability analysis is given for uniform wings. Lastly, a simple two degree of freedom aeroelastic model is presented in Appendix F that is useful for stability studies and gust response studies.

NOMENCLATURE

$\underline{A}$	Steady Aerodynamic Matrix, eq. (F-25)
A_1	Cross sectional area of individual stiffener
A_{44}, A_{45}	Steady aerodynamic coefficients, eqs. (F-27)
A_e	Enclosed area of cross section cell
A_{ij}	Laminate membrane stiffnesses for wing box covers, eqs. (10)
A_n	Fourier coefficients for thin airfoil theory, eqs. (A-4, 5)
a_o	Lift curve slope for airfoil section
a_0 - a_4	Coefficients for characteristic equation, eqs. (F-30, 31)
$\overline{C}_{12}$	Effective Poisson's ratio, eq. (62)
$\overline{C}_{26}$	Twist-camber coupling parameter, eq. (63)
$(C_{66})_{EFF}$	Effective reduced bending stiffness, eq. (23)
C_A	Aerodynamic chord
$\underline{C}^*$	Generalized stiffness matrix, eq. (F-23)
C^*_{ij}	Generalized stiffnesses, eqs. (F-7, 8, 9)
C_{ij}	Beam stiffness matrix, eq. (16)
C_S	Chord of wing section structural box
c	Circumference of structural box cell
c_d	Airfoil section drag coefficient
c_ℓ	Airfoil section lift coefficient
c_m	Airfoil section pitching moment coefficient
$\underline{D}$	Aerodynamic damping matrix, eq. (F-24)
D_{45}, D_{55}	Aerodynamic damping coefficients, eq. (F-26)
E_{11}	Young's modulus of composite material in fiber direction
$(EA)_c$	Extensional stiffness of aluminum closure channel, eq. (77)
$(EI)_c$	Bending stiffness of aluminum closure channel, eq. (69)
e	Eccentricity parameter of aerodynamic center relative to structural axis location, eq. (E-14)
F	Beam generalized internal force matrix, eq. (12)
G	Airfoil geometric factor, eq. (A-10)
H	Height of wing section structural box
h	Skin thickness of load bearing covers of the wing structural box
h'	Equivalent smeared thickness of skin and stiffeners, eq. (50)
h_k	Thickness of k-th ply of a laminate
I_2, I_3, I_4	Integrals defined in eqs. (F-15)

I_α	Mass moment of inertia of wing section about the shear center axis per unit span, eq. (F-14c)
I_α^*	Generalized mass, eq. (F-13c)
J_y	Geometric parameter defined in eq. (30)
K_{ij}	Structural box cover stiffnesses defined in eqs. (9)
k	Parameter defined in eq. (E-13)
k_{11}	Structural box cover stiffness per unit skin thickness defined in eq. (48)
k_c	Camber curvature kinematic matrix defined in eqs. (31, 32)
L'	Lift per unit span, eq. (A-1)
M	Spanwise bending moment
M*	Generalized mass defined in eq. (F-13a)
$\underline{M}^*$	Generalized mass matrix, eq. (F-22)
M'_{AC}	Pitching moment per unit span about aerodyanmic center, eq. (E-5)
M_x	Chordwise bending moment
M_y	Spanwise bending moment
M_z	Twisting moment
m	Mass per unit span of wing structure
m_x	Distributed torque given in eq. (E-4)
N	Axial force (eq. (6)), number of laminate plies (eq. (10))
N_{xs}	Membrane shear flow or stress resultant
N_{ss}	Circumferential (hoop) membrane stress resultant
N_{ss}^T	Themal stress resultant defined in eq. (34)
N_{xx}, N_{xy}, N_{yy}	Membrane stress resultants
$\overline{N}_{xx}$	Prescribed distributed running load in the wing box covers
n	Stiffening parameter defined in eq. (38d)
p_1	Pitch between parallel rows of stiffeners
Q_4, Q_5	Generalized forces defined in eqs. (F-18)
$\overline{Q}_{ij}$	Plane stress stiffnesses for each ply of a laminate
Q_y, Q_z	Beam shear force components defined in eq. (7)
q	Shear flow, dynamic pressure
q_z	Spanwise distributed loading (transverse force per unit span)
S	Beam flexibility matrix
S_α	Static unbalance per unit span defined in eq. (F-14b)
S_α^*	Generalized mass defined in eq. (F-13b)
S_{11}	Beam extensional compliance
S_{15}	Beam bending-extension coupling compliance

S_{44}	Beam twisting compliance
S_{55}	Beam spanwise bending compliance defined in eq. (68)
S_{c5}	Beam camber compliance defined in eq. (72)
T	Kinetic energy
t	Time
U, V, W	Displacement components of the beam reference axis (shear center axis)
$\overline{U}$	Elastic strain energy due to beam bending and twisting, eq. (F-3)
u, v, w	Components of the displacement vector in the (x, y, z) directions, respectively
u_1	Out-of-plane warping displacement component for beam cross section
u_4, u_5	Modal amplitudes associated with beam twisting and spanwise bending, respectively
V_∞	Freestream air velocity
v_1, w_1	Displacement components associated with in-plane warping of beam cross sections
x, y, z	Cartesian coordinates
$\overline{y}_{AC}$	Eccentricity of aerodynamic center relative to structural axis location for a wing airfoil section
α	Airfoil angle of attack, elastic rotation angle
α_d	Effective dynamic angle of attack for an airfoil section given in eq. (F-16)
β	Laminate fiber orientation parameter defined in eq. (21)
β_y, β_z	Beam cross section rotations defined in eqs. (4) and (5), respectively
δW_e	Virtual work of external forces
Δc_ℓ	Increment in airfoil section lift coefficient due to chordwise camber
ε	Maximum strain level
ε_{11}	Spanwise extensional strain in wing box covers
$\bar{\varepsilon}_{11}$	Mean extensional limit strain
ε_{22}	Chordwise strain in wing box covers
ε_{ss}	Chordwise membrane strain in wing box covers
ε_{xx}, ε_{yy}, ε_{zz}	Components of extensional strain
ζ	Thickness coordinate associated with laminated wing box cover
γ	Beam compliance coupling parameter, eq. (78)
γ_{xs}	Membrane shear strain in cell wall of wing section structural box, eq. (26)
γ_{xy}, γ_{xz}, γ_{yz}	Components of engineering shear strain
γ^0_{xy}, γ^0_{xz}	Mean spanwise transverse shear strain components
κ_{11}	Spanwise curvature, eq. (66)

κ_{22}, κ_c	Mean section chordwise camber curvature, eqs. (29) and (70)
κ_{xx}	Spanwise curvature of beam reference axis
$\phi(x)$	Elastic twist angle
ρ_∞	Freestream air density
θ_0	Dominant skin fiber orientation angle
θ_1	Stiffener orientation angle

Subscripts

AC	Refers to aerodynamic center
EFF	Refers to effective value
c	Refers to box beam closure channel
$C_A/4$	Refers to quarter chord location
i, j, k	Refers to indices assuming the values 1, 2, 6
l	Refers to lower wing box cover
u	Refers to upper wing box cover

Superscripts

l	Refers to property of a stiffener
o	Refers to property of the wing cover skin
k	Refers to identifying index
T	Refers to thermal properties

MODELING OF HIGH ASPECT RATIO COMPOSITE WINGS

Preliminary Remarks

Modeling plays a significant role in science and engineering. In fact, the way we understand our world is largely through the study of models of real systems. For the present purposes, we define "model" to be a set of rules which establishes relationships among significant variables and parameters in a physical situation.

For use in engineering design, models must be relatively simple but provide a sound description of physical behavior. Simplicity is essential as cause-effect relationships between configuration and response must be fully understood, physical mechanisms and the parameters influencing them must be clearly identified and, generally, many iterative design analysis cycles are required. Often the analysis cycles are conducted with the aid of an optimization algorithm to reach performance goals without violating constraints that would impair structural integrity or other conditions that limit usefulness or performance.

In this report, a new, simple structural model is presented which is intended for use in aeroelastic tailoring studies of high aspect ratio wings. This model has many advantages and uses.

Hopefully, it will serve to facilitate both understanding and preliminary design. By this means, the "mystery" of aeroelastic tailoring will be diminished as well.

Elastic and Aeroelastic Tailoring

A significant attribute of laminated composites is their design flexibility. The layers or plies of a laminate are, in fact, modular units which can be selected to provide distinct material properties and fiber orientations. It is possible, therefore, to "tailor" the properties of composites to meet specific design requirements.

Tailoring of composite laminates to achieve favorable or desired characteristics has been applied effectively. The swept forward wing of the X-29 Fighter is a prime example. The layup of the wing skins for this aircraft was selected to utilize overall bending-twist coupling of the wing box to avoid static torsional divergence, a chronic problem normally inherent in swept forward wing designs. This permits the swept forward wing design to be used. This type of wing configuration stalls from root to tip, which preserves aileron effectiveness and thereby prevents spin instabilities. Also, a lower wing profile drag at the transonic maneuver design point was achieved.

A second example which is currently undergoing development is the creative use of extension-twist coupling in rotor blades to achieve enhanced performance (ref. 5). The principle utilized is that the blade rotational speed, through extension-twist coupling, can be used to alter the twist of the blade to favorably influence the aerodynamics. An enhanced flight envelope and increased range are sought due to delay of blade stall in hover.

The above examples strongly indicate that tailoring can be utilized effectively if

1) The behavior in question is thoroughly understood physically;

2) The mechanism(s) is (are) clearly identified; and

3) Favorable changes of sufficient magnitude can be produced.

The cornerstone of elastic tailoring with composites is modeling. We select the well established thin-walled beam theory of Rehfield (refs. 5-7) to serve as a basis for our models of high aspect ratio composite structures, appropriately modified to predict chordwise camber deformations.

Tailored response utilizing elastic coupling mechanisms for thin-walled beams is achieved by skewing angle plies with respect to the beam axis. Two limiting archetype configurations are shown in figs. 4 and 5. The circumferentially uniform stiffness (CUS) configuration produces extension-twist coupling with bending-transverse shear as a parasitic coupling mechanism (ref. 7). The other configuration, circumferentially asymmetric stiffness (CAS), produces bending-twist coupling with extension-transverse shear as a parasitic coupling mechanism (ref. 7). The angle θ in figs. 4 and 5 denotes the dominant off-axis angle ply orientation in the upper and lower surface wall configurations. These limiting forms are interesting because they isolate the two primary independent coupling mechanisms of extension-twist and bending-twist.

Thin-Walled Composite Beam Theory

The theory of Rehfield (ref. 5) provides the basis for this work. Attention will be confined to single cell beams, which provide elementary means for exploring the new coupling mechanisms. A typical beam model and the coordinate system are shown in fig. 6.

Kinematics

The components of the displacement vector are taken in the form (refs. 5-7)

$$u = U(x) + y\beta_z(x) + z\beta_y(x) + u_1 \tag{1}$$

$$v = V(x) - z\phi(x) \tag{2}$$

$$w = W(x) + y\phi(x) \tag{3}$$

where the section rotations are

$$\beta_y = \gamma^o_{xz}(x) - W_{,x} \tag{4}$$

$$\beta_z = \gamma^o_{xy} - V_{,x} \tag{5}$$

The above expressions are valid up to moderate bending and twisting rotations and small strain states. Also, the shear center of the cross section and x-axis projection have been assumed to coincide.

The displacement contribution u_1 is the out-of-plane warping (OPW) displacement, which is familiar from the St. Venant theory of bending and twisting of beams (ref. 8). The most significant contribution to u_1 is twisting related warping. It may be expressed as (refs. 5-7)

$$u_1 = \psi\varphi,x \tag{1a}$$

where ψ is the St. Venant torsion function which characterizes out-of-plane warping due to global twisting deformation. It is thoroughly evaluated and discussed in ref. 6 for a model rotor blade. Generally, OPW displacement contributions create boundary layer zones near boundaries where they are restrained from freely developing due to a high degree of fixity. The essential physical nature of the response is not altered by OPW displacements. Tip rotation in the model rotor blade considered in ref. 6 is lowered by approximately ten percent due to twisting-related out-of-plane warping.

Nonuniform OPW effects will be ignored in the present work, as is the custom in aeroelastic studies. This is a conservative assumption for aeroelastic instability predictions.

These effects may be analyzed by superposition of boundary layer solutions in the manner utilized by Valisetty, Murthy and Rehfield (ref. 9).

Generalized Forces

The consistent generalized forces are determined with the aid of the Principle of Virtual Work (ref. 5). They are defined as

$$(N,M_y,M_z) = \oint N_{xx}\,(1,z,y)ds \tag{6}$$

$$(Q_y,Q_z,M_x) = \oint N_{xs}\left(\frac{dy}{ds}, \frac{dz}{ds}, \frac{2A_e}{c}\right)ds \tag{7}$$

Complete equilibrium equations and admissible boundary conditions appear in ref. 5. The enclosed cell area is A_e, and c is the circumference of the closed cell. The integrals are taken around the closed cell in a counterclockwise direction.

Force-Deformation Relations

Composite thin-walled construction is characterized by the membrane stiffness matrix K which relates the non-zero stress resultants to the membrane strains. The constitutive relations are

$$\begin{aligned} N_{xx} &= K_{11}\varepsilon_{xx} + K_{12}\gamma_{xs} \\ N_{xs} &= K_{12}\varepsilon_{xx} + K_{22}\gamma_{xs} \end{aligned} \tag{8}$$

The stiffnesses K_{11} corresponds to uniaxial extension, K_{22} corresponds to shear, and K_{12} is a coupling stiffness. They are related to the usual stiffness matrix A (refs. 5-7) as follows

$$\begin{aligned} K_{11} &= A_{11} - \frac{A_{12}^2}{A_{22}} \\ K_{12} &= A_{16} - \frac{A_{12}A_{26}}{A_{22}} \\ K_{22} &= A_{66} - \frac{A_{26}^2}{A_{22}} \end{aligned} \tag{9}$$

For a laminate of N plies, the stiffnesses are determined by simply adding the plane stress stiffnesses, $\overline{Q}_{ij}$, for each ply. Thus

$$A_{ij} = \sum_{k=1}^{N} \overline{Q}_{ij}^{(k)} h_k \qquad (i,j = 1,2,6) \tag{10}$$

where h_k is the thickness of the kth ply. The ply stiffnesses depend upon the material system, material form and fiber orientation.

Equations (8) describe the elastic response because the circumferential stress resultant, N_{ss}, is neglected. This is justified in the absence of internal pressure.

The deformation variables or generalized strains are easily identified from the strain expressions. Arrayed in a column matrix u they are

$$u = \left[U_{,x}\ \gamma^{o}_{xy}\ \gamma^{o}_{xz}\ \phi_{,x}\ \beta_{y,x}\ \beta_{z,x}\right]^{T} \tag{11}$$

Similarly the generalized internal forces can be put in a column matrix form as

$$F = \left[N\ Q_y\ Q_z\ M_x\ M_y\ M_z\right]^{T} \tag{12}$$

The relationship between the beam and its reference axis (the coordinate direction x) has not yet been specified; however, it is convenient to choose it in a manner that differs from that of refs. 5-7. We choose a geometric axis system that is defined such that

$$\oint y\,ds = 0 \tag{13a}$$

$$\oint z\,ds = 0 \tag{13b}$$

The x-axis, therefore, is located at the centroid of the enclosed cell area. In addition, the orientation of the y- and z-axis can be selected such that

$$\oint yz\,ds = 0 \tag{14}$$

A fixed geometric axis system is particularly convenient for studying damage processes in composite structures. As plies become damaged and lose effectiveness, the reference axes do not have to be moved.

Since the force and the deformation are linearly related, a symmetric 6 x 6 stiffness matrix, C, can then be defined such that

$$F = Cu \tag{15}$$

By virtue of the procedure and choice of axes defined above, the elements of C consist of 21 independent stiffness constants

$$(C_{11},C_{15},C_{16},C_{55},C_{56},C_{66}) = \oint K_{11}\left(1,z,y,z^2,yz,y^2\right)ds \tag{16a}$$

$$(C_{12},C_{13},C_{14},C_{25},C_{26}) = \oint K_{12}\left(\frac{dy}{ds},\frac{dz}{ds},\frac{2Ae}{c},\frac{dy}{ds}z,\frac{dy}{ds}y\right)ds \tag{16b}$$

$$(C_{35},C_{36},C_{45},C_{46}) = \oint K_{12}\left(\frac{dz}{ds}z, \frac{dz}{ds}y, \frac{2Ae}{c}z, \frac{2Ae}{c}y\right)ds \tag{16c}$$

$$(C_{22},C_{23},C_{24},C_{33},C_{34},C_{44}) = \oint K_{22}\left[\left(\frac{dy}{ds}\right)^2, \frac{dy}{ds}\frac{dz}{ds}, \frac{2Ae}{c}\frac{dy}{ds}, \left(\frac{dz}{ds}\right)^2, \frac{2Ae}{c}\frac{dz}{ds}, \left(\frac{2Ae}{c}\right)^2\right]ds \tag{16d}$$

In order to apply forces and calculate beam deformations, however, it is necessary to invert eq. (15) to obtain the compliance relationship

$$u = S\,F \tag{17}$$

where $S = C^{-1}$ is the flexibility matrix. Alternatively, the flexibility or compliance matrix may be evaluated directly from the complementary strain energy per unit length of beam (ref. 9).

In-Plane Warping Displacement

The above theory may be modified to permit evaluation of in-plane warping (IPW) displacement components. To this end, we replace eqs. (2) and (3) by the following expressions:

$$v = V(x) - z\phi(x) + v_1 \tag{18a}$$

$$w = W(x) + y\phi(x) + w_1 \tag{18b}$$

The components v_1 and w_1 are associated with IPW. The component w_1 may be identified with camber bending.

IPW effects are very important in aeronautical structures because section shape changes effect the aerodynamic characteristics of the structure. There is, therefore, the opportunity to favorably tailor the structure to enhance aerodynamic performance.

The thin-walled structure is assumed to be described adequately by classical lamination theory and the Kirchhoff hypothesis. Consequently, we have only to consider the three membrane strain components ε_{xx}, γ_{xs}, and ε_{ss}. Since the hoop stress resultant, N_{ss}, vanishes (for no internal pressure)

$$\varepsilon_{ss} = -\frac{1}{A_{22}}(A_{12}\varepsilon_{xx} + A_{26}\gamma_{xs}) \tag{19}$$

Consequently, from the strain transformation equations

$$\varepsilon_{yy} = v_{1,y} = \varepsilon_{ss}\left(\frac{dy}{ds}\right)^2 \tag{20a}$$

$$\varepsilon_{zz} = w_{1,z} = \varepsilon_{ss}\left(\frac{dz}{ds}\right)^2 \tag{20b}$$

$$\gamma_{yz} = v_{1,z} + w_{1,y} = 2\varepsilon_{ss}\left(\frac{dy}{ds}\right)\left(\frac{dz}{ds}\right) \tag{20c}$$

Eqs. (20a) - (20c) must be integrated to evaluate the IPW displacement components.

A Simple Aeroelastic Section Model

The Ideal Tailored Box Model

Our studies of tailored wings have shown the utility of the simple cross section model shown in fig. 7. This model is the result of considerable design analysis experience. We call it the "Ideal Tailored Box Model." The upper and lower covers are load bearing, while the webs are assumed to be nonstructural. The role of the webs is to preserve the closed cell load path in torsion and maintain the geometry of the section (infinite transverse shear stiffness) while not contributing to the extentional, bending and torsional stiffnesses of the beam. Mean or averaged stiffness properties are considered uniform across the section width.

Great simplicity is achieved with this model. Closed form expressions for all the stiffnesses and compliances permit rapid assessment of design changes and facilitate understanding of the cause-effect relationships between configuration and structural response. The model is useful for teaching, initial sizing in preliminary design, optimization and parametric studies, providing trend information, establishing intuitive insight into behavior on the part of the designer and isolating and identifying independent design-controlled mechanisms. Stiffness equations are summarized in Appendix B.

Model-Structure Correspondence

One use for the model is analyzing the response of an existing structure. In such an instance, we have found that a useful approach to fixing model parameters is to require correspondence of global extensional stiffness, spanwise bending stiffness, and torsional stiffness. In addition, since our model has five parameters for symmetric upper and lower cover configurations, we match global fiber orientation effects through a parameter denoted "β" in refs. 6 and 7 and an effective chordwise bending stiffness. The parameter β is defined as

$$\beta = (K_{12})^2/K_{11}K_{22} \tag{21}$$

Since only the load bearing covers contribute to the stiffnesses, it is not possible to model all of them with fidelity. Because the webs of the structural box are not modeled, the transverse shear stiffness C_{33} associated with spanwise bending and the bending-transverse shear coupling stiffness C_{36} cannot be modeled independently. A natural choice for establishing correspondence emerges for the case of chordwise compact sections.

A chordwise compact section is one for which

$$H/C_s << 1 \tag{22}$$

This is a typical characteristic that applies to most, if not all, airfoil sections. For this class of section, we assume Bernoulli-Euler behavior for spanwise bending, which is equivalent to letting C_{33} become infinitely large in the global compliance equations. The result is that transverse shear deformations are ignored for spanwise bending. Again, this restriction is not serious for the usual airfoil sections encountered in aeronautics.

Chordwise bending behavior, while affected by transverse shear deformations through the stiffness C_{22}, is controlled by the effective reduced bending stiffness $(C_{66})_{EFF}$ defined as

$$(C_{66})_{EFF} = C_{66} - (C_{36})^2 / C_{33} \qquad (23)$$

A thorough discussion of reduced bending stiffnesses appears in ref. 6. The practical result is that the structure responds to bending loads as if the bending stiffness is reduced by virtue of the presence of the bending - transverse shear coupling stiffness---in this case, C_{36}. This unwanted, parasitic effective stiffness reduction can be as great as fifty percent (refs. 6, 7). For this reason, we choose to match the reduced chordwise bending stiffness in eq. (23) as the condition for model-structure correspondence.

Application to the Langley Rotor Blade

The rotor blade studied in ref. 10 is a convenient example to illustrate model-structure correspondence. It appears in fig. 8. The results of applying the principles for matching parameters above to this blade appear in Table 1.

The results in Table 1 confirm that a high degree of correspondence has been achieved between the rotor blade and our simple aeroelastic model.

If greater physical fidelity is desired, the webs may be modeled. This, however, creates ambiguity and complexity, and much of the appealing simplicity is lost. In its present form, the Ideal Tailored Box Model includes all of the physical effects that earlier work has shown to be essential to good predictions of global behavior (refs. 5-7).

Simplified Analysis of In-Plane Warping Displacement for Chordwise Compact Sections

The differential equations which permit evaluation of IPW displacement components are given in eqs. (20). They may be simplified further for chordwise compact sections which satisfy the inequality of eq. (22). In particular, we introduce the following approximations:

$$\frac{dy}{ds} \cong 1 \ , \ \frac{dz}{ds} \cong 0 \qquad (24)$$

Consequently

$$v_{1,y} \cong \varepsilon_{ss} \qquad (25a)$$

$$w_{1,z} = \varepsilon_{zz} \cong 0 \qquad (25b)$$

$$v_{1,z} + w_{1,y} = \gamma_{yz} \cong 0 \qquad (25c)$$

Note that eqs. (25) are completely consistent with the physical approximations inherent in the Ideal Tailored Box Model.

Also consistent with this level of physical approximation is the following expression for shear strain:

$$\gamma_{xs} \cong \gamma^o_{xy} - z\phi_{,x} \qquad (26)$$

This expression is valid when spanwise transverse shear deformations are ignored $(\gamma^o_{xz} \equiv 0)$ and the section is chordwise compact. For the Ideal Tailored Box Model, the approximation corresponds to uniform shear strain in the upper and lower load bearing covers.

Equations (25b,c) correspond to an IPW displacement field of the classical Bernoulli-Euler type associated with, to this level of approximation, chordwise camber bending. The result is

$$w_1 = W_1(x,y) \tag{27a}$$

$$v_1 = - zW_{1,y} \tag{27b}$$

Consequently, with the aid eqs. (25a), (26), (27) and (1) (with OPW effects ignored)

$$\begin{aligned} v_{1,y} = - zW_{1,yy} &\equiv - (A_{22})^{-1} (A_{12}\varepsilon_{xx} + A_{26}\, \gamma_{xs}) \\ &\equiv - (A_{22})^{-1} \left[A_{12}\, (U_{,x} + z\beta_{y,x} + y\beta_{z,x}) + A_{26}(\gamma^o_{xy} - z\phi_{,x})\right] \end{aligned} \tag{28}$$

The left hand side of eq. (28), which suggests a linear variation with z, is not congruent with the right hand side which reflects a more complex functional form. This situation may be resolved in a number of ways. We choose to satisfy eq. (28) in an average sense. That is, we define the mean camber curvature κ_c to be

$$\begin{aligned} \kappa_c &\equiv (J_y)^{-1} \oint z\varepsilon_{yy}\, ds \\ &= - W_{1,yy} \end{aligned} \tag{29}$$

where

$$J_y = \oint z^2\, ds \tag{30}$$

With the aid of eq. (28)

$$\kappa_c = - k_c^T u \tag{31}$$

where k_c is the camber curvature kinematic matrix with the elements

$$k_{c1} = (J_y)^{-1} \oint (A_{12}\, z/\, A_{22})\, ds \tag{32a}$$

$$k_{c2} = (J_y)^{-1} \oint (A_{26}\, z/\, A_{22})\, ds \tag{32b}$$

$$k_{c3} = 0 \tag{32c}$$

$$k_{c4} = -(J_y)^{-1} \oint (A_{26} z^2 / A_{22})\, ds \tag{32d}$$

$$k_{c5} = (J_y)^{-1} \oint (A_{12} z^2 / A_{22})\, ds \tag{32e}$$

$$k_{c6} = (J_y)^{-1} \oint (A_{12} yz / A_{22})\, ds \tag{32f}$$

and u is defined in eq. (11). Equation (31) supplements the matrix equation (15) and extends the theory of Rehfield (refs. 5-7) to include estimates of IPW displacements.

In Appendix A we use thin airfoil theory to predict section lift and pitching moment coefficients in terms of the mean camber curvature κ_c. Thus, the aerodynamic consequences of tailored elastic camber deformations are evaluated in a simple, straight-forward manner.

CAMBER PRODUCING CONCEPTS

Fundamental Camber Principle

Elastically produced camber is created by establishing a differential chordwise membrane strain between the upper and lower box covers while preserving the structural box. This is depicted in fig. 9. There are a number of ways of accomplishing the differential strain.

It is helpful to consider the general thermoelastic chordwise strain for a laminate according to membrane theory. The relationship is

$$\varepsilon_{ss} = (A_{22})^{-1} \left(N_{ss} + N_{ss}^T - A_{12}\, \varepsilon_{xx} - A_{26}\, \gamma_{xs} \right) \tag{33}$$

where N_{ss}^T is the thermal stress resultant defined as

$$N_{ss}^T = \sum_{k=1}^{N} \int_{h_k} \left(Q_{21}\, \varepsilon_{xx}^T + Q_{22}\, \varepsilon_{ss}^T + Q_{26}\, \gamma_{xs}^T \right) d\zeta \tag{34}$$

The stiffness coefficients $\overline{Q}_{ij}$ are evaluated at the appropriate temperatures. The strains ε_{xx}^T, ε_{ss}^T and γ_{xs}^T are due to thermal effects only, and the thickness coordinate is ζ. The first term in eq. (33) due to the chordwise stress resultant N_{ss} is influenced by internal pressure in the box. The second term involving N_{ss}^T is due to thermal expansion. The term proportional to A_{12} is proportional to the spanwise strain due to extension and bending. Finally, the term proportional to A_{26} is activated by transverse shear strain and twisting.

It is possible to conceive of tailored configurations that exaggerate each of these physical effects. We refer to them as the pressure, thermal, bending and twisting concepts or methods for producing elastic camber deformations. The different mechanisms are illustrated in figs. 10 and 11. The pressure and thermal methods are of secondary importance as sufficiently large chordwise strain differentials cannot be produced for reasonable parameter values and current

composite materials. The primary mechanisms that offer practical potential are the bending and twisting methods. These two methods will be treated in detail subsequently.

Another method of producing elastic chordwise camber was discovered late in the program and has not been thoroughly evaluated. We call it the "Unsymmetrical Cover Bending Method." It can best be explained by referring to fig. 10. Two bending mechanisms are presented --- Global Camber Bending and Local Cover Bending. Both mechanisms can be enhanced by unsymmetrical wall and stiffener configurations that produce local extension-bending coupling in the stiffened wall. Exploration of this mechanism requires another level of modeling. As it is a major undertaking, we propose to study it under a future contract or grant.

The Bending Method

The bending method of creating elastically produced chordwise camber utilizes camber-bending elastic coupling illustrated in fig. 10. We could equally well have called this "Exaggerated Poisson Expansion." This method creates anticlastic chordwise bending deformation due to spanwise bending. The mechanism is differential Poisson expansion of the upper and lower wing box covers. This is a naturally occurring phenomenon, even for isotropic material structures. If the properties of composite skin and unidirectional stiffeners are aggressively utilized, however, it is possible to create tailored configurations where the Poisson effects are dominant characteristics rather than secondary ones. The objective, referring to eq. (33), is to tailor the structure in such a way that the effective Poisson ratio (A_{12}/ A_{22}) is large. Then, for identical upper and lower covers, spanwise bending strains will produce substantial chordwise camber.

The results to date utilizing this method have been impressive. Using reasonable values for angle of attack, Exaggerated Poisson Expansion can produce a section lift enhancement of up to fifteen percent for a transport aircraft airfoil section. In addition, this mechanism can be utilized without interfering with elastic deformations due to spanwise bending and twisting as balanced, symmetric cover configurations may be employed.

The Twisting Method

The twisting method of creating camber is based upon the use of camber-twist elastic coupling illustrated in fig. 10. This method, again referring to eq. (33), is to tailor the structure in order to produce large values of the effective extension-shear coupling parameter (A_{26} / A_{22}). In contrast to camber-bending elastic coupling, this mechanism exists only in unbalanced cover configurations. In addition, the effective Poisson expansion due to (A_{12} / A_{22}) will also be present, so the camber-bending mechanism will be activated simultaneously. Thus, a thorough design and optimization study is required to select the "best" configuration.

Also, in contrast to pure camber-bending balanced symmetric cover configurations, the unbalanced covers give rise to configurations which are globally circumferentially asymmetric structures (fig. 5) which possess global spanwise bending-twist elastic coupling. In general, therefore, the system design is more involved for utilization of the twisting method of producing camber. This provides an opportunity, however, to simultaneously tailor spanwise bending, spanwise twisting and camber deformations.

On the basis of camber production alone, twist-camber coupling can achieve camber and section lift coefficients comparable to camber-bending coupling. It must be remembered, however, that the configurations that are "best" for the utilization of the respective methods are physically quite distinct. The difficulty of dealing with unbalanced configurations is somewhat of an impediment to implementing this mechanism. Unbalanced configurations lead to difficulties associated with avoiding warping, twisting and bending distortions in manufacture.

Secondary Camber Mechanisms

The remaining two elastic camber producing mechanisms are illustrated in fig. 11. The third concept which utilizes internal pressure we call "Internal Pressure With Dissimilar Covers" (IPWDC). The fundamental idea behind the IPWDC mechanism is to use dissimilar covers such that the stiffness A_{22} of the upper cover is much less than that of the lower cover. Under the action of positive internal pressure chordwise (and spanwise) tensile stress resultants are produced which stretch the covers in the chordwise direction. Since the upper cover stretches chordwise more than the lower cover and the integrity of the structural box is maintained, camber deformation results.

Unlike the two deformation mechanisms treated earlier, camber deformation in this case is present as long as the internal pressure acts. Thus, if fuel pressure alone (15-20 psi) is used, little control over the camber can be exercised. The possibility of creating an artificial positive pressure which can be controlled is a consideration, but it adds difficulties of its own.

Unfortunately, an evaluation of this concept shows that this is a weak mechanism. For extreme structural configurations and typical fuel pressures, the resulting contribution to the lift coefficient is insignificant. Consequently, after the initial evaluation, study of this method was discontinued.

A fourth mechanism, Augmented Thermal Expansion (ATE), has also been evaluated. Like IPWDC, the basic idea is to create a greater chordwise strain in the upper cover of the box than the lower, thereby producing a camber deformation. In this case, thermal expansion strains are augmented by intentional local heating of the upper cover to produce up to 400F temperature differences between the covers. This mechanism is also weak and appears to be of no practical value by itself. After the initial evaluation, study of this idea was discontinued as well. Section lift coefficient increments less than three percent are created by this mechanism.

Closing Remarks

We have introduced the methods that we have created to produce elastic chordwise camber deformations in this section. The secondary methods will not be discussed further as they do not appear to be practical by themselves. Two parallel design analyses will be presented for the bending and twisting methods subsequently for a transport wing application. Also, the results of an experimental program to evaluate the bending method will be presented later.

DESIGN ANALYSIS METHODOLOGY - BENDING METHOD

Preliminary Remarks

Our beam-like analysis together with the simple Ideal Tailored Box section model have been created for use in the preliminary or conceptual phase of design. The design analysis methodology that we have developed is correspondingly appropriate and consistent with the level required at this stage of the design process. In contrast to the previous work of others (refs. 1, 4), we will not tailor specific configurations to specific mission requirements. Instead we seek scientific understanding of behavior and design concepts which accentuate camber producing deformations. A generic transport wing serves as a vehicle for evaluating camber producing configurations.

The wing box model appears in fig. 12. Only the structural box covers are assumed to be load bearing in keeping with our Ideal Tailored Box modeling approach. The model is based upon the center wing structural box of the Lockheed C-130 transport. This avoids the complexity of wing sweep. All dimensions other than skin thicknesses are those of the C-130.

For study of the bending method, a balanced configuration with identical upper and lower covers has been selected. The material properties correspond to AS4/3501-6 graphite-epoxy; they appear in Table 2.

Basic Configurations - Bending Method

Camber without the presence of other forms of section deformation can be produced by creating balanced configurations of skin layup and stiffeners with respect to the stiffened beam's axis. Under pure bending, no twisting will occur. A typical stiffener-skin pattern appears in fig. 13.

The stiffeners are taken to be made of unidirectional composite material with rectangular cross sections of the type that may be created by winding or weaving technology. Also, [0]-degree stiffeners parallel to the beam axis may be added for structural efficiency. These stiffeners enhance overall bending stiffness without affecting the camber creating mechanism.

Since membrane behavior is considered for the upper and lower wing box covers, local bending effects due to cover buckling or postbuckling are excluded at this level of modeling. The influence of the box webs are neglected for convenience in keeping with the Ideal Tailored Box Model.

A single skin fiber orientation angle θ_o (fig. 13) is considered. This is not overly restrictive as [0] and [90] plies may be added without altering the camber-bending coupling significantly. For the final result we want both efficient load bearing ability and sufficient camber-bending coupling.

This camber producing concept requires that a large effective Poisson's ratio be given to the wing covers. This can be accomplished by utilizing the balanced stiffener pattern and a balanced skin layup as shown in fig. 13, with both upper and lower covers identical in stiffness. The skin and stiffener orientation angles θ_o and θ_1, together with appropriate dimensions, are selected to produce a large Poisson's ratio while carrying the basic bending loads. Let x denote the spanwise coordinate and y a chordwise coordinate. For membrane behavior in the covers

$$N_{xx} = A_{11}\,\varepsilon_{xx} + A_{12}\,\varepsilon_{yy} \tag{35a}$$

$$N_{yy} = A_{12}\,\varepsilon_{xx} + A_{22}\,\varepsilon_{yy} \tag{35b}$$

$$N_{xy} = A_{66}\,\gamma_{xy} \tag{35c}$$

The membrane stress resultants are N_{xx}, N_{yy} and N_{xy}, the membrane strains are ε_{xx}, ε_{yy}, and γ_{xy} and the A_{ij}'s are membrane stiffnesses as before.

The stiffnesses are composed of two contributions, one due to the skin and the other due to the stiffeners. The influence of stiffeners is accounted for in an averaged manner. The stiffeners are "smeared" or "averaged" over the area of the skin. The stiffnesses may be written as

$$A_{ij} = A^{o}_{ij} + A^{1}_{ij} \tag{36}$$

We adopt the convention that superscripts "o" and "1" refer to the skin and stiffeners, respectively. For a laminated skin of N plies, the skin stiffnesses are determined by simply adding the plane stress stiffnesses, $\overline{Q}_{ij}$, for each ply. Thus

$$A^{o}_{ij} = \sum_{k=1}^{N} \overline{Q}^{(k)}_{ij} h_k \quad (i,j = 1, 2, 6) \tag{37}$$

where h_k is the thickness of the k-th ply. The ply stiffnesses depend upon the material system, material form (fabric or tape, for example) and fiber orientation.

The stiffeners carry only axial loads and their effects are "smeared" over the surface. These stiffness contributions are

$$A^{1}_{11} = 2E^{1}_{11}\, hn \cos^4\theta_1 \tag{38a}$$

$$A^{1}_{12} = 2E^{1}_{11}\, hn \sin^2\theta_1 \cos^2\theta_1 = A^{1}_{66} \tag{38b}$$

$$A^{1}_{22} = 2E^{1}_{11}\, hn \sin^4\theta_1 \tag{38c}$$

The extensional modulus of the stiffeners is E^{1}_{11}, h is the skin thickness, n is the stiffening parameter that reflects the stiffener spatial distribution and pattern. Equations (38) are valid for balanced pairs of stiffeners oriented at angles of $\pm\,\theta_1$.

The stiffening parameter n is defined as

$$n = A_1 / p_1\, h \tag{38d}$$

The cross sectional area of an individual stiffener is A_1 and p_1 is the pitch or distance between parallel rows of stiffeners. The stiffener orientation angle is θ_1 as shown in fig. 13.

By virtue of high aspect ratio wing geometry, the chordwise stress resultant N_{yy} is quite small and will be ignored. Thus

$$N_{yy} \approx 0 \tag{39}$$

This permits the equations to be reduced. The results are

$$\varepsilon_{yy} = -\,(A_{12} / A_{22})\, \varepsilon_{xx} \tag{40}$$

$$N_{xx} = K_{11}\, \varepsilon_{xx} \tag{41}$$

where $$K_{11} = A_{11} - (A_{12})^2 / A_{22} \tag{42}$$

The effective extensional membrane stiffness is K_{11}. The effective Poisson's ratio, which is related to camber, is (A_{12} / A_{22}).

It remains to relate the lift on the airfoil section to the elastically produced camber deformation. The incremental contribution to the section lift coefficient due to elastic camber may be expressed as (eq. (A-8), Appendix A)

$$\Delta c_\ell = G(H/2)\, \kappa_c \tag{43}$$

This equation is based upon linear two-dimensional thin airfoil theory. The factor G is a geometric factor that depends on the cross sectional shape, structural box dimensions and overall section dimensions. It is given in eq. (A-10), Appendix A. Note that the factor $(H/2)\, \kappa_c$ is simply the

maximum chordwise bending strain. For uniform cover properties, the only camber curvature kinematic parameter is k_{C5}.

$$k_{C5} = A_{12} / A_{22} \tag{44}$$

The bending strain is related to the section rotation as follows

$$\beta_{y,x} = -2\varepsilon / H \tag{45}$$

where ε is the maximum strain level for bending with the upper fibers in compression (upwardly convex spanwise bending of the wing). Thus, from eqs. (31) and (43) - (45)

$$\Delta C_\ell = G(A_{12} / A_{22})\varepsilon \tag{46}$$

Equation (46), although simple in form, conveys a significant amount of physical information. The factor G contains all of the geometric information about the section which includes the structural chord (C_s), the aerodynamic chord (C_A), and the airfoil thickness or structural box depth (H). The effective Poisson's ratio (A_{12} / A_{22}) enters in direct proportion to the increment in section lift coefficient. Thus, maximizing Poisson's ratio will maximize the section lift coefficient. The allowable strain level is actually a material property. Clearly, there are lift benefits to selecting a material system with a high strain-to-failure.

Design Analysis - Bending Method

A design analysis algorithm has been created for evaluating the benefits of tailored camber. An allowable strain level for bending related response and a distributed axial loading in the covers are assigned initially. The running axial cover stiffness can be directly estimated.

$$K_{11} = \overline{N}_{xx} / \varepsilon \tag{47}$$

The distributed running load in the cover is $\overline{N}_{xx}$. The strain level ε is the allowable spanwise bending strain.

It is convenient to define the membrane stiffness per unit skin thickness k_{11} as

$$k_{11} = K_{11} / h \tag{48}$$

This stiffness parameter may be calculated directly from lamination theory and a knowledge of the stiffener pattern. It permits the skin thickness to be evaluated as

$$h = \overline{N}_{xx} / k_{11}\,\varepsilon \tag{49}$$

An appropriate measure of structural weight for configurations fabricated from one material is the equivalent smeared thickness of skin and stiffeners denoted h'. It is

$$h' = h(1+2n) \tag{50}$$

This equation is based upon a balanced stiffener spatial distribution and pattern.

The incremental contribution to the section lift coefficient due to elastic camber may be estimated directly from eqn. (46).

The design analysis proceeds as follows:

1. A configuration is selected and k_{11} is determined;
2. The skin thickness is found using eq. (49);
3. The lift coefficient contribution is calculated using eq. (46);
4. The weight related measure of the lift created is evaluated from the parameter

$$\Delta c_\ell \; / \; h'$$

5. Parametric and optimization studies can be conducted based upon the lift created (eq. (47)) or lift per unit of structural weight (step 4).

In attempting to optimize the aerodynamic benefits, we have found that there are two optimum designs that are of interest. These are a "weight" optimum which corresponds to the maximum lift per unit structural weight. There is also a "lift" optimum that corresponds to maximum absolute lift. Experience indicates a large weight penalty accompanies the transition from weight to lift optimum designs.

Results and Discussion

Benchmark Wing Cover Design

A benchmark configuration was created and analyzed for which no effort was made to create elastically produced camber. This configuration carries the design level bending strain and utilizes AS4/3501-6 graphite-epoxy as a material system. The stiffeners are unidirectional and oriented at [0] degrees to the wing beam axis. The skin is composed of only [±45] plies.

The overall level of stiffening remains comparable (but not necessarily equal) in all designs. Also the design extensional strain level ε is taken as 4500 microinches per inch. The applied running load $\bar{N}_{xx}$ is set at 25,000 pounds per inch, a value consistent with the center wing of a large transport.

Bending Method Design Study

A sampling of design results is presented in figs. 14-19. They are based upon C-130 overall dimensions (fig. 12) and AS4/3501-6 graphite-epoxy properties. Results appear in fig. 14 for an unstiffened design. An optimum fiber orientation for unidirectional material is found to be approximately 26 degrees.

These results are put in perspective by the information presented in fig. 15. Curves corresponding to four levels of stiffening illustrate clearly how effective balanced stiffeners are at enhancing Poisson effects. Values of n corresponding to 0.0, 0.5, 1.0 and 1.5 are associated with skin only and light, medium and heavy stiffening, respectively.

A fully weight optimized design is represented in fig. 16. This was determined with the aid of the commercially available computer program "Eureka" (ref. 11). A maximum value of $\Delta c_\ell / h'$ is

obtained which, in this instance, corresponds to stiffener orientations of approximately 15.6 degrees.

A design based upon maximizing the total lift appears in fig. 17. A maximum value of Δc_ℓ is obtained which, in this instance, corresponds to stiffener orientations of 20.8 degrees. Note that the weight optimum design (WOD) is different from the lift optimum design (LOD).

Our studies indicate that the total lift produced by the WOD is lower than for the LOD. The additional weight required to increase total lift above the WOD level may be substantial, however. It appears that efforts to produce weight efficient designs are warranted.

Another intuitive design concept is one in which the orientation of the unidirectional skin plies and the stiffeners are the same. This "equal angle design" (EAD) concept is appealing because of its simplicity and relative case of fabrication.

Equal angle design results are presented in figs. 18 and 19. A WOD analysis appears in fig. 18. These results compare favorably with those in fig. 16. In Fig. 19 a LOD analysis is shown. These results must be compared to those of fig. 17. The EAD concept yields results which are practically indistinguishable from fully optimized designs.

Optimal values for the bending method designs are presented in table 3. The results correspond to n = 1.5, which is considered to be heavy stiffening. It is to be noted that the section lift coefficient increments for both the weight optimum design (WOD) and lift optimum design (LOD) are large enough to be of practical interest. As a reference, the basic lift contribution due to angle of attack from linear thin airfoil theory is

$$\Delta c_\ell \equiv 0.110\,\alpha \tag{51}$$

where α, the angle of attack, is given in degrees.

The transition from the WOD to the LOD corresponds to an approximate increase in section lift coefficient of 18 percent. The weight increase, however, is 56 percent. Thus, as mentioned earlier, a substantial weight penalty is required for the additional lift. Also, the two designs correspond to totally different configurations.

Even though no effort was made to produce elastic camber with the benchmark design, there is a small contribution due to anticlastic curvature. The transition from the benchmark design to the WOD corresponds to an increase of 234 percent in section lift coefficient for a weight increase of only 11 percent. This suggests that elastic camber tailoring is weight efficient.

Concluding Remarks

The design studies provide valuable information. Perhaps the most significant finding is that WOD and LOD configurations are distinct and that heavy weight penalties are associated with obtaining lift above the WOD level. It appears that the lift enhancement obtainable by elastically tailored camber is large enough to be of practical significance.

DESIGN ANALYSIS METHODOLOGY - TWISTING METHOD

Preliminary Remarks

As indicated earlier, the twisting method of creating camber deformations requires unbalanced cover configurations arranged in a globally circumferentially asymmetric structure (fig. 5). Apart from these differences, the models and analyses parallel those described earlier for the bending method.

Basic Configurations - Twisting Method

The upper and lower covers are identical and arranged in a manner that we have earlier called a circumferentially asymmetric configuration. This type of configuration produces bending-twist coupling in addition to the camber studied here. Figure 20 shows the arrangement of the covers. The fiber orientation indicated in the figure corresponds to the dominant off axis fiber direction.

The stiffeners are taken to be unidirectional configurations as before. Also, [0]-degree stiffeners parallel to the beam axis may be added for structural efficiency. These stiffeners enhance overall bending stiffness without affecting the camber creating mechanism. A single stiffener orientation angle θ_1 and a single skin fiber orientation angle θ_o are considered.

For membrane behavior in the covers

$$N_{xx} = A_{11}\,\varepsilon_{xx} + A_{12}\,\varepsilon_{yy} + A_{16}\,\gamma_{xy} \tag{52a}$$

$$N_{yy} = A_{12}\,\varepsilon_{xx} + A_{22}\,\varepsilon_{yy} + A_{26}\,\gamma_{xy} \tag{52b}$$

$$N_{xy} = A_{16}\,\varepsilon_{xx} + A_{26}\,\varepsilon_{yy} + A_{66}\,\gamma_{xy} \tag{52c}$$

As before we write the stiffnesses in the form given in eq. (36). For this unbalanced stiffener pattern, however, the stiffness contributions due to the stiffeners are

$$A^1_{11} = E^1_{11}\,hn\,\cos^4\theta_1 \tag{53a}$$

$$A^1_{12} = E^1_{11}\,hn\,\sin^2\theta_1\,\cos^2\theta_1 = A^1_{66} \tag{53b}$$

$$A^1_{16} = E^1_{11}\,hn\,\sin\theta_1\,\cos^3\theta_1 \tag{53c}$$

$$A^1_{22} = E^1_{11}\,hn\,\sin^4\theta_1 \tag{53d}$$

$$A^1_{26} = E^1_{11}\,hn\,\sin^3\theta_1\,\cos\theta_1 \tag{53e}$$

In addition, from eq. (39)

$$\varepsilon_{yy} = -(A_{22})^{-1}\,(A_{12}\,\varepsilon_{xx} + A_{26}\,\gamma_{xy}) \tag{54}$$

This equation is the basis for camber prediction.

With the aid of eq. (54), eqs. (52) may be reduced to two equations in terms of the two membrane strains ε_{xx} and γ_{xy}.

$$N_{xx} = K_{11}\,\varepsilon_{xx} + K_{12}\,\gamma_{xy} \tag{55a}$$

$$N_{xy} = K_{12}\,\varepsilon_{xx} + K_{22}\,\gamma_{xy} \tag{55b}$$

The membrane stiffnesses K_{ij} for uniaxial conditions are

$$K_{11} = A_{11} - (A_{12})^2 / A_{22} \tag{42}$$

$$K_{12} = A_{16} - A_{12}\,A_{26} / A_{22} \tag{56}$$

$$K_{22} = A_{66} - (A_{26})^2 / A_{22} \tag{57}$$

As the effects of smeared stiffeners are included in the A_{ij} stiffnesses, this is a generalization of the expressions used in refs. (5-7). These equations are, therefore, valid for a wide class of stiffened structures.

For uniform cover properties, there are two camber curvature kinematic parameters---k_{C5}, given by eq. (44), and k_{C4}. The latter is

$$k_{C4} = - A_{26} / A_{22} \tag{58}$$

Therefore, from eq. (31)

$$\kappa_c = (A_{26} / A_{22})\,\phi_{,x} - (A_{12} / A_{22})\,\beta_{y,x} \tag{59}$$

We also have the relationship

$$\gamma_{xy} = -\frac{H}{2}\,\phi_{,x} = (K_{22})^{-1}(-\,q - K_{12}\,\varepsilon_{xx}) \tag{60}$$

The shear flow in the closed box is q (positive counterclockwise). It seems more appropriate to work with shear flow than shear strain as it is within a definite range for transports. Therefore, with $\beta_{y,x}$ given by eq. (45)

$$\kappa_c = (2 / H)(\overline{C}_{12}\,\varepsilon + \overline{C}_{26}\,q / K_{22}) \tag{61}$$

The parameter $\overline{C}_{12}$ is an effective Poisson's ratio is given by

$$\overline{C}_{12} = \frac{A_{12}}{A_{22}} - \frac{A_{26}}{A_{22}}\frac{K_{12}}{K_{22}} \tag{62}$$

The parameter $\overline{C}_{26}$ characterizes the coupling between twist and camber. It is

$$\overline{C}_{26} = A_{26} / A_{22} \tag{63}$$

Consequently, in place of eq. (46) we have the relationship

$$\Delta c_\ell = G(\overline{C}_{12}\,\varepsilon + \overline{C}_{26}\,q / K_{22}) \tag{64}$$

This result permits the increment of section lift coefficient to be evaluated for these unbalanced configurations.

Results and Discussion

Twisting Method Design Study

A design analysis algorithm that is similar to that described for the bending method has been utilized to explore the camber-twist mechanism. In all of our studies, the shear flow q has been taken as 5000 lb./in. Material properties, as before, correspond to the AS4/3501-6 graphite-epoxy system (table 2). The essential differences in methodology consist of the use of eq. (64) to evaluate the increment in section lift coefficient and the following expression for the effective thickness of skin and stiffeners:

$$h' = h(1+n) \tag{65}$$

This equation accounts for the unbalanced stiffener configuration (fig. 20).

A sampling of design results are presented in figs. 21-27. Results appear in fig. 21 for $\overline{C}_{26}$, the parameter that directly measures the extent of twist-camber coupling, for an unstiffened design. An optimum fiber orientation for unidirectional material is found to be approximately 37 degrees. These results are put in perspective by information presented in figs. 22 and 23. Heavy stiffening corresponding to n = 1.5 has been assumed throughout for the stiffened configurations. These figures show that the maximum twist-camber coupling occurs for a fiber orientation of 30-45 degrees for the skin and a stiffener orientation of 24-34 degrees.

When all of the factors in eq. (64) are taken into account for the lift coefficient calculation, the situation is different. A weight related measure of the lift created is evaluated from the parameter $\left(\Delta c_\ell / h'\right)$. This parameter appears in figs. 24 and 25. Clearly the "best" stiffener orientation is zero degrees (spanwise) and the skin fiber orientation is between 30-45 degrees.

An absolute measure of lift per unit span, $\left(\Delta c_\ell / h'\right)$, appears in figs. 26 and 27. The stiffener orientation for maximum lift is zero degrees. The "best" fiber orientation for the skin is approximately 45 degrees. As reported earlier, the weight optimum design differs from the lift optimum design.

Optimal values for twisting method designs are presented in table 4. The absolute section lift coefficient increments achieved by this method are somewhat less than for the bending method. They are large enough to be of practical interest and the corresponding weights (thicknesses) are less. On the basis of the parameter $\left(\Delta c_\ell / h'\right)$ (inches^{-1}), the twisting method gives 0.295 in.$^{-1}$ and the bending method yields 0.299 in.$^{-1}$ for a weight optimal design. Therefore, on a relative basis, the two methods are competitive.

If absolute lift is important, the twisting method is more efficient. Twisting method designs and bending method designs correspond to entirely different configurations, however. There are, therefore, manufacturing factors which would enter into the decision of which method to adopt.

Concluding Remarks

The optimum lift parameters obtained from these designs are comparable to those found earlier for the bending method. It would appear, therefore, that the additional complexity of unbalanced designs should be avoided and the former mechanism utilized. This suggestion, however, pertains only to camber effects. Since spanwise bending-twist coupling is also present for the unbalanced designs, its influence must be accounted for in making an overall assessment.

EXPERIMENTAL EVALUATION OF TAILORED WING BOXES WITH ELASTICALLY PRODUCED CHORDWISE CAMBER

Introductory Remarks

In this section, some of the unique considerations that are associated with the experimental evaluation of chordwise deformable wing structures are addressed. Since chordwise elastic camber deformations are desired and must be free to develop, traditional experimental methodology cannot be used. An experimental methodology based upon the use of a flexible sling support and load application system has been created and utilized to evaluate a model box beam experimentally.

Experimental Methodology

Attention is restricted to the bending method of creating elastically produced chordwise camber deformation. This method produces an intentionally exaggerated form of anticlastic chordwise curvature, which is a natural response to spanwise bending. The key to successfully using this approach is to create large effective Poisson's ratios in the wing box covers while preserving the essential integrity of the box cross section.

The "best" test to perform in order to evaluate and validate camber production experimentally is a four-point bending test. This test method creates a gage section in the specimen that is exposed to a pure spanwise bending moment only, a simple state of loading that isolates the desired effect of anticlastic curvature. The challenge, of course, is to create a way of performing the test that utilizes methods of load application and support that permit chordwise camber deformations to occur freely.

Test Specimen Design

The box beam test specimen (fig. 28) has been designed with three factors in mind. First, due to the dimensions of our laminating press, the box covers are limited to a maximum length of twenty inches. The cover layup is taken to be [±26] in keeping with our optimized design without stiffeners (fig. 14). Second, to prevent the covers from buckling under the four point bending loading, a cover width of four inches and a thickness of twelve plies has been selected. This also is in concert with the third factor, which is to produce measurable strain levels.

To prevent the covers from buckling, it is necessary to predict the buckling load of the box beam covers. The bending stiffness of the beam was determined using the cross sectional geometry of the box and material properties of the laminate and aluminum channel. Two methods have been used to calculate the buckling load of the box covers and the results compare well with each other. The properties of AS4/3501-6 graphite-epoxy have been used in the design analysis for the covers (table 2).

The first method used was to derive the buckling equations for an orthotropic plate with two opposing edges fixed and two opposing edges simply supported opposing ends. A closed form solution for a buckling problem with these boundary conditions does not exist, so the commercially available numerical solution program "Theorist" (ref. 12) was used to solve for the determinant of the buckling equation. This solution yields a buckling load of 1,016 lbs, which in turn relates to a strain level of 1,565$\mu\varepsilon$. The second method used was to determine the ratio of buckling loads for a simply supported isotropic plate to that of a fixed-fixed, simply supported isotropic plate with the same aspect ratio. This factor was then used to determine the buckling load of the orthotropic fixed-fixed simply supported plate from that of a simply supported on all sides orthotropic plate. The resulting buckling load and strain level were determined to be 1,102 lbs. and 1,701 $\mu\varepsilon$, respectively. Thus, in view of the approximate nature of the second method, the results compare rather well.

Experimental Methodology

A number of possible approaches for performing the four-point bending tests were devised and thoroughly evaluated. With the help of Dr. Damodar Ambur of the NASA Langley Research Center, the "Sling Supported Method" was selected for implementation. Figure 29 illustrates this approach in schematic form. An attractive feature of this method is the fact that the entire assembly is placed in the hydraulic grips of our 75 kip MTS universal testing machine and pulled in tension. The flexible slings of nylon strap material are used to both support the test specimen and apply the four-point loading. This concept would seem to provide minimal resistance to the elastically produced camber deformations.

In addition to testing the wing box, a series of component and coupon tests and a detailed finite element analysis of the fixtures were performed. Measured property data on coupon tests were used for correlating the test results with theory in the second method of camber correlation, which is discussed subsequently.

All specimen response measurements were made with resistance strain gages. While displacement measurements would have been useful, the floating nature of the test setup makes them extremely inconvenient and potentially unreliable. A diagram showing the strain gage nomenclature and locations appears in fig. 30.

Results and Discussion

Basic Strain Gage Data

Strain gage data appear in figs. 31-33 as functions of applied bending moment. Figure 31 shows data from the chordwise strain gages. The zero reference line is provided because, in a theoretically perfect test, the top and bottom gage readings should be symmetrically located about this reference line.

Data from the two spanwise centrally located gages appear in fig. 32. Again the zero reference line is provided. Ideally, the two gages should read the opposite of each other.

Data from the two outer or remote spanwise gages mounted on the bottom surface are presented in fig. 33. These data were used, together with turnbuckle adjustments, to balance out the load application system with a small amount of preload applied. Theoretically, if the test conditions were ideal, the data from these two gages would be identical. This would correspond to perfect four-point bending conditions.

The above test results suggest that the objectives of the experiment were met, and the behavior reflected is as anticipated.

Of particular interest is the ability of the structure to produce global chordwise camber curvature. This capability was optimized for the box covers with the [±26] ply layup for AS4/3501-6 graphite-epoxy. Several basic relations are needed to interpret the measured data.

Elementary Mechanics Model

The first relationship involves the spanwise curvature and membrane strains in the box. Let "1" denote the spanwise direction and "2" the normal chordwise direction. If the usual Bernoulli-Euler assumption, which is valid under pure bending, is adopted, we can write

$$\kappa_{11} = \text{Spanwise Curvature} = \left(\varepsilon^{\ell}_{11} - \varepsilon^{u}_{11}\right)/(H+h) \tag{66}$$

where κ_{11} is the spanwise curvature, ε_{11} is the spanwise membrane extensional strain, H is the depth of the box, h is the cover thickness and the subscripts "ℓ" and "u" refer to the lower and upper covers of the box, respectively.

The second relation provides the elastic law relating spanwise curvature and bending moment. It is, in the notation of ref. 5,

$$\kappa_{11} = S_{55}\, M_y \tag{67}$$

The spanwise bending moment is M_y, and S_{55} is the spanwise bending compliance. It is related to the stiffness, C_{55}, as follows (ref. 5):

$$S_{55} = (C_{55})^{-1} \tag{68}$$

and

$$\begin{aligned} C_{55} &= \text{Spanwise Bending Stiffness} \\ &= 2C_s\, K_{11}\left(\frac{H}{2}\right)^2 + 2(EI)_c \end{aligned} \tag{69}$$

In eq. (69), C_s denotes the structural chord or width of the box, $(EI)_c$ is the bending stiffness of the aluminum closure channel (fig. 28) about a chordwise parallel axis, and K_{11} is the spanwise extensional stiffness of the box covers. For balanced cover configurations and uniaxial stress conditions

$$\varepsilon_{22} = -\left(A_{12} / A_{22}\right) \varepsilon_{11} \tag{40}$$

The ratio (A_{12}/A_{22}) is the effective Poisson's ratio for the laminated covers.

From classical Bernoulli-Euler bending theory

$$\kappa_{22} \equiv \kappa_c \text{ the Camber Curvature}$$

$$= \left(A_{12} / A_{22}\right) \kappa_{11} \tag{70a}$$

$$= \left(A_{12} / A_{22}\right) S_{55}\, M_y \tag{70b}$$

$$= \left(\varepsilon_{22}^{u} - \varepsilon_{22}^{\ell}\right) / (H+h) \qquad (70c)$$

Equation (70c) is analogous to eq. (66), and ε_{22} is the chordwise extensional membrane strain. Consequently, we define the camber bending compliance such that

$$\kappa_c = S_{c5} M_y \qquad (71)$$

and the camber compliance is

$$S_{c5} = (A_{12} / A_{22}) S_{55} \qquad (72)$$

Camber Correlation

The most desirable way to correlate theory and experiment is to use measured properties on the actual test specimen itself in the theoretical calculations. This is because there is batch-to-batch variation in composite materials themselves and some amount of variation from part-to-part due to processing. This is normal for composite structures and is accounted for by using the allowable properties used in structural design and analysis. Our purposes here, however, are to evaluate (1) actual versus theoretical elastic camber production, (2) the suitability of the test methodology, and (3) the validity of the model that has been created for use in design analysis. With these objectives in mind, our correlation study proceeded in a direct manner along two paths.

The first path or method is based upon using the experimentally determined spanwise bending compliance as the wing box cover primary load-bearing elastic characteristic. This compliance is readily determined from the plot of experimental data shown in fig. 34. This figure is based upon the use of eqs. (66) and (67). The measured spanwise bending compliance, S_{55}, together with the theoretical value of the effective Poisson's ratio of 1.26 and eq. (72) permits an estimate of the camber compliance to be calculated. This value is compared with the experimentally determined one obtained from fig. 35 in table 5. The "experimental" value is based upon eqs. (70c) and (71).

While the agreement reflected in table 5 is excellent, another way of interpreting this information is that (A_{12}/A_{22}) can be found experimentally from measured compliances (figs. 34, 35) and eq. (72). This yields an effective Poisson's ratio of 1.27, which is in good agreement with the value assumed in the design analysis (1.26).

The second method presumes that the box specimen is imperfect. Both the chordwise and spanwise strain gage data taken during the four point bending test (figs. 31, 32) suggest that a small mean spanwise strain is present. The test was repeated with the specimen position reversed with respect to sling support and loading system. The results were identical to the first test indicating that the specimen and not the test setup was responsible for the lack of symmetry of the data about the reference lines.

In keeping with our approach of using measured properties on the actual test specimen in the theoretical calculations for evaluating the adequacy of our model, a second type of test was conducted on the box specimen. T he ends of the box were machined to be flat and parallel, and a compression test was conducted with the box flat-ended between the testing machine platens. Strain gage data were taken as a function of applied compressive load. These data permitted the extensional stiffness K_{11} and the equivalent imperfection of the specimen to be evaluated.

Our imperfect model of the specimen presumes that (unwanted) bending-extension coupling is present in the box specimen. This coupling is due to manufacturing irregularities in the box such as differences in the covers or lack of parallelism of the closure channels. As a consequence, there

is a mean extensional strain $\bar{\varepsilon}_{11}$ present in the four point bending test. This mean strain is evaluated as

$$\bar{\varepsilon}_{11} = (\varepsilon^u_{11} + \varepsilon^\ell_{11})/2 \tag{73}$$

With the bending-extension coupling present, we have the equations

$$\bar{\varepsilon}_{11} = S_{11}\, N + S_{15}\, M \tag{74a}$$

$$\kappa_{11} = S_{15}\, N + S_{55}\, M \tag{74b}$$

In the four point bending test, the axial force N is zero. Consequently, from eq. (74a)

$$\bar{\varepsilon}_{11} = S_{15}\, M \tag{75}$$

A plot of this equation is given in fig. 36. The bending-extension coupling compliance S_{15}, therefore, is determined from this figure. Note that this compliance is a small negative value (-0.079 in-lbs^{-1}).

In the flat-ended compression test, the box specimen experiences an applied compressive force N_o and an unknown bending moment. This bending moment corresponds to the compressive load N_o being applied at a distance e from the central geometric axis. This situation is described by the equations

$$\bar{\varepsilon}_{11} = -(S_{11} + e\, S_{15})\, N_o \tag{76a}$$

$$\kappa_{11} = -(S_{15} + e\, S_{55})\, N_o \tag{76b}$$

Figures 37 and 38 contain plots of these equations obtained from compression test data. With S_{55} and S_{15} previously determined from the bending test, these figures permit the extensional compliance S_{11} and the load eccentricity e to be evaluated. The results are: $S_{11} = 0.161 \times 10^{-6}\,(\text{lb})^{-1}$ and e = 0.023 in.

From elementary rule of mixtures considerations, we write

$$C_{11} = 2C_s\, \bar{K}_{11} + 2\,(EA)_c \tag{77}$$

The mean cover stiffness is $\bar{K}_{11}$ and $(EA)_c$ is the extensional stiffness of the closure channels. By analogy with the parameter β, we introduce the coupling parameter γ defined such that

$$\gamma = (S_{15})^2 / S_{11}\, S_{55} = (C_{15})^2 / C_{11}\, C_{55} \tag{78}$$

The magnitude of this parameter is a convenient measure of the unwanted bending - extension coupling. It has the value 0.046 for the box specimen, thus indicating only a small degree of imperfection. The inverse of eqs. (74) is

$$N = C_{11}\, \bar{\varepsilon}_{11} + C_{15}\, \kappa_{11} \tag{79a}$$

$$M = C_{15}\, \bar{\varepsilon}_{11} + C_{55}\, \kappa_{11} \tag{79b}$$

where

$$C_{11} = [S_{11}(1-\gamma)]^{-1} \tag{80a}$$

$$C_{15} = -\gamma / S_{15}(1-\gamma) \tag{80b}$$

$$C_{55} = [S_{55}](1-\gamma)^{-1} \tag{80c}$$

The mean cover stiffness $\overline{K}_{11}$ is determined with the aid of eqs. (77) and (80a). The bending stiffness C_{55} is found from eqs. (80c) and (69).

The correlation of theory and experiment by this second method requires that the coupling parameter γ and the measured mean cover stiffness $\overline{K}_{11}$ (0.521×10^6 lb.) be used in the theoretical calculations. If this is done, the correlation of spanwise bending compliance predictions and experimentally determined values can be made. The results appear in table 6. A similar correlation for chordwise camber compliance is given in table 7. These comparisons show excellent agreement between our model predictions and the experiments.

Concluding Remarks

In this section, we have addressed the unique considerations that are associated with the experimental evaluation of chordwise deformable wing structures. Since chordwise elastic camber deformations are desired and must be free to develop, traditional experimental methodology cannot be used. An experimental methodology based upon the use of a flexible sling support and load application system has been created and utilized to evaluate a model box beam experimentally.

Experimental data correlates extremely well with design analysis predictions based upon a beam-like model for the global properties of camber compliance and spanwise bending compliance. Local strain measurements exhibit trends in agreement with intuition but which depart slightly from theoretical perfection in terms of upper and lower cover asymmetry. This behavior has been explained by accounting for unwanted bending-extension coupling present in the box specimen, which was quantitatively evaluated by performing an additional compression test and appropriately analyzing the data.

Overall, a solid basis for the design of box structures based upon the bending method of elastic camber production has been confirmed by the experiments.

Since the agreement between finite element simulations and the beam-like predictions is excellent and the correlation with experiments is very good here, we consider that the design of high aspect chordwise deformable wings by utilizing the bending method of producing camber is on firm ground.

CONCLUSIONS AND RECOMMENDATIONS

Structural models and design analysis methodology have been created for composite primary aircraft structures that are appropriate for the preliminary or conceptual phase of design. Emphasis has been given to high aspect ratio wings and the potential of aeroelastic tailoring to enhance lift production. This research focuses upon understanding, modeling, tailoring mechanisms and creating design concepts that accentuate individual behavioral characteristics. As the roles of wing bending and twisting deformations are rather well understood, attention has been directed to elastically produced chordwise camber. A scientific understanding of behavior and design

concepts which accentuate camber producing deformations are presented and applied to a generic transport wing.

Modeling has been validated by extensive finite element simulation (Appendix C) and by selected experiments on a model box beam specimen. All of the results confirm the validity of the thin-walled composite beam model of Rehfield (refs. 5-7) as it has been extended herein to predict in-plane warping displacements. Consequently, we believe that the modeling and design analysis methodology that has been created can be applied with a high degree of confidence to high aspect ratio wing structures without significant discontinuities.

Summary of Accomplishments

While earlier work by others clearly showed the potential of elastic tailoring, primarily in the context of low aspect ratio plate-like lifting surfaces and the X-29 Technology Demonstrator, it remained to establish a firm grasp of the cause-effect relationships between configuration and response, to clearly identify the parameters which control the tailoring process, and to establish a rational design methodology for future applications. A synopsis of the original contributions of the research follows. The contributions logically fall into two natural categories---"modeling, design analysis, and structural concepts" and "experimental methodology development."

Modeling, Design Analysis and Structural Concepts

- Created modeling technology for thin-walled composite beam structures which includes all essential nonclassical effects and chordwise deformation modes.
- Isolated and identified distinct elastic coupling mechanisms and the parameters which influence them to establish a basis for design and understanding.
- Created a technology for elastically producing camber in wings, applied it to transport wings and demonstrated significant lift enhancement.
- Developed structural concepts for chordwise deformable wing ribs (Appendix D).
- Demonstrated the efficiency and effectiveness of grid stiffened configurations for elastic tailoring applications.
- Created two-dimensional aerodynamic modeling approaches for steady flow around chordwise deformable airfoils (Appendix A).
- Discovered distinct "weight" and "lift" optimum designs.
- Created and applied new section models for wing box structures (Appendix B) and a "typical section" model for aeroelastic studies (Appendix F).
- Correlated mechanics model predictions with extensive finite element simulations (Appendix C).
- Performed an exploratory static aeroelastic instability study for chordwise deformable wings (Appendix E).

Experimental Methodology Development

- Developed an experimental methodology for bending testing of chordwise deformable box structures, applied it to a model box beam, and correlated the experimental results with theoretical predictions.

An entire area of research and application --- chordwise deformable wings --- has been defined and developed. A foundation of appropriate models, structural design methodology and design concepts have been created and presented which offer new options for future aircraft. It appears that lift enhancements of sufficient magnitude can be produced to render this type of wing tailoring of practical interest, and the basic understanding and design analysis methodology now exist to explore the potential of these ideas.

Recommendations for Future Work

This project, in our opinion, has been very successful. Our bending-related camber producing concept has been thoroughly evaluated by design analysis, extensive finite element simulation and carefully designed experiments. It is ready for a "real world" evaluation.

Below is a list of tasks that we believe should be completed to carry us toward the ultimate goal of an Advanced Technology Wing.

- Understand the interaction of wing elastic camber, twist and bending;
- Understand the interaction of wing sweep and elastically tailored deformation modes, camber in particular,
- Create technology for "smart" adaptive control to be used in conjunction with elastic tailoring;
- Study performance-related advantages of advanced technology wings;
- Understand the aeroelasticity of advanced technology wings;
- Understand, design and predict damage/failure processes in unbalanced laminated composite structures;
- Develop material selection criteria for elastic tailoring applications;
- Understand and predict residual processing effects in elastically tailored configurations; and
- Create scaling laws for subscale models.

ACKNOWLEDGMENTS

This research was sponsored by the NASA Langley Research Center under Advanced Composites Technology Program Contract NAS1-18754. This support is gratefully acknowledged. A particular debt is owed to Dr. Damodar R. Ambur, the NASA Project Engineer, for his help with the development of the experimental methodology and his wise counsel. In addition, we thank Dr. T. J. Petersen of the Boeing Commercial Airplane Group for supplying us with the composite material, which was Fortafil 3(c)/8601 graphite-epoxy unidirectional tape.

Other contributors to this research include: Michael W. Holl, who assisted with the design analysis and finite element analysis; Richard D. Pickings, who performed the finite element correlation study; Michael L. Fentress, who collaborated on the experimental phase of the program; Jonathan Lee, who helped with the development of the models; and Debbie Fowler and Tatiana Fallis, who typed the manuscript. The authors gratefully acknowledge the significant contributions made by these individuals.

We also acknowledge Drs. Damodar R. Ambur and James H. Starnes, Jr. for reading the manuscript and giving us constructive suggestions.

REFERENCES

1. Shirk, M.H., Hertz, T.J. and Weisshaar, T.A., "A Survey of Aeroelastic Tailoring-Theory, Practice, Promise," Journal of Aircraft, Vol. 23, No. 1, January 1986, pp. 6-18.

2. Rehfield, L.W., Chang, S., Pickings, R.D., Zischka, P.J. and Holl, M.W., "Tailored Composite Wings With Elastically Produced Chordwise Camber," NASA Conference Publication 3104, Part 2, 1991, pp. 1037-1047.

3. Rehfield, L.W., Chang, S., Zischka, P.J., Pickings, R.D. and Holl, M.W., "Tailoring of Composite Wing Structures for Elastically Produced Camber Deformations," AIAA Paper No. 91-1186, Proceedings of the 32nd AIAA Structures, Structural Dynamics and Materials Conference, April 8-10, 1991, Baltimore, MD, Part 3, pp. 2123-2127.

4. Rogers, W.A., Braymen, W.W. and Shirk, M.H., "Design, Analysis, and Model Tests of an Aeroelastically Tailored Lifting Surface," AIAA Paper No. 81-1673, AIAA Aircraft Systems and Technology Conference, August 11-13, 1981, Dayton, OH.

5. Rehfield, L.W., "Design Analysis Methodology for Composite Rotor Blades," Proceedings of the Seventh DoD/NASA Conference on Fibrous Composites in Structural Design, AFWAL-TR-85-3094, June 1985, pp. (V(a)-1)-(V(a)-15).

6. Rehfield, L.W., Hodges, D.H., and Atilgan, A.R., "Nonclassical Behavior of Thin-Walled Beams with Closed Cross Sections, Journal of the American Helicopter Society, Vol. 35, No. 2, April 1990, pp. 42-50.

7. Rehfield, L.W. and Atilgan, A.R., "Toward Understanding the Tailoring Mechanisms for Thin-Walled Composites Tubular Beams," Proceedings of the First USSR-US Symposium on Mechanics of Composite Materials, 23-25 May 1989, Riga, Latvia, USSR, ASME, pp. 187-196.

8. Love, A.E.H., A Treatise on the Mathematical Theory of Elasticity, Fourth Edition, Dover Publications, New York, 1944, Chapter XV, pp. 329-348.

9. Valisetty, R.R., Murthy, P.L.N. and Rehfield, L.W., "An Ideal Clamping Analysis for a Cross-Ply Laminate," Journal of Composite Materials, Vol. 22, No. 2, February 1988, pp. 136-153.

10. Hodges, R.V., Nixon, M.W. and Rehfield, L.W., "Comparison of Composite Rotor Blade Models: Beam Analysis and an MSC Nastran Shell Element Model," NASA Technical Memorandum 89024, January 1987.

11. Anonymous, Eureka: The Solver, Owner's Handbook, Borland International, Inc., Scotts Valley, California, 1987.

12. Anonymous, Theorist Reference Manual, Second Printing, Prescience Corp., San Francisco, California, 1991.

Property	Rotor Blade	ITB Model
Extensional Stiffness, C_{11} (lb)	0.8332×10^6	Matched
Spanwise Bending Stiffness, C_{55} (lb-in^2)	0.1337×10^5	Matched
Torsional Stiffness, C_{44} (lb-in^2)	0.9747×10^4	Matched
Effective Chordwise Bending Stiffness, $(C_{66})_{EFF}$ (lb-in^2)	0.0806×10^6	Matched
Chordwise Transverse Shear Stiffness, C_{22} (lb)	0.1651×10^6	0.1519×10^6
Extension-Twist Coupling Stiffness , C_{14} (lb-in)	-0.6294×10^5	-0.6309×10^5
Bending-Transverse Shear Coupling Stiffness, C_{25} (lb-in)	0.3147×10^5	0.3153×10^5

TABLE 1. - COMPARISON OF IDEAL TAILORED BOX MODEL TO ACTUAL LANGLEY ROTOR BLADE

FIBER DIRECTION TENSION MODULUS, E_{11} (MSI)	20.0
TRANSVERSE DIRECTION, TENSION MODULUS, E_{22} (MSI)	1.7
IN-PLANE SHEAR MODULUS, G_{12} (MSI)	0.85
POISSON'S RATIO, ν_{12}	0.30

TABLE 2. - NOMINAL UNIDIRECTIONAL MECHANICAL PROPERTIES FOR AS4/3501-6 GRAPHITE - EPOXY (ROOM TEMPERATURE, DRY)

	ΔC_t	h' (IN.)
LIFT OPTIMUM	0.138	0.610
WEIGHT OPTIMUM	0.117	0.391
BENCHMARK	0.035	0.353

TABLE 3. - OPTIMUM VALUES - BENDING METHOD (n = 1.5)

	ΔC_t	h' (IN.)
LIFT OPTIMUM	0.125	0.429
WEIGHT OPTIMUM	0.109	0.369
BENCHMARK	0.035	0.353

TABLE 4. - OPTIMUM VALUES - TWISTING METHOD (n = 1.5)

	ANALYSIS	EXPERIMENT
CAMBER COMPLIANCE	1.075	1.080
$(LB\text{-}IN^2)^{-1} \times 10^6$		
PERCENT DIFFERENCE	----	0.5

TABLE 5. - CAMBER CORRELATION-METHOD 1

	ANALYSIS	EXPERIMENT
SPANWISE BENDING	0.82	0.85
COMPLIANCE		
$(LB\text{-}IN^2)^{-1} \times 10^6$		
PERCENT DIFFERENCE	----	3.7

TABLE 6. - SPANWISE BENDING CORRELATION-METHOD 2

	ANALYSIS	EXPERIMENT
CAMBER COMPLIANCE $(LB\text{-}IN^2)^{-1} \times 10^6$	1.03	1.08
PERCENT DIFFERENCE	----	4.9

TABLE 7. - CAMBER CORRELATION-METHOD 3

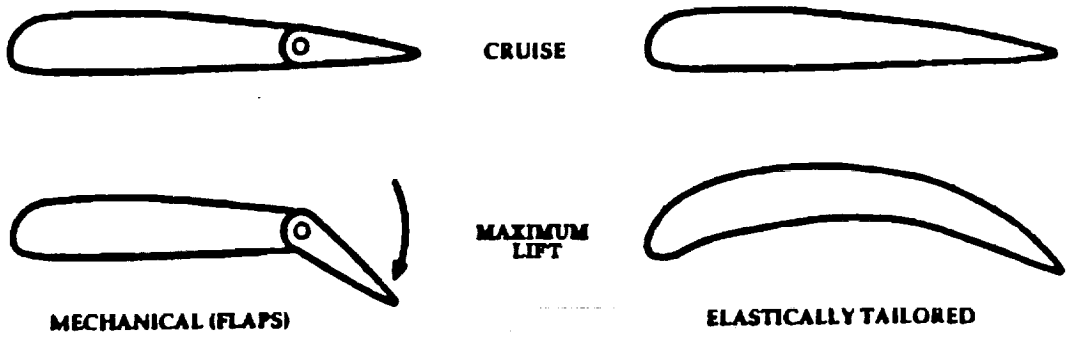

FIGURE 1. - METHODS OF INCREASING AIRFOIL LIFT

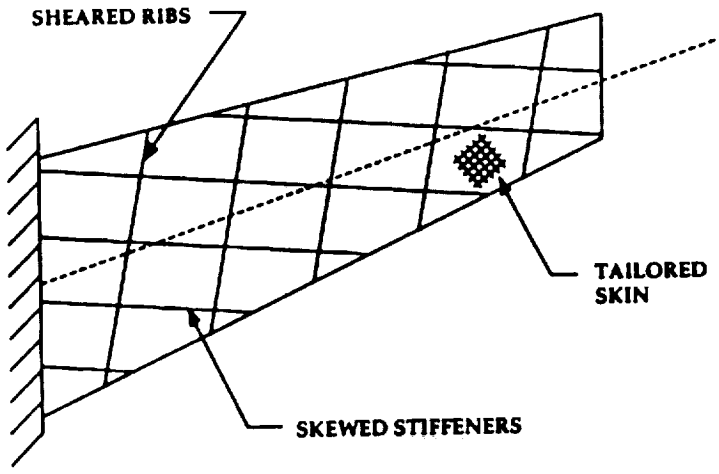

FIGURE 2. - METHODS FOR PRODUCING ELASTIC COUPLING IN HIGH ASPECT RATIO WINGS

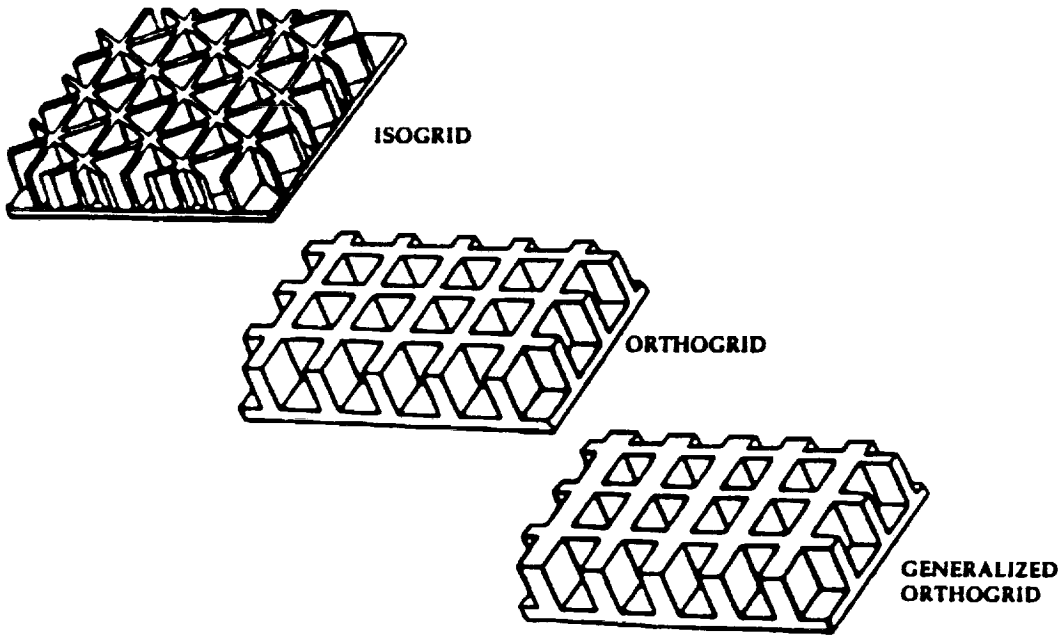

FIGURE 3. - GRID CONFIGURATIONS

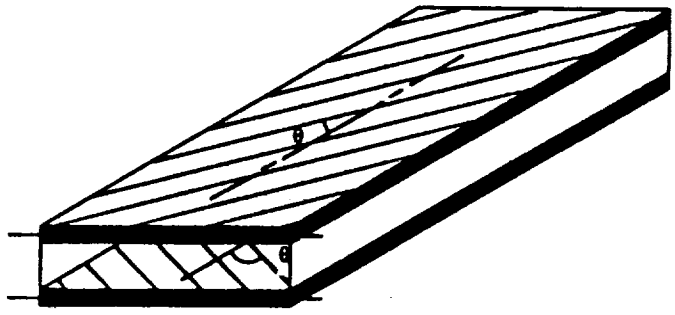

FIGURE 4. - PLY ORIENTATION FOR CIRCUMFERENTIALLY UNIFORM STIFFNESS

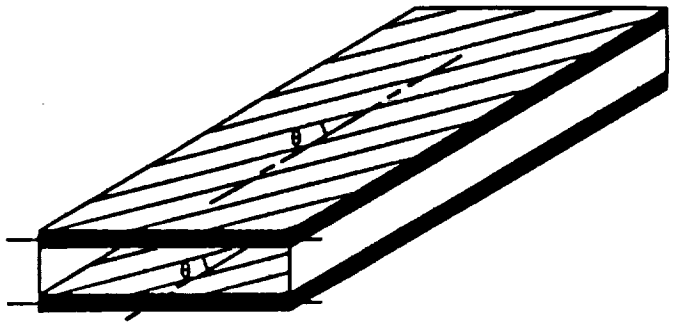

FIGURE 5. - PLY ORIENTATION FOR CIRCUMFERENTIALLY ASYMMETRICAL STIFFNESS

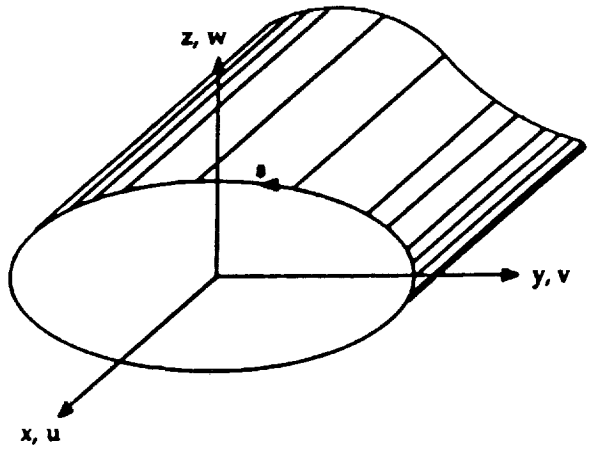

FIGURE 6. - CLOSED CELL THIN WALL BEAM MODEL

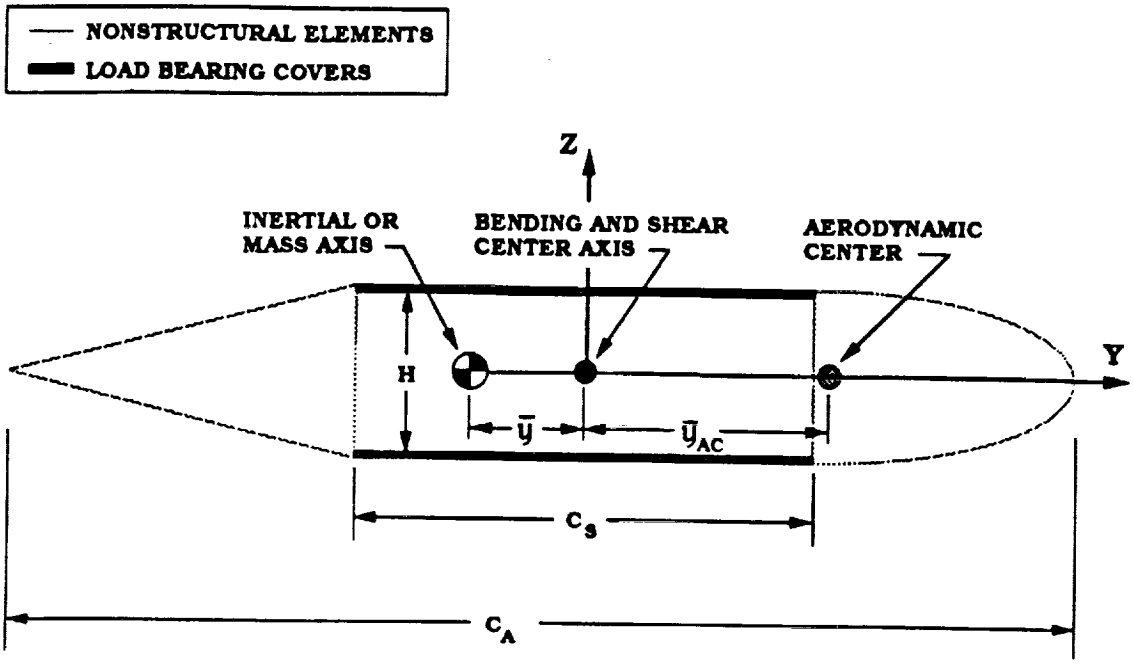

FIGURE 7. - IDEAL TAILORED BOX MODEL

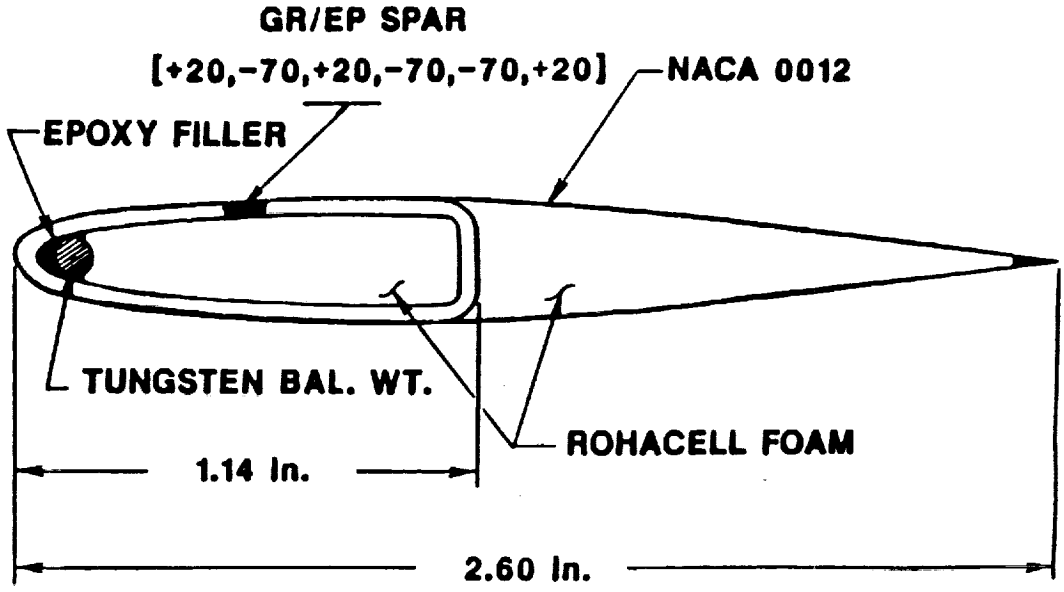

FIGURE 8. - LANGLEY ROTOR BLADE

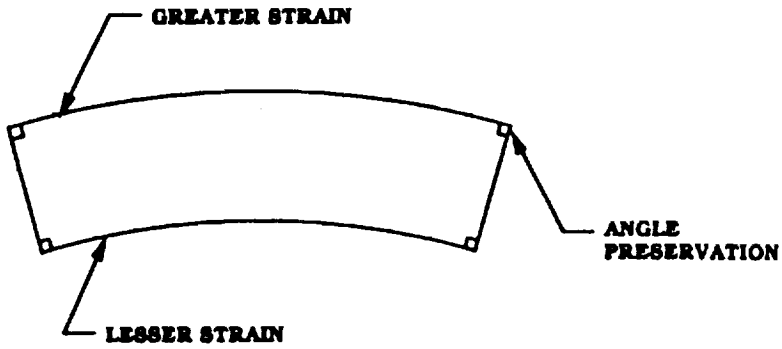

FIGURE 9. - FUNDAMENTAL CAMBER PRINCIPLE
(ANTICLASTIC CURVATURE OF CROSS SECTION)

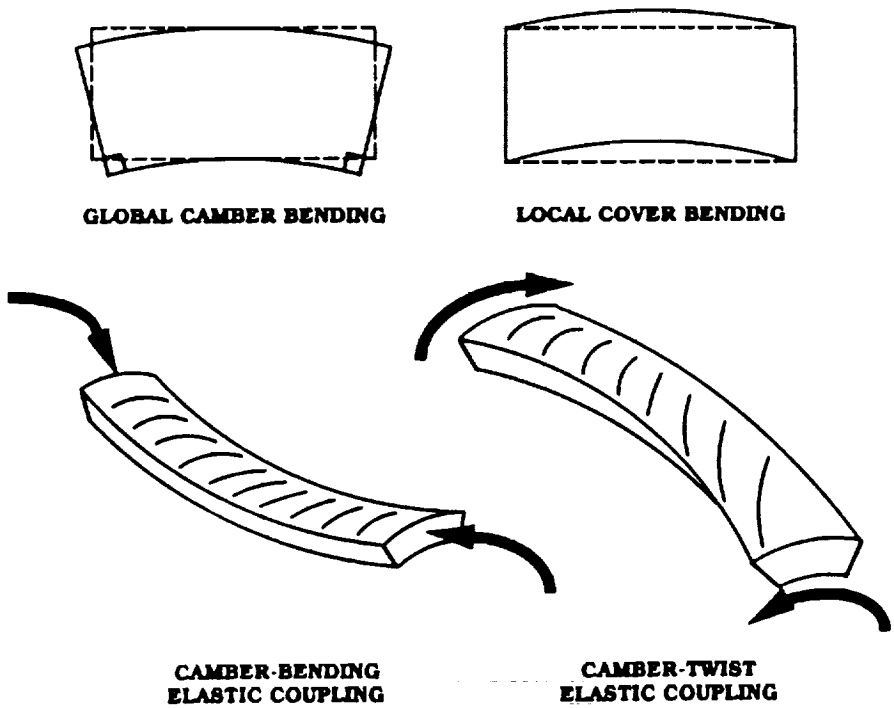

FIGURE 10. - CAMBER-RELATED DEFORMATION MECHANISMS

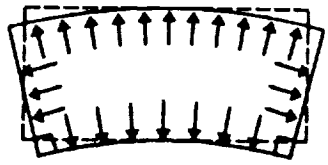

DIFFERENTIAL CHORDWISE COVER STRAIN
BY INTERNAL PRESSURE

DIFFERENTIAL CHORDWISE COVER STRAIN
BY THERMAL EXPANSION

FIGURE 11. - SECONDARY CAMBER MECHANISMS

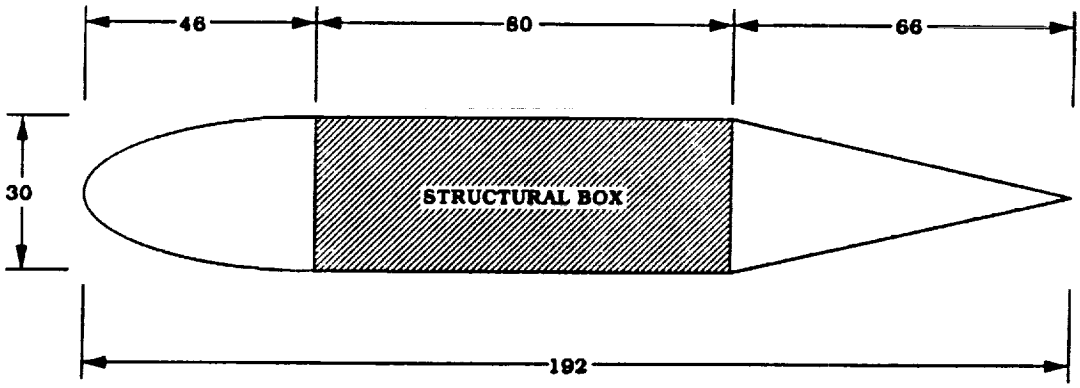

FIGURE 12.- C-130 CENTER WING BOX MODEL
(UNITS ARE INCHES)

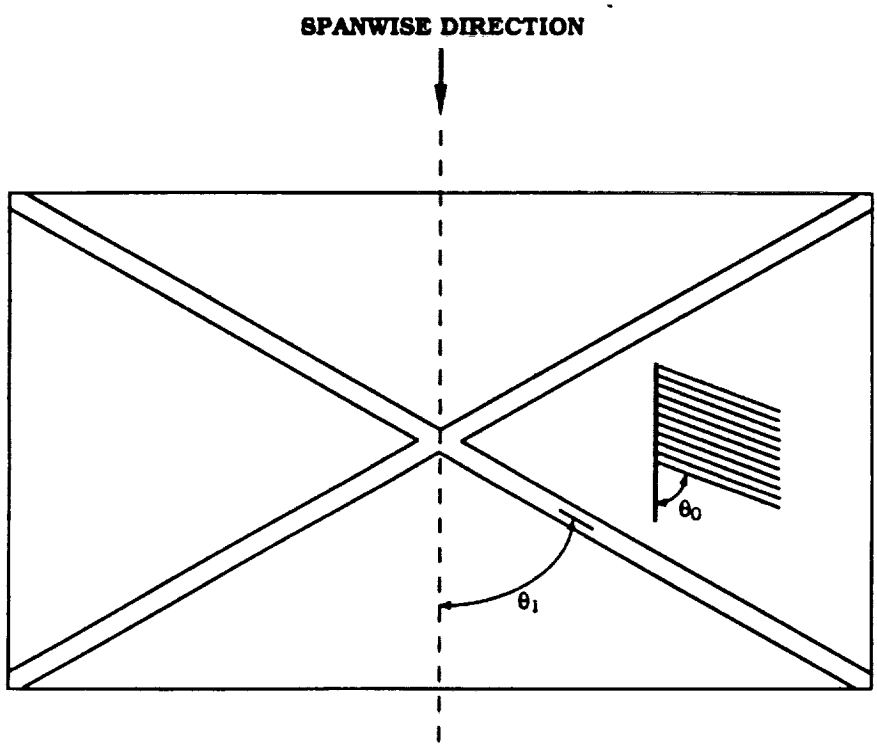

FIGURE 13. - BALANCED SKIN AND STIFFENER PATTERN

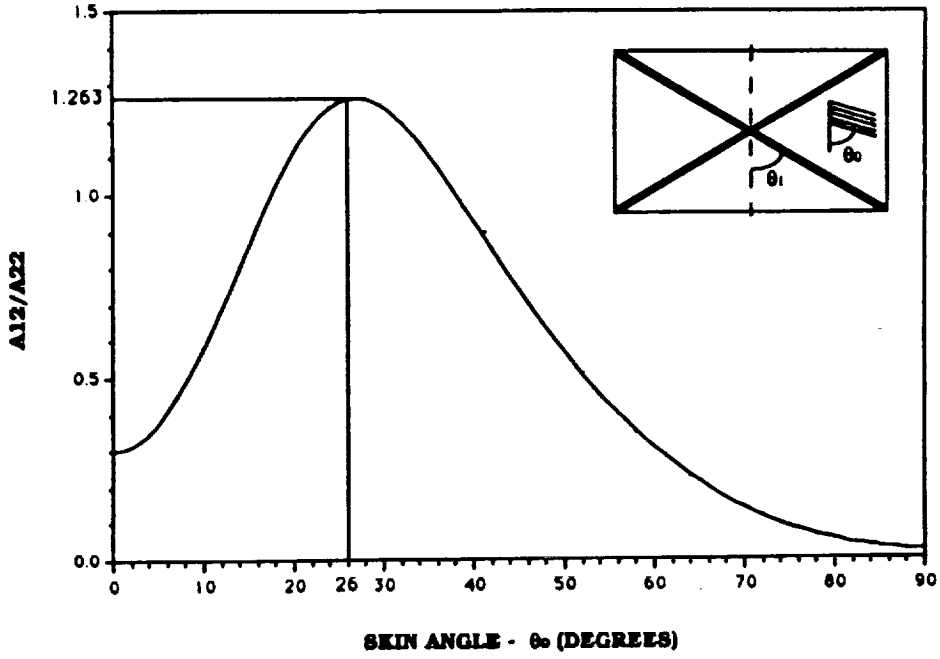

FIGURE 14. - EFFECTIVE POISSON RATIO - SKIN ONLY

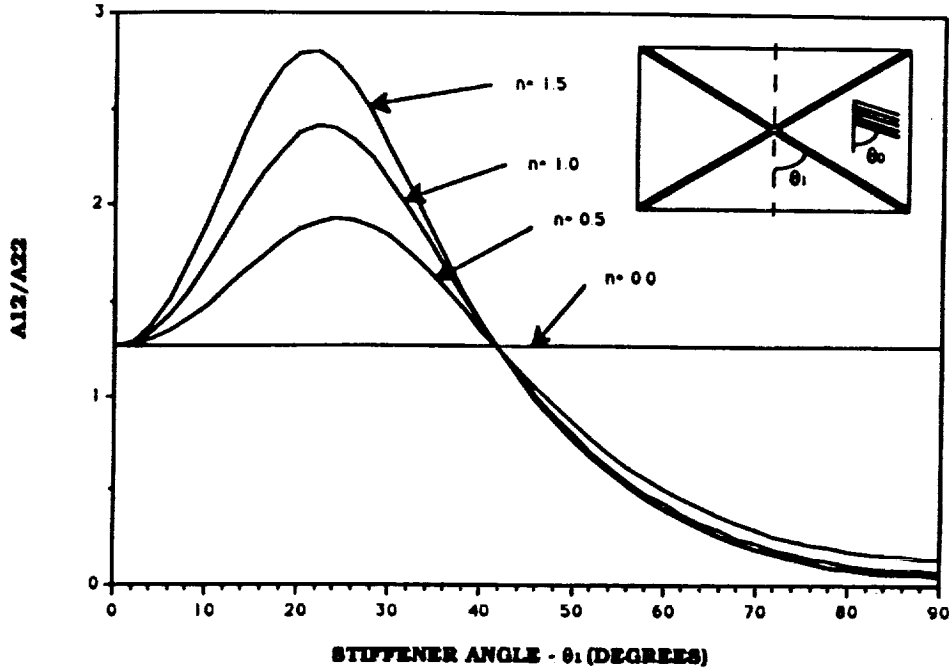

FIGURE 15. - EFFECTIVE POISSON RATIO - STIFFENED SKIN FOR θ_o = 26 DEGREES

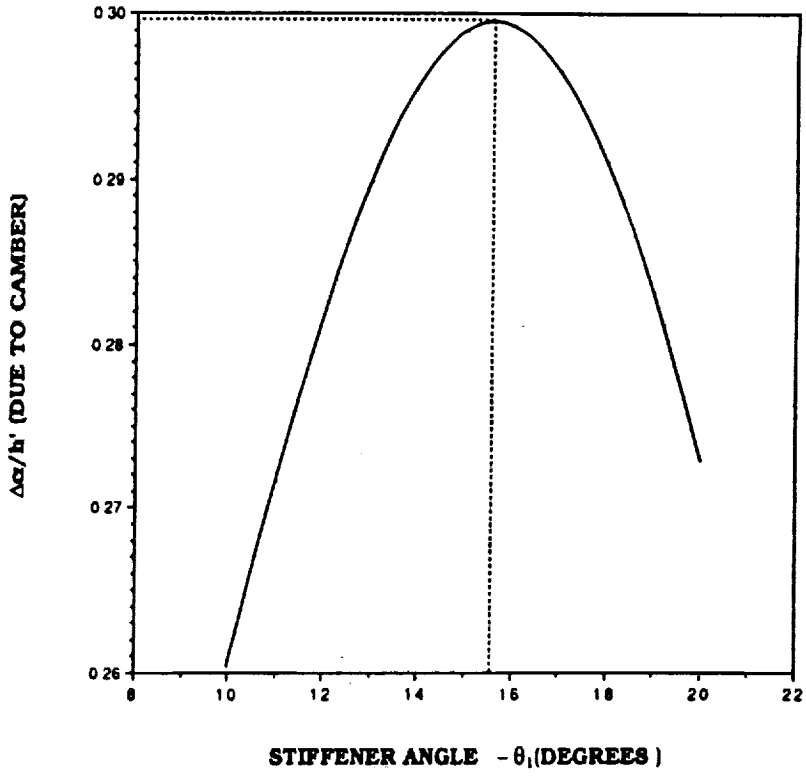

FIGURE 16.- WEIGHT OPTIMUM DESIGN - θ_o=12.6 DEGREES, n=1.5

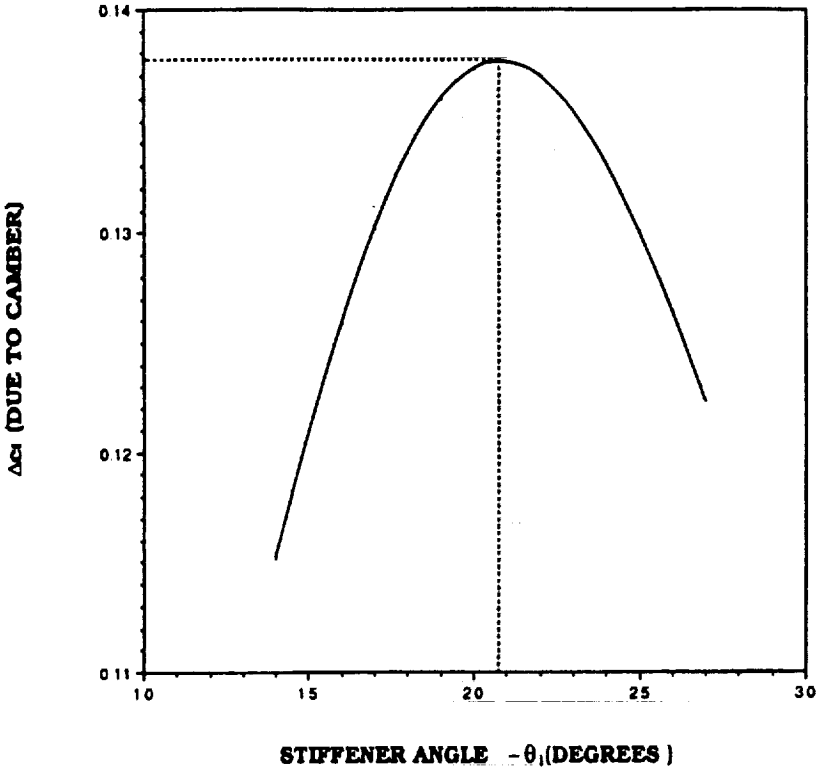

FIGURE 17.- LIFT OPTIMUM DESIGN - θ_0=18.9 DEGREES, n=1.5

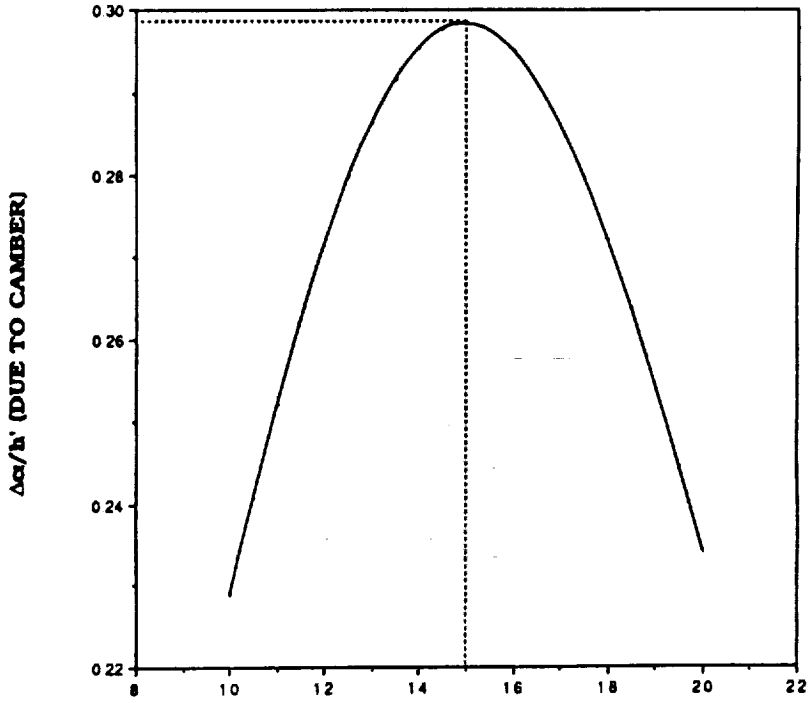

FIGURE 18.- EQUAL ANGLE WEIGHT OPTIMUM DESIGN - n=1.5

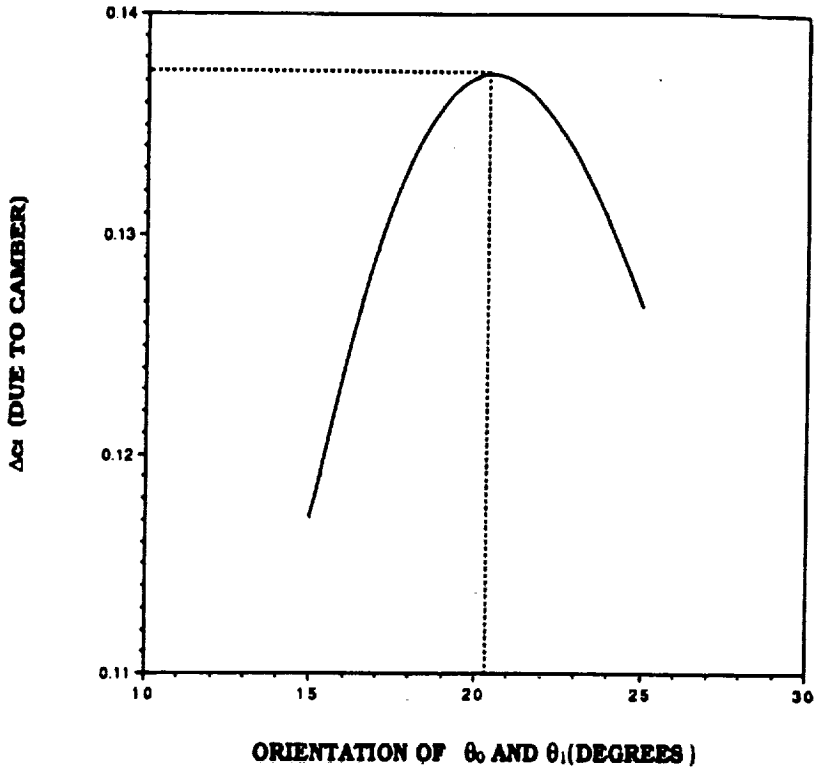

FIGURE 19.- EQUAL ANGLE LIFT OPTIMUM DESIGN - n=1.5

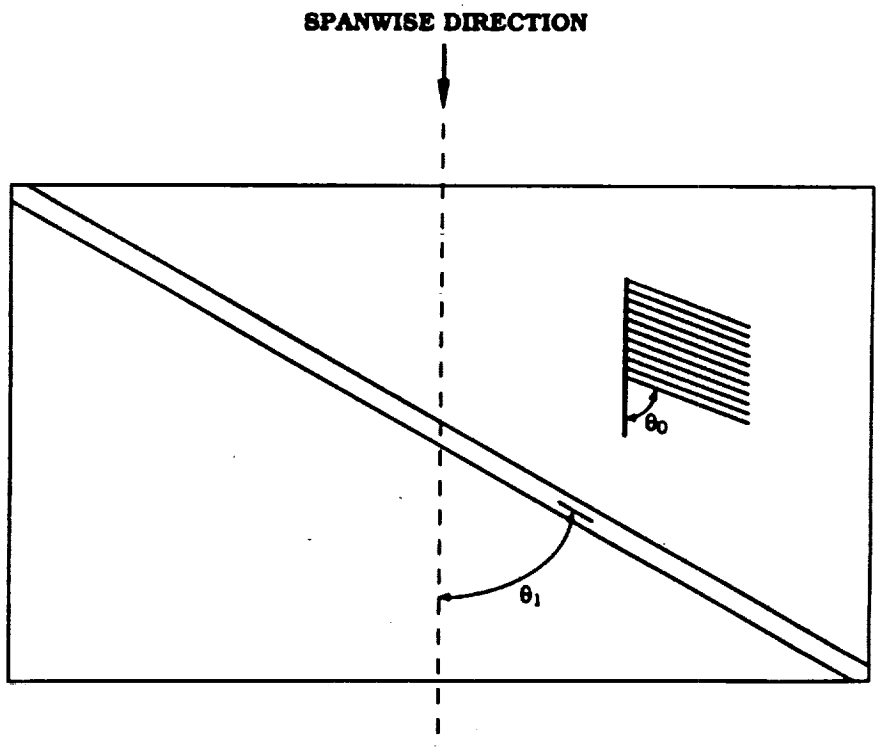

FIGURE 20. - UNBALANCED SKIN AND STIFFENER PATTERN

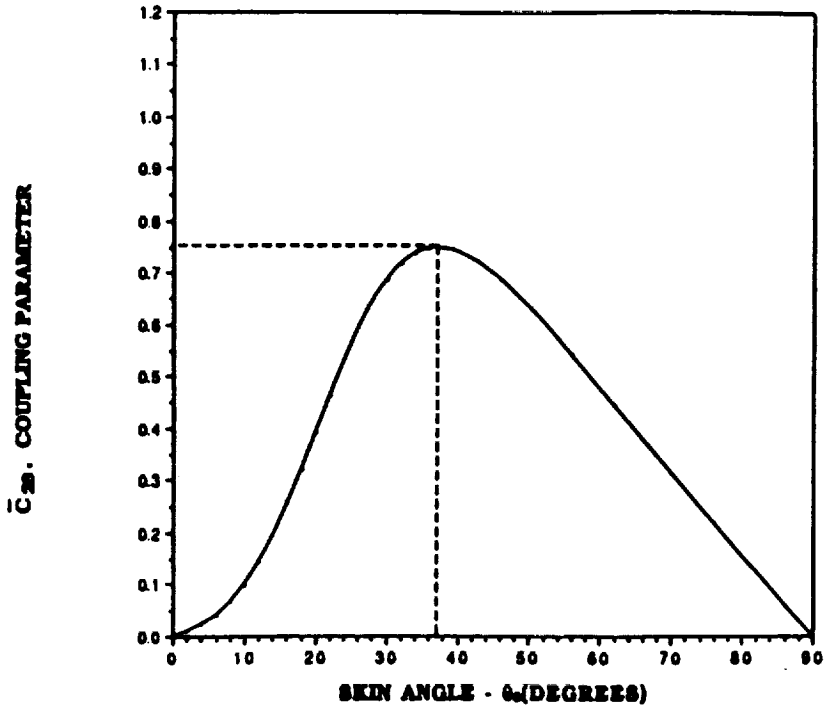

FIGURE 21. - COUPLING PARAMETER - SKIN ONLY

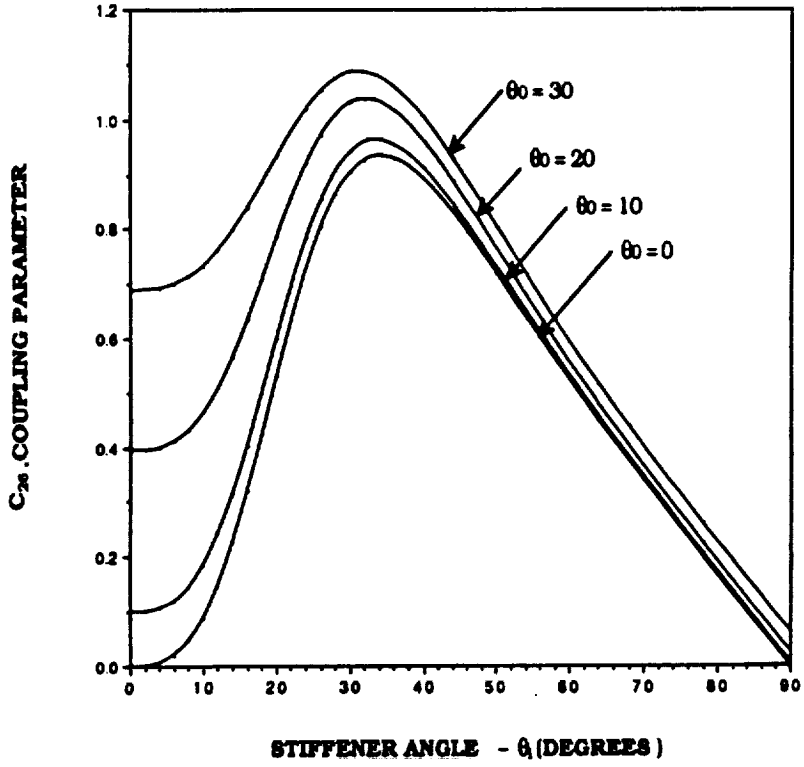

FIGURE 22.- COUPLING PARAMETER (n=1.5)

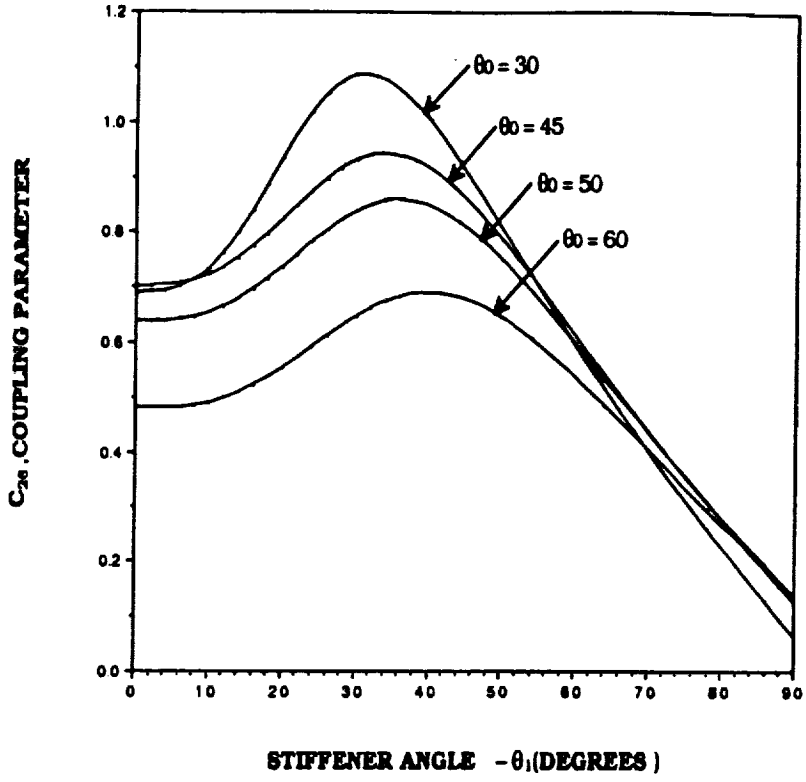

FIGURE 23.- COUPLING PARAMETER (n=1.5)

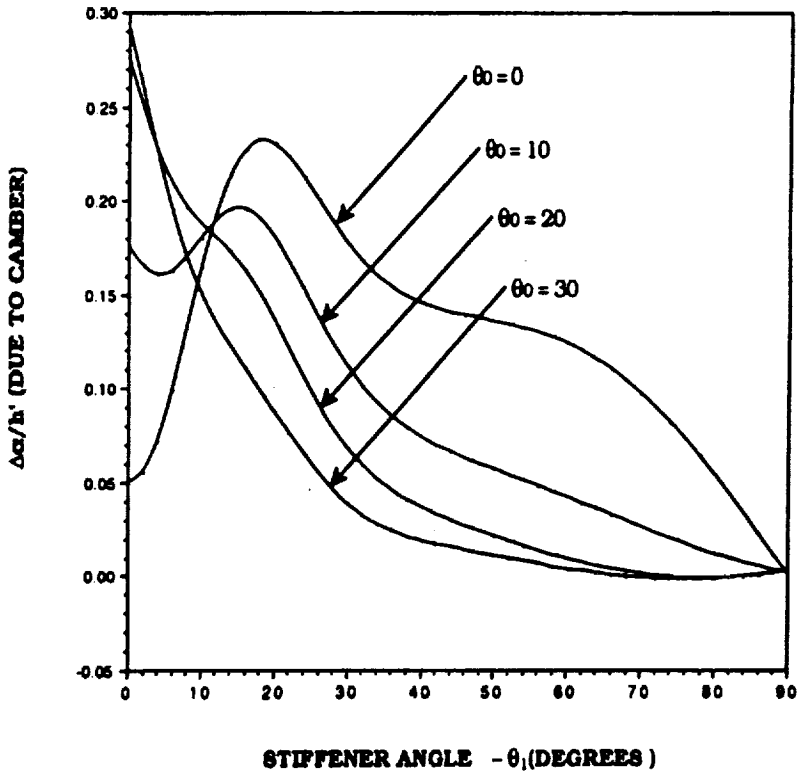

FIGURE 24.- WEIGHT OPTIMUM DESIGN (n=1.5)

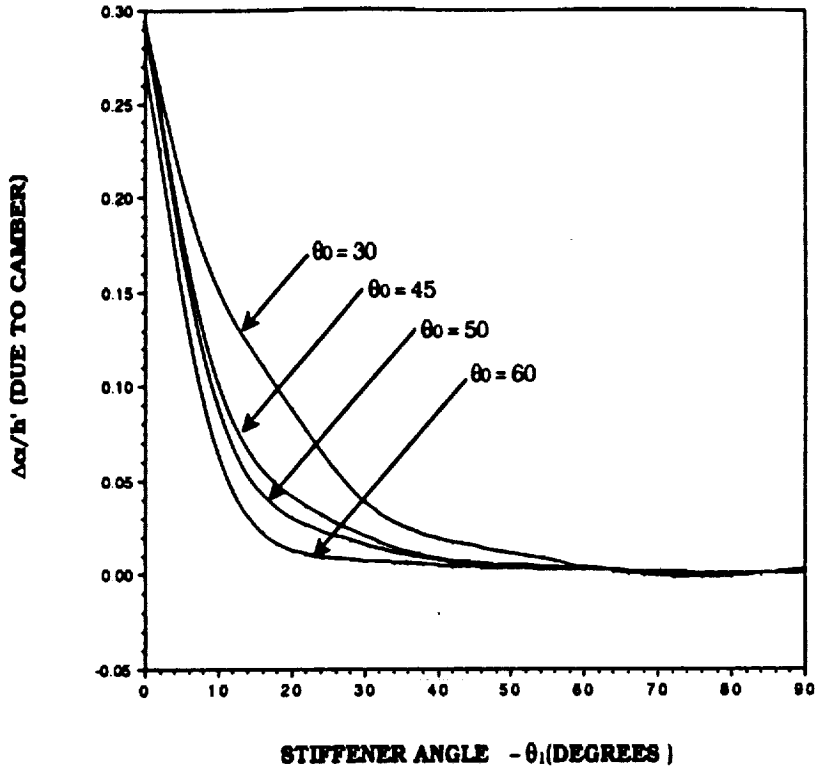

FIGURE 25.- WEIGHT OPTIMUM DESIGN (n=1.5)

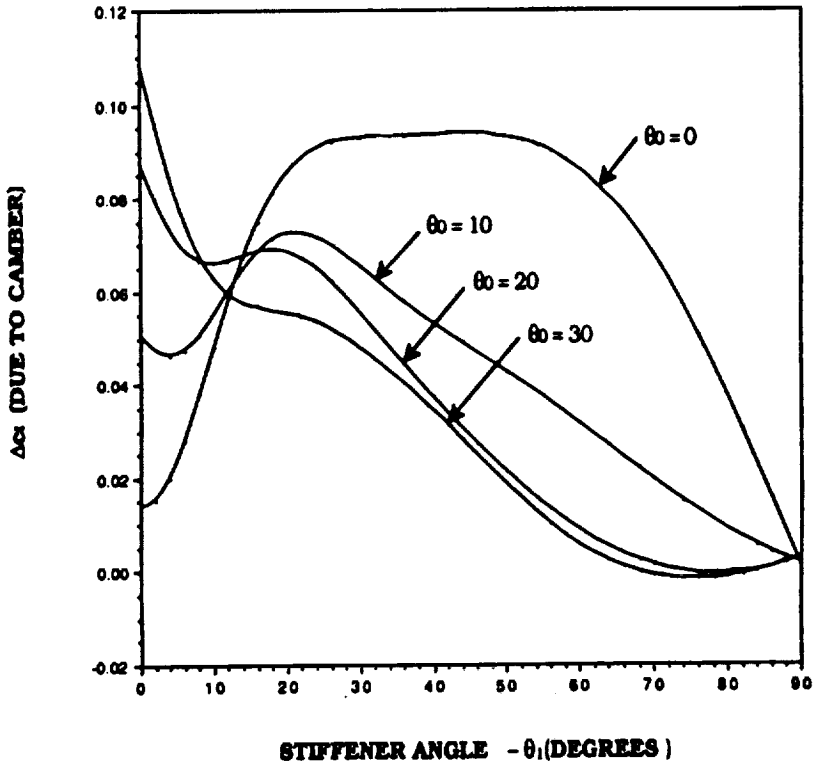

FIGURE 26. - LIFT OPTIMUM DESIGN (n=1.5)

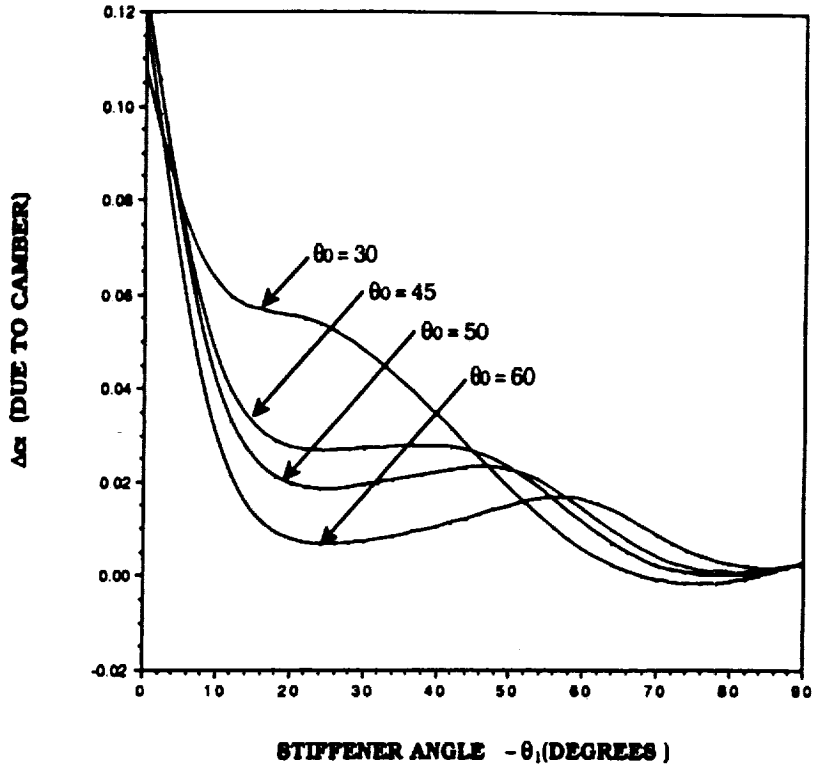

FIGURE 27. - LIFT OPTIMUM DESIGN (n=1.5)

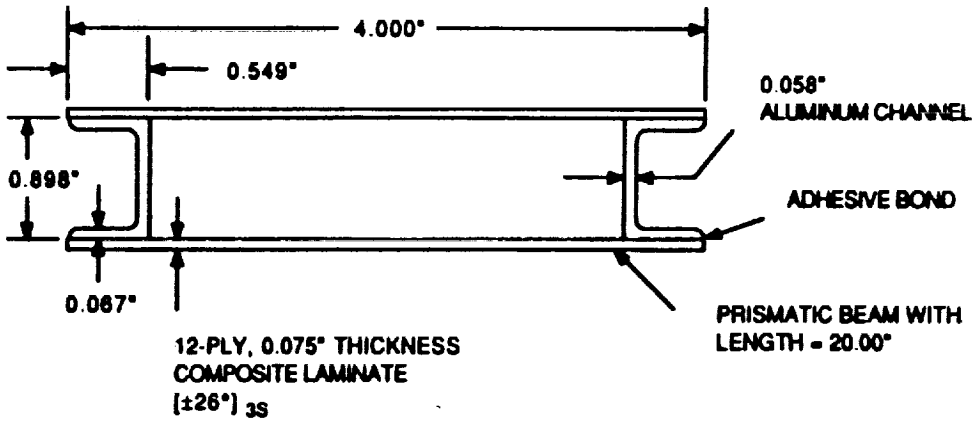

FIGURE 28. - BOX BEAM TEST SPECIMEN

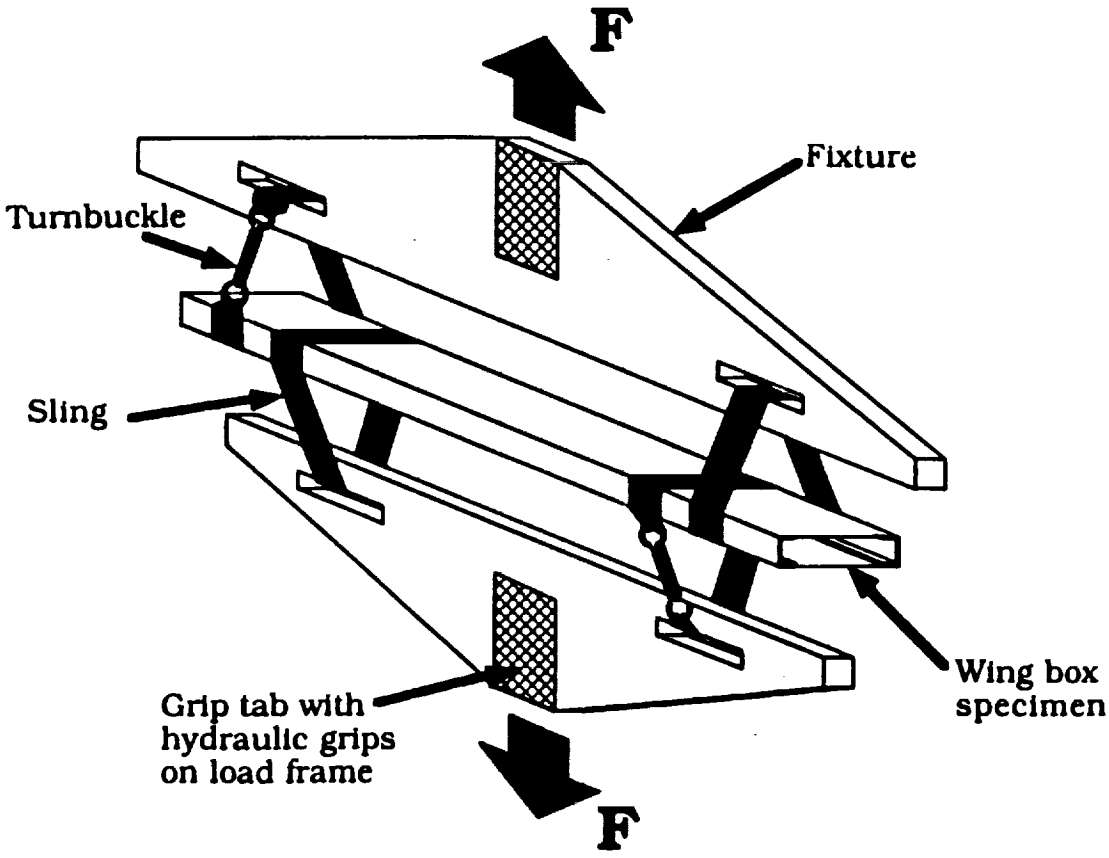

FIGURE 29. - OVERALL TEST CONFIGURATION

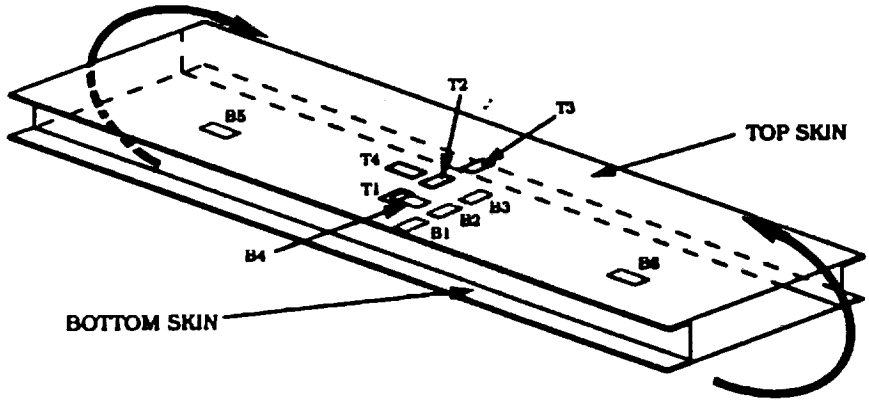

FIGURE 30. - STRAIN GAGE NOMENCLATURE AND LOCATIONS ON BOX BEAM

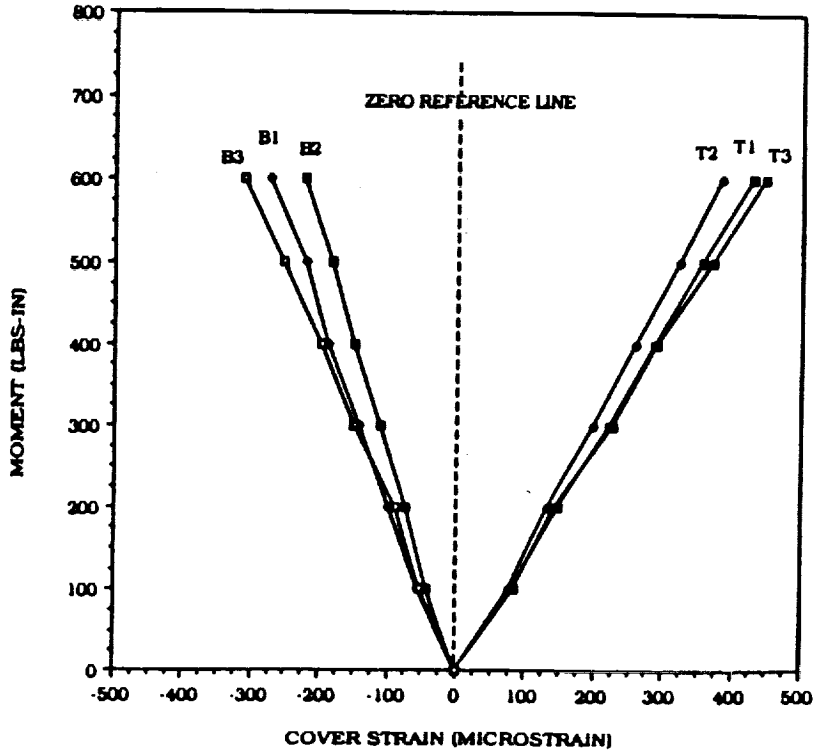

FIGURE 31. - BENDING MOMENT VS CHORDWISE GAGE STRAIN

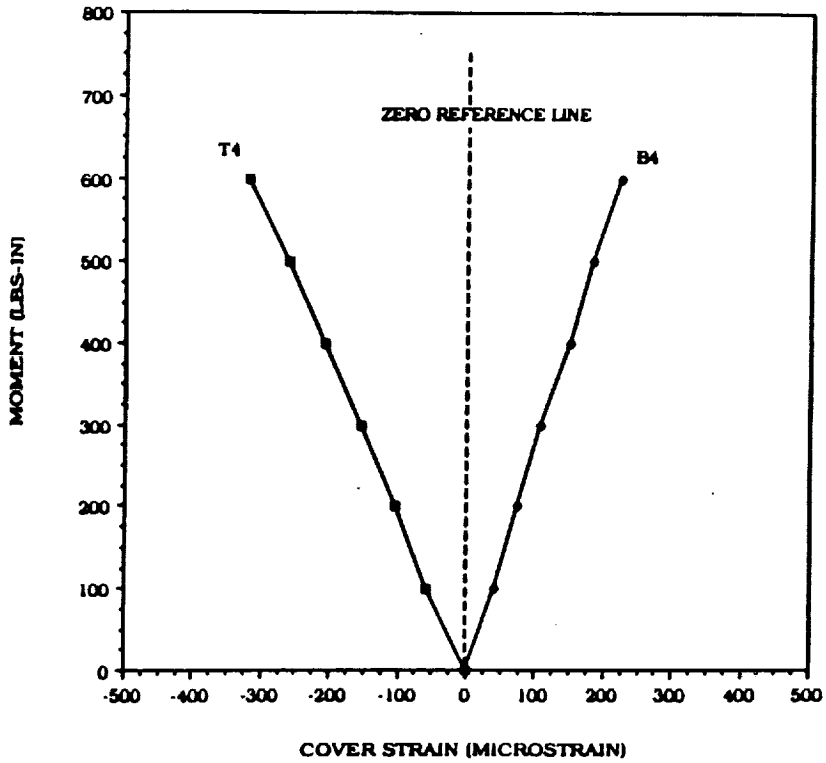

FIGURE 32. - BENDING MOMENT VS SPANWISE GAGE STRAIN

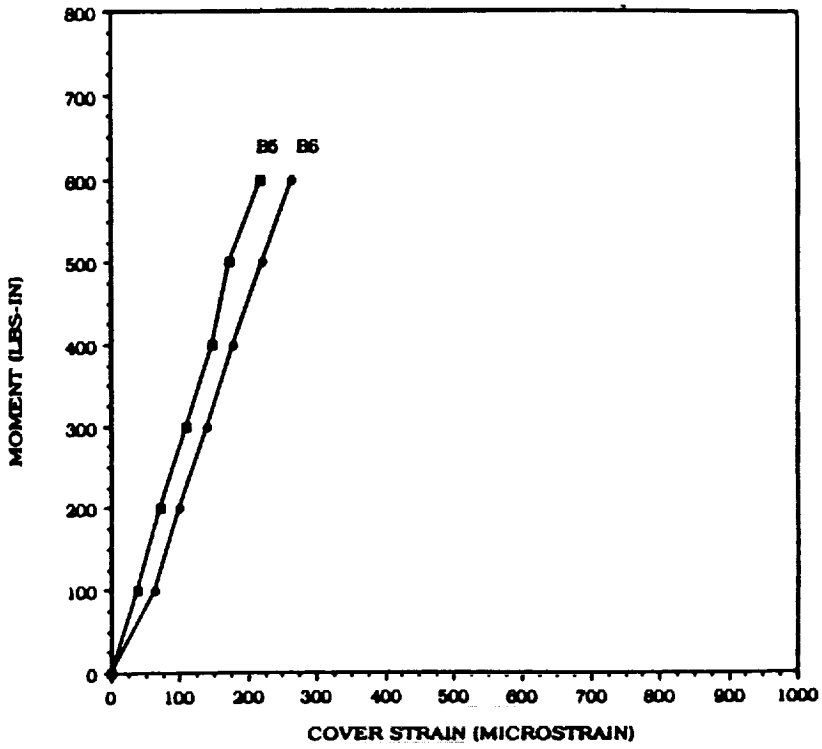

FIGURE 33. - BENDING MOMENT VS OUTER SPANWISE GAGE STRAIN

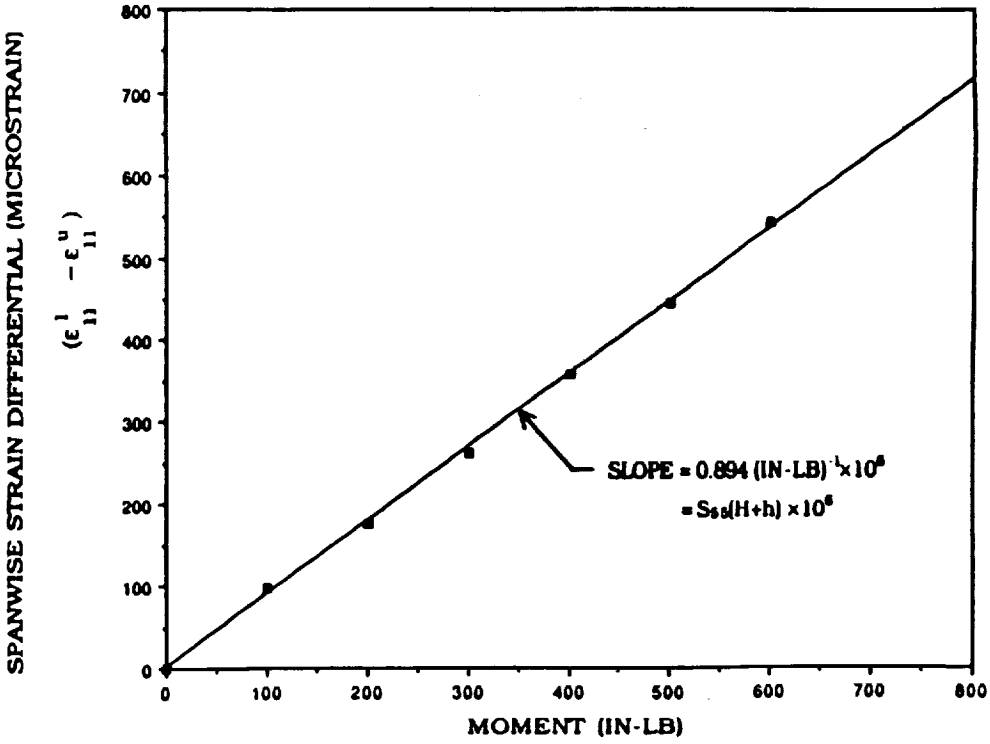

FIGURE 34. - SPANWISE STRAIN DIFFERENTIAL VS. APPLIED MOMENT

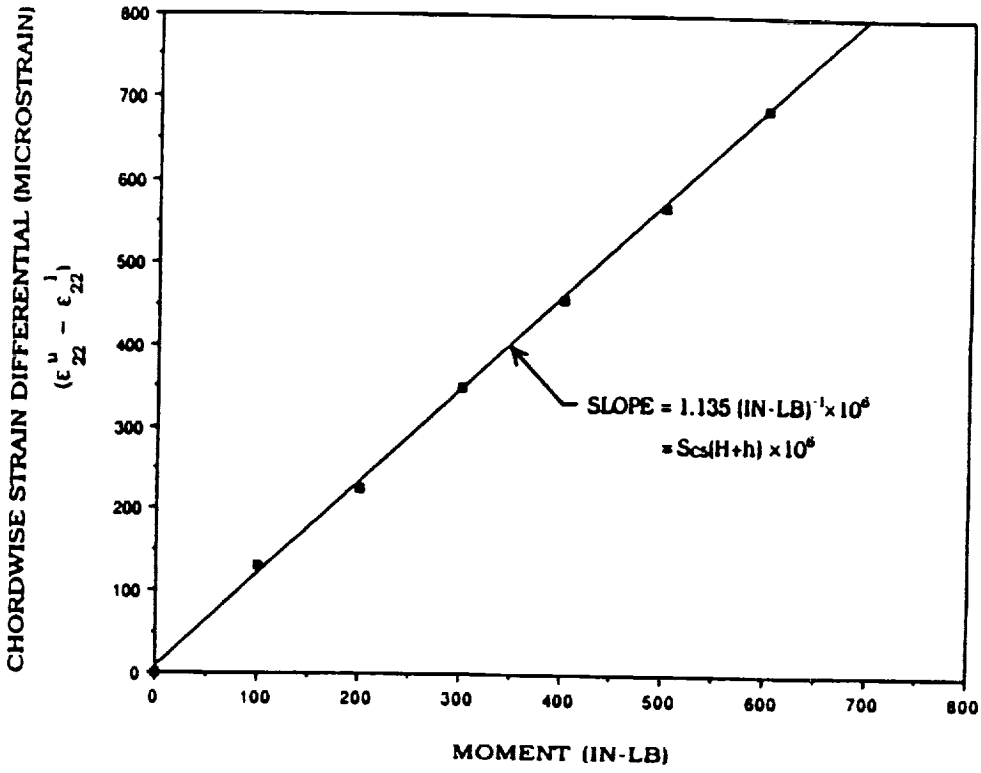

FIGURE 35. - CHORDWISE STRAIN DIFFERENTIAL VS. APPLIED MOMENT

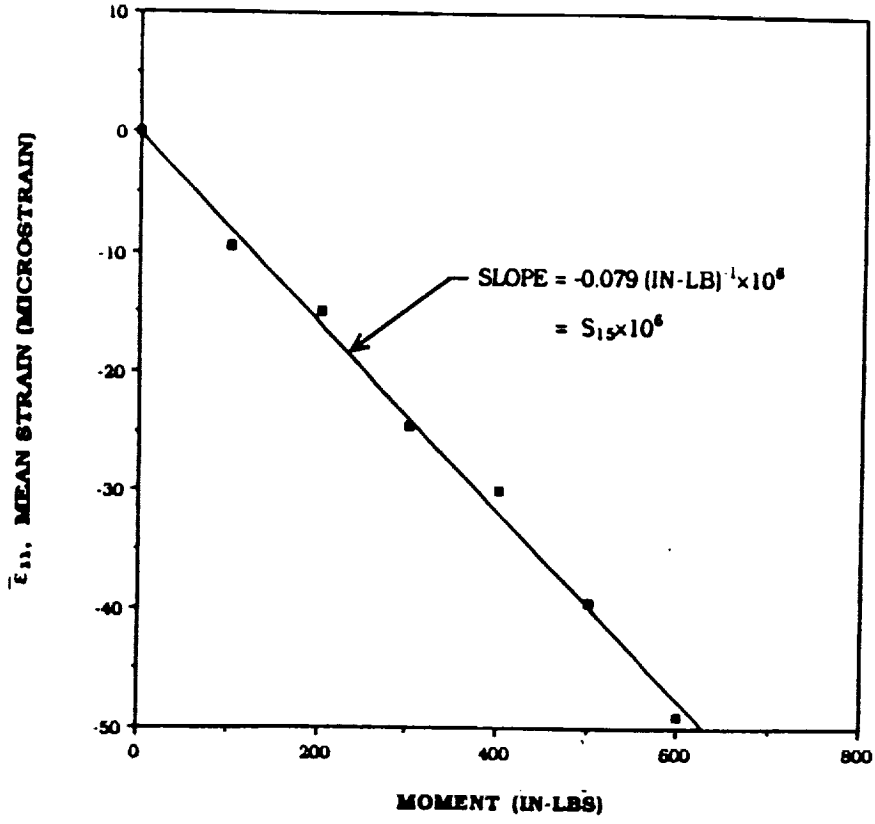

FIGURE 36. - AVERAGE STRAIN VS. BENDING MOMENT - BENDING TEST

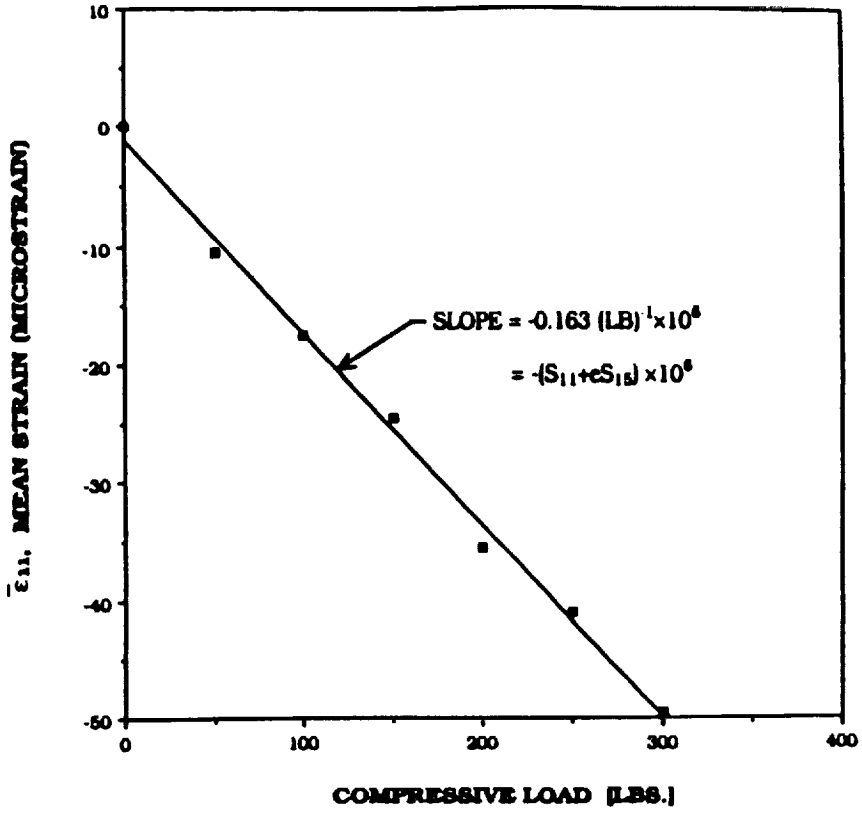

FIGURE 37. - AVERAGE STRAIN VS. COMPRESSIVE LOAD - COMPRESSION TEST

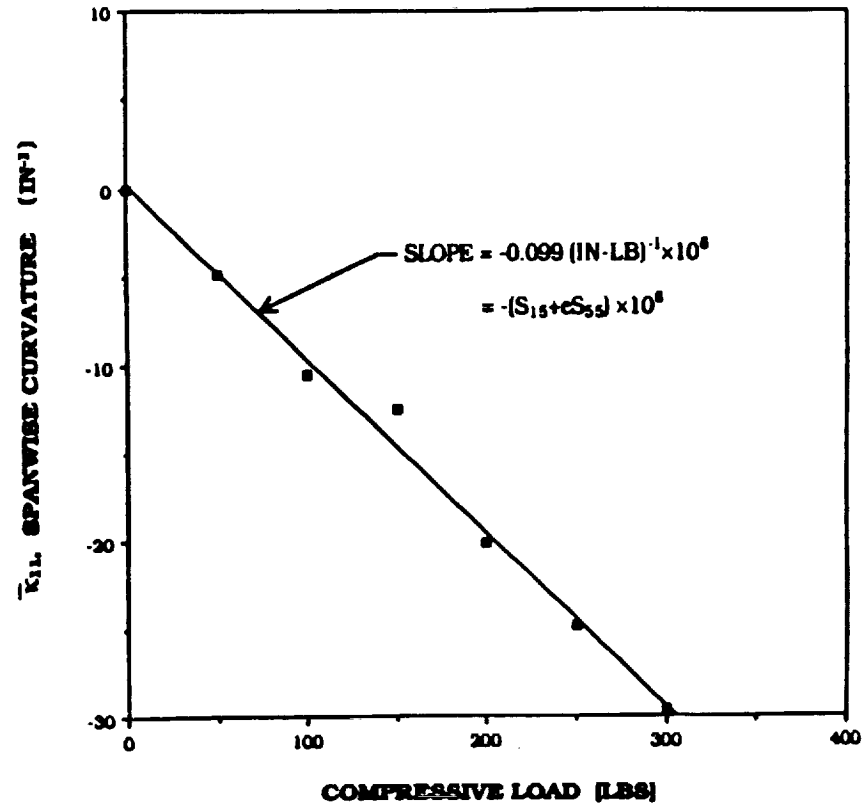

FIGURE 38. - CURVATURE VS. COMPRESSIVE LOAD - COMPRESSION TEST

APPENDIX A

AERODYNAMICS OF WINGS WITH ELASTICALLY PRODUCED CAMBER

A wing can be divided into finite airfoil sections. These sections are commonly categorized by three aerodynamic quantities: nondimensional lift, pitching moment, and drag. Symbolically they are c_ℓ, c_m, and c_d. Thin airfoil theory is used in this study to calculate aerodynamic coefficients. One assumption of thin airfoil theory is that the flow is inviscid, therefore c_d is not calculated. It is the viscosity of the fluid that produces skin friction drag and three-dimensional flow patterns that are responsible for lift induced drag.

For a given value of α the corresponding lift per unit span is given by

$$L = c_\ell \, (1/2) \, \rho_\infty \, (V_\infty)^2 \, C_A \qquad \text{(A-1)}$$

This equation shows that lift is directly proportional to velocity squared. For the safety of passengers and aircraft, it is desirable to have as small a V_∞ during take-off and landing as is possible. This means design an airfoil with a large $C_{\ell,max}$. The maximum nondimensional lift coefficient is influenced by both the thickness distribution along the airfoil and the curvature of the mean camber line. For an aircraft designed to cruise at speeds close to Mach one, a thick airfoil section and large curvature lead to unacceptably high drag.

Another aerodynamic quantity that is of interest is the nondimensional pitching moment, c_m. This is used to quantify the amount of pitching moment an airfoil section produces. It is common to record this value at the quarter chord location of an airfoil, $c_{m,c_A/4}$.

Thin Airfoil Theory

Thin airfoil theory is used in this study because it allows for an understanding of the problem through a closed form solution which yields reliable results (refs. A-1 and A-2). This method of analysis models an airfoil as a streamline of the surrounding flow by the use of a vortex sheet placed along the airfoil's chord line. The vortex sheet has a variable strength represented by γ. Once the distribution in γ along the vortex sheet is determined, the lift and pitching moment of the airfoil can be calculated.

The fundamental equation of thin airfoil theory, equation (A-2), states that the camber line of an airfoil is a streamline of the surrounding flow.

$$V_\infty\left(\alpha - \frac{dz}{dx}\right) = -\frac{1}{2\pi}\int_0^c \frac{\gamma(\xi)}{(x-\xi)}\,d\xi \qquad \text{(A-2)}$$

The free stream velocity is V_∞, α is the airfoil angle of attack to the free stream flow, z is the vertical distance of the mean camber line above the chord line, and dz/dx is the slope of the airfoil's mean camber line. For the present purposes, x is the chordwise coordinate. To aid in the

integration substitute for the dummy variable ξ, $\xi = (c/2)\,[1 - \cos(\theta)]$ and $d\xi = (c/2)\sin(\theta)\,d\theta$. The bounds of integration become 0 to π. The solution to (A-2) is

$$\gamma(\theta) = 2V_\infty\left(A_0\frac{1+\cos(\theta)}{\sin(\theta)} + \sum_{n=1}^{\infty} A_n \sin(n\theta)\right). \qquad \text{(A-3)}$$

Substituting (A-3) into equation (A-2) and solving yields a Fourier cosine series. The coefficients of this series are

$$A_0 = \alpha - \frac{1}{\pi}\int_0^{\pi}\frac{dz}{dx}\,d\theta_0 \qquad \text{(A-4)}$$

and

$$A_n = \frac{2}{\pi}\int_0^{\pi}\frac{dz}{dx}\cos(n\theta_0)\,d\theta_0, \quad (n = 1, 2, 3,\ldots) \qquad \text{(A-5)}$$

The parameter θ_0 is a dummy variable of integration.

Once the Fourier coefficients have been determined, and the substituted into equation (A-3), the nondimensional lift and pitching moment coefficients can be determined. They are (ref. A-1)

$$c_\ell = \pi\,(2A_0 + A_1) \qquad \text{(A-6)}$$

and

$$c_{m,c_A/4} = \frac{\pi}{4}(A_2 - A_1) \qquad \text{(A-7)}$$

If the Fourier coefficients A_0, A_1, A_2 are determined for the case of a centrally located structural wing box, where the leading and trailing edges are of the same length, equation (A-6) and (A-7) become

$$c_\ell = 2\pi\alpha + G\left(\frac{H}{2}\kappa_c\right) \qquad \text{(A-8)}$$

and

$$c_{m,c_A/4} = -\frac{1}{8}GH\kappa_c \qquad \text{(A-9)}$$

where G is a coefficient that depends on the geometry of the wing cross section.

$$G = \frac{C_s}{H}\left[\frac{(\pi - 2\theta_1)}{\cos\theta_1} + 2\sin\theta_1\right] \qquad \text{(A-10)}$$

and

$$\theta_1 = \cos^{-1}\left(C_s/C_A\right) \qquad \text{(A-11)}$$

For our study, the dimensions for a C-130 wing were used, and G equals 10.349.

To solve for the coefficients, the slope of the camber line over the length of the chord needs to be defined. This requires the derivation of an equation for the slope of a deformable camber line which is a function of the structural dimensions and loading conditions of the wing being studied. For our initial study, the chord line of the structural box was assumed to deform into an arc with a radius of constant curvature. The leading and trailing edges are nonstructural and therefore do not deform in shape. They simply rotate along with the structural chord such that the rotations of the chord lines maintain geometric compatible at all times.

A brief explanation of the solution procedure for the calculation of the lift and pitching moment coefficients is presented here. The detailed analysis and procedure are given in ref. A-3.

1) Determine the radius of curvature of the wing's structural box for a specified loading and allowable strain level.
2) Calculate the slopes of the leading edge, trailing edge and structural box camber lines.
3) Solve equations (A-4) and (A-5) for the Fourier Series Coefficients A_0, A_1, and A_2.
4) Use equations (A-6) and (A-7) to determine the nondimensional lift and pitching moment coefficients.

References

A-1. Bertin, J.J. and Smith, M.L., Aerodynamics for Engineers, Prentice-Hall, Inc., 1979, pp. 109-125.

A-2. Anderson, J.D., Fundamentals of Aerodynamics, McGraw-Hill Book Company, 1984, pp. 204-217.

A-3. Zischka, P.Z., "Aerodynamics of Wings with Elastically Produced Camber", MS Thesis, University of California, Davis, CA, 1991.

APPENDIX B

PROPERTIES OF THE IDEAL TAILORED BOX MODEL

The Ideal Tailored Box model shown in fig. 7 consists of load bearing covers with webs which are infinitely stiff in transverse shear. This idealized configuration possesses chordwise structural symmetry about the geometric center of the structural box with structural chord c_s. In addition, the load bearing covers have distinct uniform properties. The elastic properties of this simple model are readily evaluated in closed form. As indicated earlier, the suggested approach for model-structure correspondence is intended to be used with this model.

The following convention is adopted: superscripts "u" and "l" identify properties of the upper and lower covers (fig.7), respectively. The nonzero direct stiffnesses are C_{11}, C_{22}, C_{33} (infinite), C_{44}, C_{55} and C_{66}. The nonzero coupling stiffnesses are C_{12}, C_{14}, C_{15}, C_{24}, C_{25} and C_{45}. All stiffnesses are evaluated using equations (16). The results are

$$C_{11} = \left(K^u_{11} + K^l_{11}\right) c_s \qquad \text{(B-1)}$$

$$C_{12} = \left(-K^u_{12} + K^l_{12}\right) c_s \qquad \text{(B-2)}$$

$$C_{14} = \left(K^u_{12} + K^l_{12}\right) c_s H \qquad \text{(B-3)}$$

$$C_{15} = \left(K^u_{11} - K^l_{11}\right) c_s H / 2 \qquad \text{(B-4)}$$

$$C_{22} = \left(K^u_{22} + K^l_{22}\right) c_s \qquad \text{(B-5)}$$

$$C_{24} = \left(-K^u_{22} + K^l_{22}\right) c_s H \qquad \text{(B-6)}$$

$$C_{25} = -\left(K^u_{12} + K^l_{12}\right) c_s H / 2 \qquad \text{(B-7)}$$

$$C_{33} \rightarrow \infty \qquad \text{(B-8)}$$

$$C_{44} = \left(K^u_{22} + K^l_{22}\right) c_s H^2 \qquad \text{(B-9)}$$

$$C_{45} = \left(K^u_{12} - K^l_{12}\right) c_s H^2 / 2 \qquad \text{(B-10)}$$

$$C_{55} = \left(K^u_{11} + K^l_{11}\right) c_s H^2 / 4 \qquad \text{(B-11)}$$

$$C_{66} = \left(K^u_{11} + K^l_{11}\right) c_s^3 / 12 \qquad \text{(B-12)}$$

APPENDIX C

FINITE ELEMENT CORRELATION

The design analysis model is beam-like and based upon ref. C-1. In order to verify that the engineering assumptions of this elementary type of theory are valid, a correlation study has been undertaken. Benchmark configurations have been selected, analyzed by elementary theory and modeled and analyzed by the finite element method for the loading case of pure bending. Finite element correlation studies have been conducted for two similar structural box configurations. The first is the box shown in Fig. C-1 with the laminated composite covers bonded to the channel sections. The second is an otherwise identical box with the covers bolted to the channel sections as shown in Fig. C-2. These configurations were under consideration for laboratory tests.

ANSYS (ref. C-2), a general-purpose commercial finite element code, was used to create the finite element models of the box prototypes. Two separate models were built to analyze the boxes with bolted-on and bonded-on laminate covers. Each model utilized 441 nodes and 360 elements. The only differences between the two models were the constraint equations used to model the interface between the flanges of the aluminum channels and the laminates. Fig. C-3 shows the overall configuration of the models.

Shell elements were used to model the thin-walled boxes. The element used from the ANSYS element library was the STIF 43, an isoparametric quadrilateral shell element. The STIF 43 was chosen over the more standard STIF 63 because of its superior response to in-plane shear. Bolts were modeled as rigid links at the bolt locations between the aluminum and the laminate. The connection between the channel flange and the laminate for the bonded model was modeled by using rigid links between all of the node pairs along the interface surface. This creates the assumption that the bond is perfect, which leads to good correlation with experimental results for a similar box beam configuration. In order to obtain pure bending conditions, the beams were loaded by the use of enforced displacements at the end of the beam near the origin. Displacements were enforced to insure that the cross sections remained planar at the loaded ends.

A comparison of results showing camber curvature of the top and bottom covers for the bolted and bonded cases is given in Table C-1. The camber curvature from the finite element model was found to be constant along the beam length for both cases. This result corresponds the prediction by the classical theory. Fig. C-4 shows the deflected shapes predicted by the finite element model and the classical model for the bolted configuration. The deflected shapes are nearly identical.

Agreements between classical models and the finite element models are excellent. Examination of the results indicates that the theory is very accurate for the cases studied, and, therefore, should provide an excellent basis for further tailoring studies.

References

C-1. Rehfield, L.W., "Design Analysis Methodology for Composite Rotor Blades," *Proceedings of the Seventh DoD/NASA Conference on Fibrous Composites in Structural Design*, AFWAL-TR-85-3094, June 1985, pp. (V(a)-1)-(V(a)-15).

C-2. Kohnke, P.C., ANSYS Engineering Analysis System Theoretical Manual, Revision 4.4, Swanson Analysis Systems, Inc., Houston, PA, 1989.

	CHORDWISE CAMBER CURVATURE (IN^{-1})	
MODEL TYPE	BOLTED	BONDED
CLASSICAL	0.01040	0.00954
FINITE ELEMENT	0.01054	0.00947
PERCENT DIFFERENCE	1.1	-0.7

TABLE C-1. - FINITE ELEMENT CORRELATION STUDY

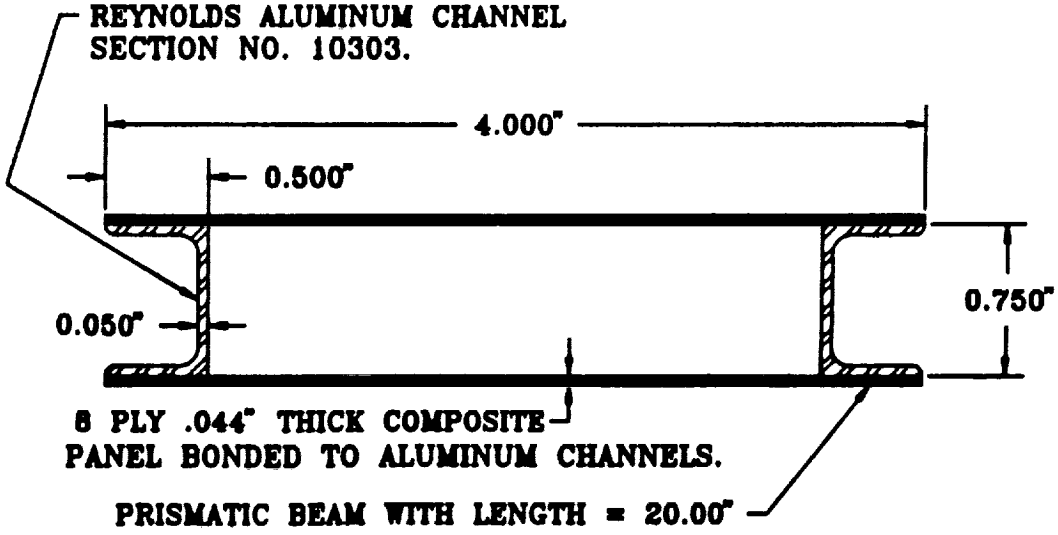

FIGURE C-1. - BOX BEAM WITH BONDED COVERS

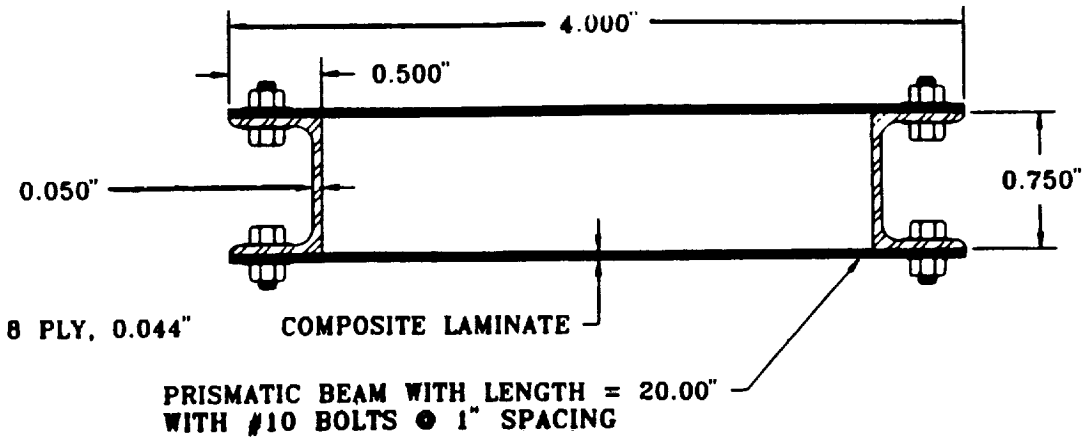

FIGURE C-2. - BOX BEAM WITH BOLTED COVERS

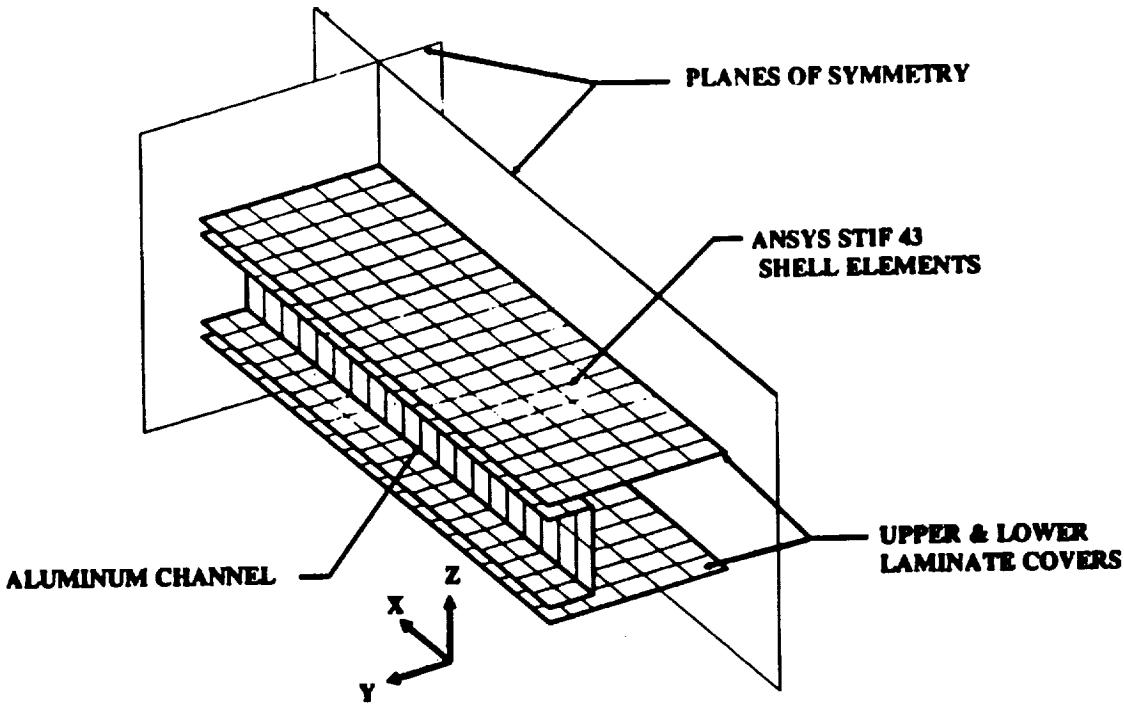

FIGURE C-3. - FINITE ELEMENT MODEL

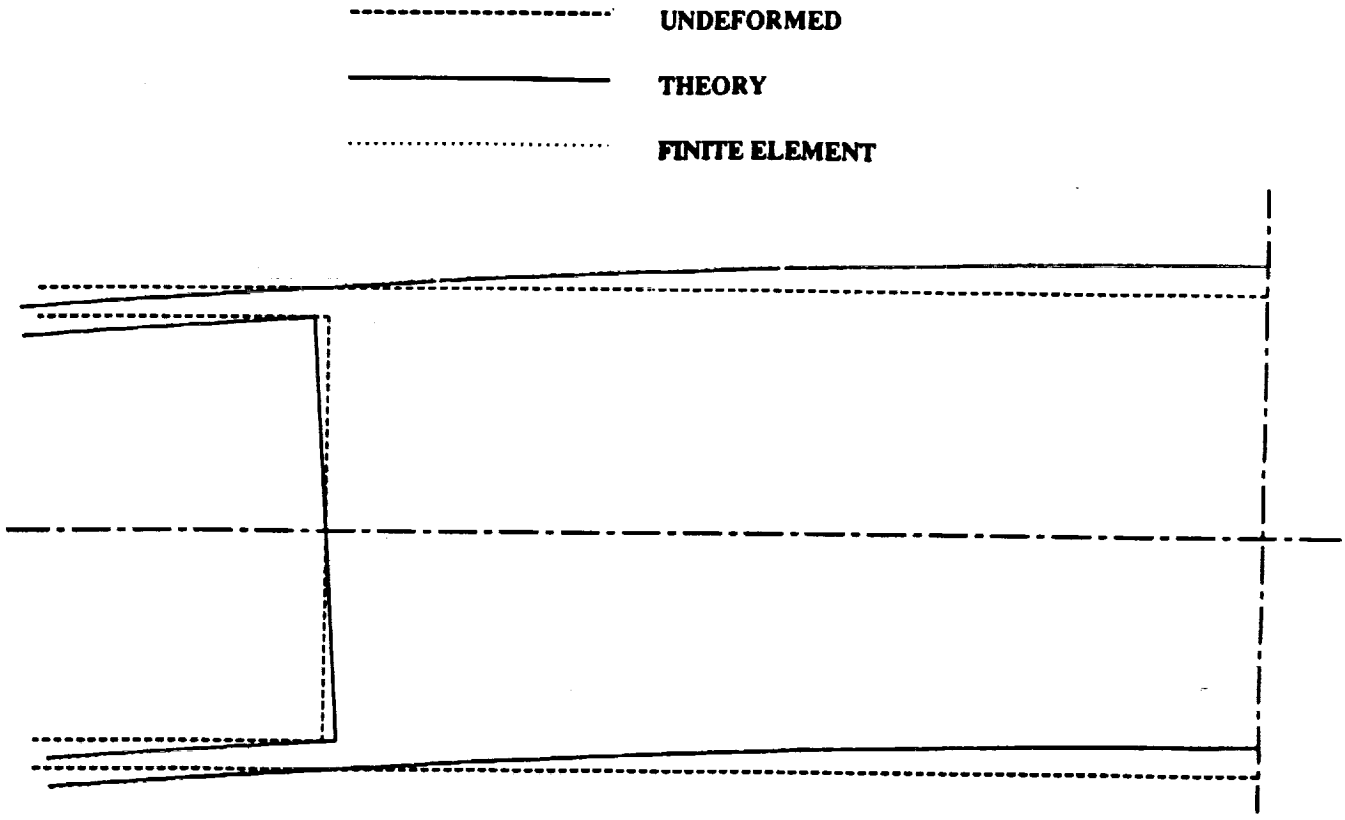

FIGURE C-4. – CAMBER DEFORMATION OF BOX WITH BOLTED COVERS

APPENDIX D

RIB CONCEPTS FOR CHORDWISE DEFORMABLE WINGS

Along with the development of elastically tailored chordwise deformable wings, it is necessary to design a compatible rib structure that allows the chordwise deformation to occur while still performing some of the traditional functions of a rib. A traditional rib is designed to: 1) preserve the cross section geometry, 2) distribute pressure loads to the spars and stiffeners, 3) support the wing covers, and 4) serve as attachment locations for system equipment. The new chordwise deformable rib still transfers pressure loads and provides cover support, but it must allow the cross section geometry to camber. Five new rib design concepts appear in figs. D1-D5.

Figure D-1 shows the Vertical Column Support type of rib structure. This style of rib is attractive because it is easily joined to the proposed grid stiffening structure of the wing box. Due to the method of constructing the grid structure, convenient points of attachment for the columns are created. To minimize the restraint of rib on chordwise deformation, it is proposed to use universal joints to attach the columns to the grid. The grid structure needs to be sized such that the columns can be placed at the proper spanwise intervals so that they support the covers against general instability buckling modes.

The Accordion Rib, unlike the column supports, provides continuous chordwise support to the covers while still allowing differential expansion of the upper and lower structural wing box covers. The Accordion Rib looks much like the pleated portion of an accordion. The pleats will conform to the grid structure as shown in fig. D-2.

The Diagonal Rib Structures, figs. D-3 and D-4, consist of diagonal columns fastened to the grid structure like the Vertical Columns via universal joints. Figure D-3 shows the Segmented Diagonal Columns jointed at their intersection while fig. D-4, Crossed Diagonal Columns, shows no midsection joint.

The Floating Rib Structure, fig. D-5, is constructed of crossed diagonal ribs with one end fastened with a universal joint and the other free to float. The floating end rests on an abrasion pad that attaches to the upper and lower wing covers.

A detailed design analysis is required for sizing the individual elements in these configurations. These suggestions should prove useful as technology for chordwise deformable wings advances.

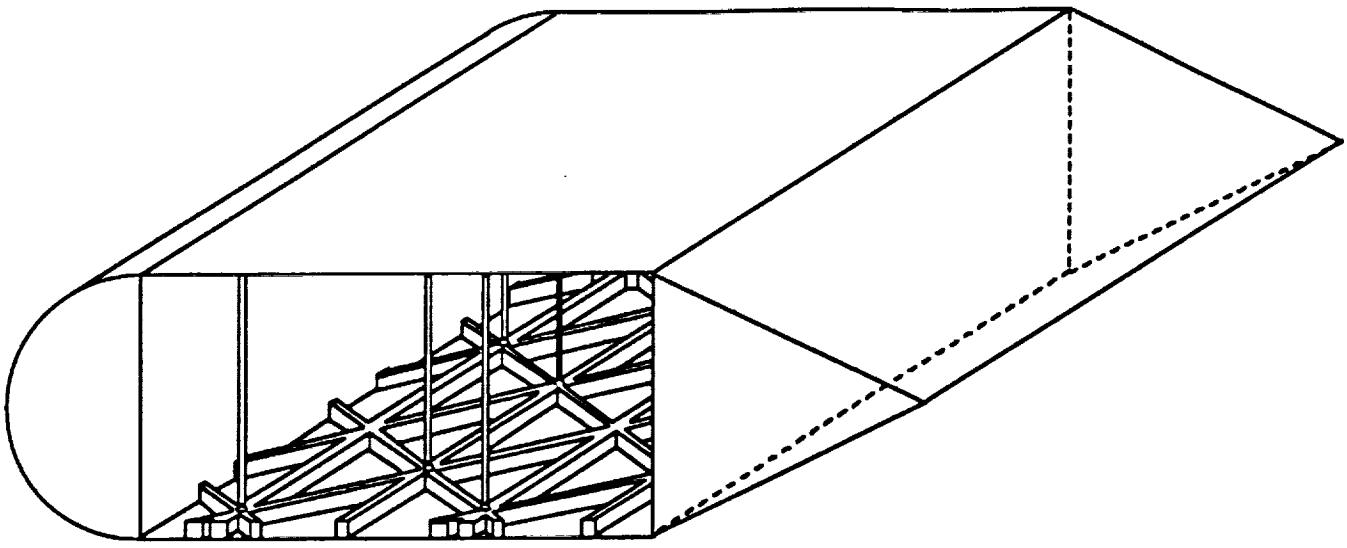

FIGURE D-1. VERTICAL COLUMN SUPPORT

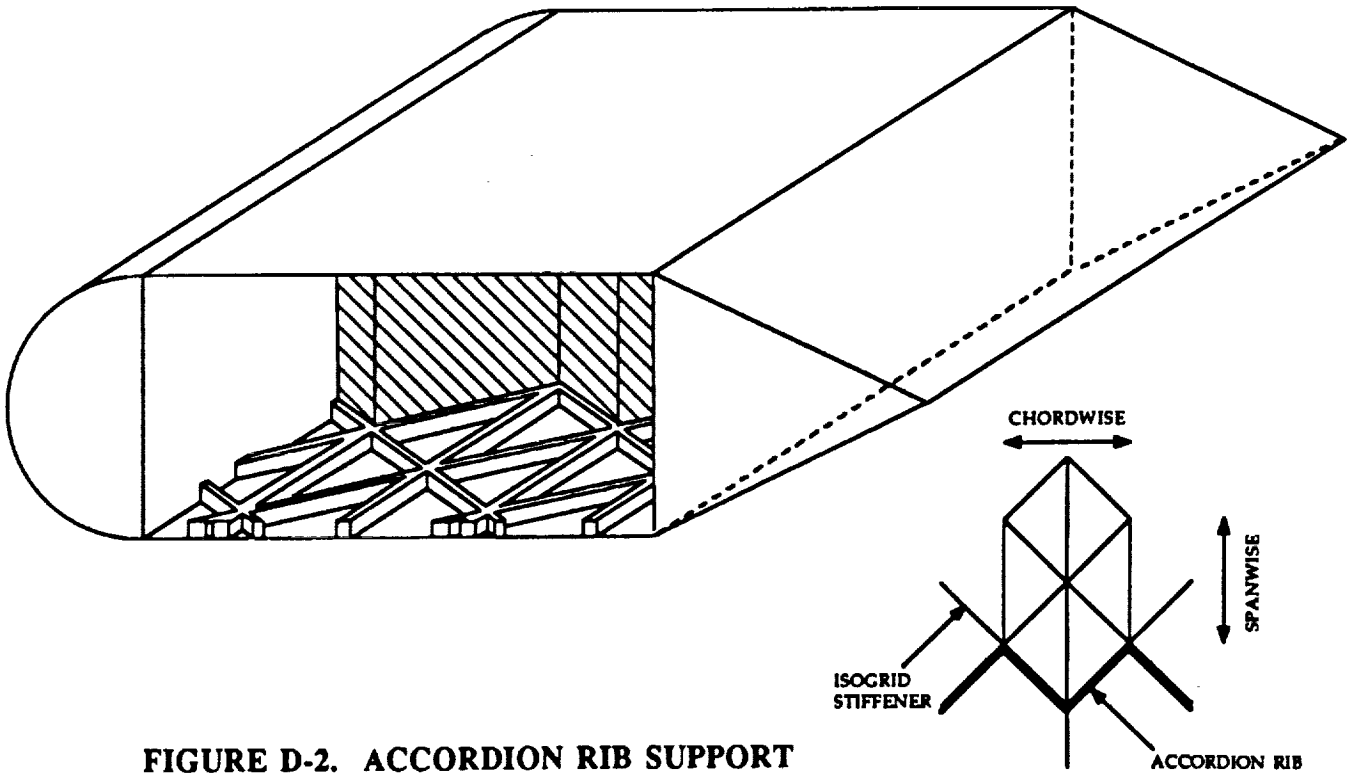

FIGURE D-2. ACCORDION RIB SUPPORT

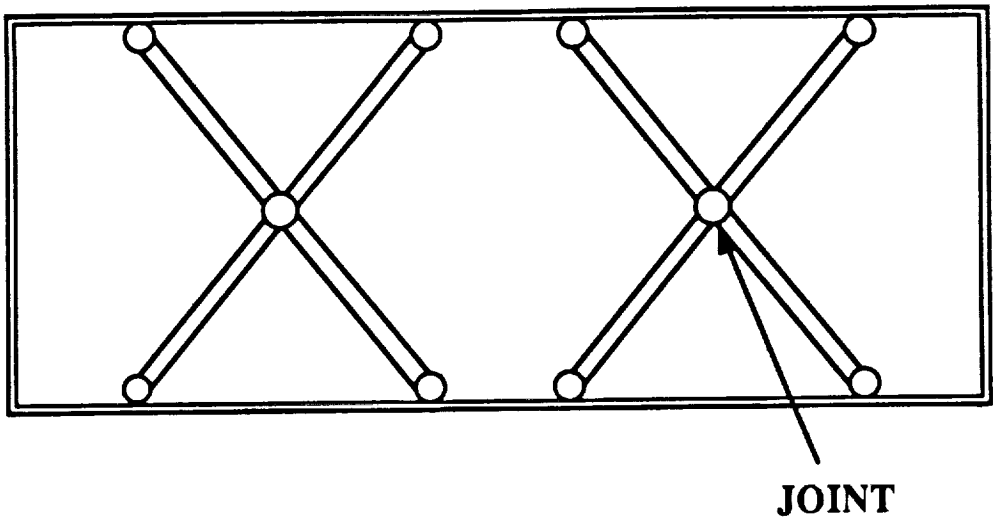

FIGURE D-3. SEGMENTED DIAGONAL COLUMNS WITH MIDSECTION JOINTS

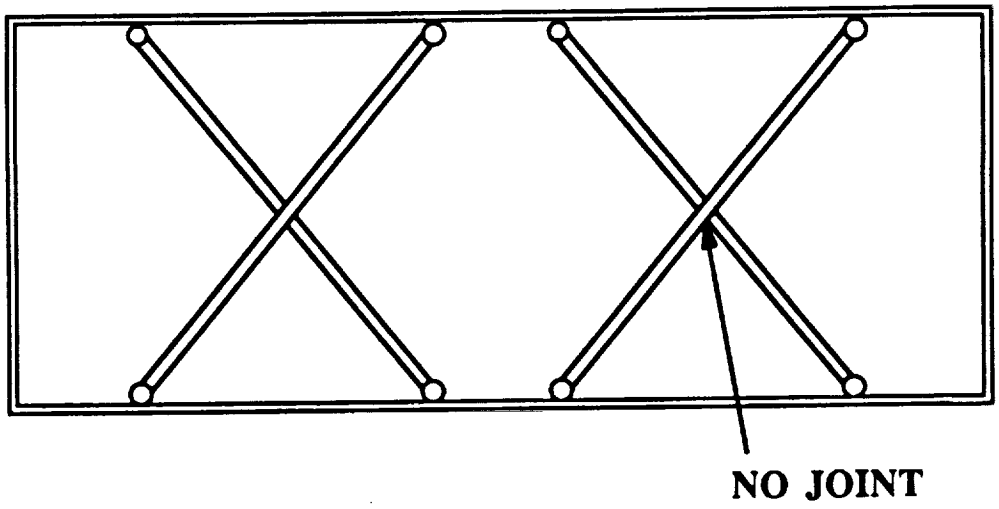

FIGURE D-4. SEGMENTED DIAGONAL SUPPORTS WITHOUT MIDSECTION JOINTS

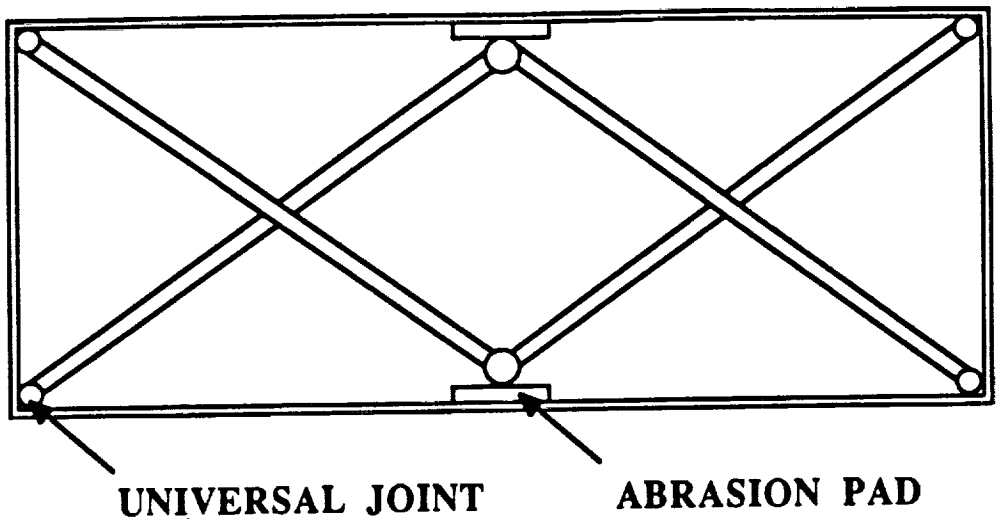

FIGURE D-5. FLOATING RIB STRUCTURE

APPENDIX E

A STATIC AEROELASTIC ANALYSIS OF CHORDWISE DEFORMABLE WINGS

Preliminary Remarks

Here we explore the possibility of what may be called "bending divergence". The occurrence of a static instability of this type arises because wing bending produces positive camber, which, in turn, produces additional lift, and, hence, increased bending of the wing. There also remains the potential threat of torsional divergence or, due to elastic coupling, some coupled form of bending - torsion instability.

Static instability is detected by a linearized set of equations that correspond to a disturbance from an equilibrium flight condition. The physics of the disturbed state is usually described by homogeneous equations without prescribed external generalized forces. Non-trivial solutions to the homogeneous equations correspond to static instability. For this reason, we need only consider the homogeneous equations of static equilibrium. The non-trivial solutions correspond to adjacent equilibrium states from the basic state under consideration.

Basic Theory

Divergence will be explored in a very simple context. Consider a uniform straight wing that is described aerodynamically by quasi-steady incompressible strip theory. The wing is designed with spanwise bending - camber elastic coupling. The section lift increment produces the following distributed loading q_z:

$$q_z = c_l c_A q \tag{E-1}$$

with the section lift coefficient given by

$$c_l = a_o \alpha + GH\kappa_c / 2 \tag{E-2}$$

and

$$q = \frac{1}{2} \rho_\infty V_\infty^2 \tag{E-3}$$

is the dynamic pressure. In addition, there is a distributed torque about the shear center axis; it is given by (fig. 7)

$$m_x = M'_{AC} + \bar{y}_{AC} q_z \tag{E-4}$$

where M'_{AC} is pitching moment per unit span about the aerodynamic center.

$$M'_{AC} = c_{MAC} c_A^2 q \tag{E-5}$$

where

$$c_{MAC} = - GH\kappa_c / 8 \qquad \text{(E-6)}$$

The equilibrium equations are

$$Q_{z,x} + q_z = 0 \qquad \text{(z - force)} \qquad \text{(E-7)}$$

$$M_{y,x} = Q_z \qquad \text{(y - moment)} \qquad \text{(E-8)}$$

$$M_{x,x} + m_x = 0 \qquad \text{(x - moment)} \qquad \text{(E-9)}$$

For constitutive relations, a classical bending theory approximation without direct transverse shear deformations is taken.

$$\kappa_{xx} = - \ W_{,xx} = S_{55}M_y \qquad \text{(E-10)}$$

$$\kappa_c = - \ S_{c5}M_y \qquad \text{(E-11)}$$

$$\alpha_{,x} = S_{44}M_x \qquad \text{(E-12)}$$

We have bowed to tradition and denoted α, the increment in angle of attack, as the elastic rotation angle.

Divergence Analysis

Equation (E-8) is used to eliminate the shear force Q_z in eq. (E-7). The equilibrium equations (E-7) and (E-9), therefore, with the aid of eqs. (E-1) - (E-6) and (E-10) - (E-12), may be written as

$$C_A q a_o \alpha + M_{y,xx} - k^2 M_y = 0 \qquad \text{(E-7a)}$$

$$C_{44}\alpha_{,xx} + C_A^2 e a_o q \alpha - c_A k^2 \left(e - \frac{1}{4}\right) M_y = 0 \qquad \text{(E-9a)}$$

where

$$k^2 = \frac{GH}{2} C_A q S_{c5} \qquad \text{(E-13)}$$

and

$$e = \bar{y}_{AC} / C_A \qquad \text{(E-14)}$$

To the level of approximation of a thin airfoil in incompressible flow and the assumption of a chordwise centrally located structural box, e = 1/4 and eq. (E-9a) reduces to

$$C_{44}\alpha_{,xx} + C_A^2 e a_o q \alpha = 0 \qquad \text{(E-15)}$$

This is the usual equation for torsional divergence. Consequently, we conclude that torsional divergence is unaffected by elastic chordwise camber within the limits of this model.

If there is no torsional divergence, we set $\alpha = 0$ in eq. (E-7a). Then

$$M_{y,xx} - k^2 M_y = 0 \qquad \text{(E-16)}$$

The general form of solutions to this equation is

$$M_y = C_1 \sinh(kx) + C_2 \cosh(kx) \qquad \text{(E-17)}$$

Consider the wing fixed at the root (x = 0) and free at tip (x = L). Consequently, at x = L

$$M_y(L) = 0 \qquad \text{(E-18)}$$

$$Q_z(L) = M_{y,x}(L) = 0 \qquad \text{(E-19)}$$

These conditions lead to

$$\begin{bmatrix} \sinh(kL) & \cosh(kL) \\ k\cosh(kL) & k\sinh(kL) \end{bmatrix} \begin{bmatrix} C_1 \\ C_2 \end{bmatrix} = \begin{bmatrix} 0 \\ 0 \end{bmatrix} \qquad \text{(E-20)}$$

Only trivial solutions can be found to this system of equation. Either $C_1 = C_2 = 0$ (no bending response) or k = 0, which corresponds to $V_\infty = 0$.

Concluding Remarks

A static aeroelastic analysis has been performed for a uniform wing in incompressible flow. On the basis of the analysis of this elementary model, it is concluded that the only static instability is torsional divergence, and it is unaffected by elastic chordwise camber. It remains to explore the effects of wing sweep and supersonic flight conditions. However, in subsonic flight, we expect no strong interaction between camber and twist for the case of spanwise bending - camber designed-in coupling.

APPENDIX F

AN ELEMENTARY MODEL FOR STRUCTURAL DYNAMICS

Introduction

Typical section models were created by aeroelastic pioneers to provide insight into behavior and provide trend information before the age of computers. A thorough discussion of these models is presented by Bisplinghoff and Ashley (ref. F-1). Initially, section model properties were defined to correspond to a single "typical" section, usually taken to be the section at the three-quarter span location. Dynamic response was determined by solving a system of ordinary differential equations with time as the independent variable. Even today, typical section models remain useful for teaching, promoting physical understanding and providing trend information.

Theoretical models with the same complexity as the typical section type can be developed using a different physical basis for defining the parameters of the models. Perhaps the most direct way is to use Lagrange's equations and a single generalized displacement for each distinct type of physical displacement variable. For continuous systems, this is accomplished easily by taking a single mode to represent each physical displacement variable. This approach is adopted here. It is perhaps more appropriate to call such a model an "energy-based section model."

Elementary models of this type are particularly useful for exploring trends in dynamic situations such as flutter, gust response and transient dynamic structural response. Dynamic stress predictions may be inadequate for design purposes, but overall displacement response predictions are usually informative as are flutter predictions. Modal truncation errors must be evaluated on the usual bases such as natural frequency and mode shape.

Basic Theory

We restrict our attention to uniform straight wings with chordwise compact sections. In addition, we consider only spanwise bending and twisting types of deformation. The transverse displacement is given by

$$u = v = 0 \tag{F-1}$$

$$w = W(x,t) + y\alpha(x,t) \tag{F-2}$$

All section warping effects are neglected. Refer to fig. F-1.

Neglecting the effects of transverse shear deformations, the strain energy associated with spanwise bending and twisting is

$$\overline{U} = \frac{1}{2}\int_0^L \left[C_{55}(W_{,xx})^2 + 2C_{45}\alpha_{,x}(- W_{,xx}) + C_{44}(\alpha_{,x})^2\right] dx \tag{F-3}$$

The semi-span of the wing is L. If the wing is clamped at the root x = 0, we assume the following forms for W and α:

$$W = u_5(t)\,(1 - \cos(\pi x/2L)) \tag{F-4}$$

$$\alpha = u_4(t)\sin(\pi x/2L) \tag{F-5}$$

The generalized displacements are the modal amplitudes u_5 and u_4, which are functions of time only.

For a uniform wing and these assumed modes, the strain energy is

$$\overline{U} = \frac{1}{2}\left[C^*_{55}u_5^2 + 2C^*_{45}u_4u_5 + C^*_{44}u_4^2\right] \tag{F-6}$$

where the generalized stiffnesses are

$$C^*_{44} = \pi^2 C_{44} / 8L \tag{F-7}$$

$$C^*_{45} = -\pi^3 C_{45} / 16L^2 \tag{F-8}$$

$$C^*_{55} = \pi^4 C_{55} / 32L^3 \tag{F-9}$$

The kinetic energy, T, for spanwise bending and twisting motion is

$$T = \frac{1}{2}\int_h \int_{C_A} \int_0^L \rho(\dot{w})\, dz\, dy\, dx = \frac{1}{2}\left[I^*_\alpha(\dot{u}_4)^2 + 2S^*_\alpha\dot{u}_4\dot{u}_5 + M^*(\dot{u}_5)^2\right] \tag{F-12}$$

where

$$M^* = mL\,(3/2 - 4/\pi) \tag{F-13a}$$

$$S^*_\alpha = S_\alpha L/\pi \tag{F-13b}$$

$$I^*_\alpha = I_\alpha L / 2 \tag{F-13c}$$

and

$$m = \int_h \int_{C_A} \rho\, dz\, dy, \qquad \text{mass/unit span} \tag{F-14a}$$

$$S_\alpha = \int_h \int_{C_A} \rho y\, dz\, dy, \qquad \text{static unbalance/unit span} \tag{F-14b}$$

$$I_\alpha = \int_h \int_{C_A} \rho y^2\, dz\, dy, \qquad \text{mass moment of inertia about the shear center axis/unit span} \tag{F-14c}$$

The following integrals were useful for evaluating the generalized masses in eqs. (F-13):

$$I_2 = \int_0^L \sin^2\left(\frac{\pi x}{2L}\right) dx = L / 2 \tag{F-15a}$$

$$I_3 = \int_0^L \sin\left(\frac{\pi x}{2L}\right)\cos\left(\frac{\pi x}{2L}\right) dx = L/\pi \qquad \text{(F-15b)}$$

$$I_4 = \int_0^L 2\sin^2\left(\frac{\pi x}{4L}\right)\sin\left(\frac{\pi x}{2L}\right) dx = L/\pi \qquad \text{(F-15c)}$$

The virtual work of the external forces is evaluated using strip theory aerodynamics with an effective dynamic angle of attack α_d defined as

$$\alpha_d = \alpha - \dot{w} / V_\infty \qquad \text{(F-16)}$$

The result is

$$\delta W_e = \int_0^L q_z\, \delta W\, dx = \int_0^L L\left(\delta W + \bar{y}_{AC}\, \delta\alpha\right) dx = Q_4 \delta u_4 + Q_5 \delta u_5 \qquad \text{(F-17)}$$

where the generalized forces are

$$Q_4 = a_0 C_A q L \bar{y}_{AC}\left(u_4 / 2 - 4\dot{u}_5 / \pi V_\infty\right) \qquad \text{(F-18a)}$$

$$Q_5 = a_0 C_A q L\left(4u_4 / \pi - (3/2 - 4/\pi)\,\dot{u}_5 / 8V_\infty\right) \qquad \text{(F-18b)}$$

With the aid of Lagrange's equations, the following equations of motion are obtained:

$$I_\alpha^* \ddot{u}_4 + S_\alpha^* \ddot{u}_5 + C_{44}^* u_4 + C_{45}^* u_5 - Q_4 = 0 \qquad \text{(F-19a)}$$

$$S_\alpha^* \ddot{u}_4 + M^* \ddot{u}_5 + C_{45}^* u_4 + C_{55}^* u_5 - Q_5 = 0 \qquad \text{(F-19b)}$$

Equation (F-19a) physically corresponds to the moment of momentum about the shear center axis. Equation (F-19b) physically corresponds to transverse linear momentum. The equations represent motion due to a small disturbance from an equilibrium state and correspond to what we call an energy-based section model.

Stability Considerations

It is convenient to write eqs. (F-19a,b) in matrix form. We introduce the following notation:

$$\underline{M}^* \ddot{\underline{u}} + \underline{D}\,\dot{\underline{u}} + \underline{C}^* \underline{u} = \underline{A}\,\underline{u} \qquad \text{(F-20)}$$

$$\underline{u} = (u_4 u_5)^T \qquad \text{(Generalized Displacement Vector)} \qquad \text{(F-21)}$$

$$\underline{M}^* = \begin{bmatrix} I_\alpha^* & S_\alpha^* \\ S_\alpha^* & M^* \end{bmatrix} \qquad \text{(Generalized Mass Matrix)} \qquad \text{(F-22)}$$

$$\underline{C}^* = \begin{bmatrix} C^*_{44} & C^*_{45} \\ C^*_{45} & C^*_{55} \end{bmatrix} \qquad \text{(Generalized Stiffness Matrix)} \qquad \text{(F-23)}$$

$$\underline{D} = \begin{bmatrix} 0 & D_{45} \\ 0 & D_{55} \end{bmatrix} \qquad \text{(Aerodynamic Damping Matrix)} \qquad \text{(F-24)}$$

$$\underline{A} = \begin{bmatrix} A_{44} & 0 \\ A_{45} & 0 \end{bmatrix} \qquad \text{(Steady Aerodynamic Matrix)} \qquad \text{(F-25)}$$

where

$$(D_{45}, D_{55}) = \frac{a_0 C_A q L}{V_\infty}\left(\frac{\bar{y}_{AC}}{\pi}, \left(\frac{3}{2} - \frac{4}{\pi}\right)\right) \qquad \text{(F-26)}$$

$$(A_{44}, A_{45}) = a_0 C_A q L\left(\frac{\bar{y}_{AC}}{2}, \frac{1}{\pi}\right) \qquad \text{(F-27)}$$

This notation facilitates understanding by identifying the physical nature of the individual terms.

Equations (F-20) constitute of system of linear homogeneous ordinary differential equations with constant coefficients. Solutions are of the form

$$(u_4, u_5) = (\bar{A}_4, \bar{A}_5)\, e^{pt} \qquad \text{(F-28)}$$

The constants $\bar{A}_4$ and $\bar{A}_5$ are modal amplitudes. The substitution of eq. (F-28) into eq. (F-20) yields the following system of equations:

$$\left[\underline{M}^* p^2 + \underline{D} p + (\underline{C}^* - \underline{A})\right]\begin{bmatrix} \bar{A}_4 \\ \bar{A}_5 \end{bmatrix} = \begin{bmatrix} 0 \\ 0 \end{bmatrix} \qquad \text{(F-29)}$$

Non-trivial solutions correspond to the vanishing of the determinant of the coefficient matrix.

The determinant of the coefficient matrix corresponds to the following characteristic equation:

$$a_0 p^4 + a_1 p^3 + a_2 p^2 + a_3 p + a_4 = 0 \qquad \text{(F-30)}$$

The coefficients in this equation are

$$a_0 = M^* I^*_\alpha - (S^*_\alpha)^2 \qquad \text{(F-31a)}$$

$$a_1 = I^*_\alpha D_{55} - S^*_\alpha D_{45} \qquad \text{(F-31b)}$$

$$a_2 = I^*_\alpha C^*_{55} + M^*(C^*_{44} - A_{44}) - S^*_\alpha(2C^*_{45} - A_{45}) \qquad \text{(F-31c)}$$

$$a_3 = D_{55}(C^*_{44} - A_{44}) - D_{45}(C^*_{45} - A_{45}) \qquad \text{(F-31d)}$$

$$a_4 = C^*_{55}(C^*_{44} - A_{44}) - C^*_{45}(C^*_{45} - A_{45}) \qquad \text{(F-31e)}$$

Information on stability can be obtained without actually solving eq. (F-30). There are two necessary conditions for none of the roots $p_1, \ldots, p_4$ of eq. (F-30) to have positive real parts. These conditions are (ref. F-2):

1. All of the coefficients a_0, ..., a_4 of the characteristic polynomial must have the same sign.
2. None of the coefficients are zero.

Since these conditions are only necessary, their satisfaction does not guarantee stability. They may be used, however, to identify unstable situations quite easily. Necessary and sufficient conditions for stability are provided by the Routh-Hurwitz criterion (ref. F-1).

In the special case $a_4 = 0$, there are two zero roots to eq. (F-30). This condition corresponds to static instability or divergence. It is identified with a critical value of the dynamic pressure q.

Parametric Studies

A parametric study has been conducted for a model box beam specimen with cross sectional geometry shown in fig. 28. Fifty percent of the laminate thickness is taken to be [0] plies and fifty percent to be angle plies with orientation angle [θ]. The laminated covers, therefore, have unbalanced ply layups. The laminate material properties are given in table 2. In addition, the following parameter values were selected for this study:

$a_0 = 2\pi$, $c_A = 2\ c_s = 8.00$ in, $L = 64.00$ in
$V_\infty = 550.00$ mph $= 9684$ in/sec
Air density (at sea level) $\rho_\infty = 0.114 \times 10^{-6}$ lb-sec^2/in^4
Laminate density: 0.1477×10^{-3} lb-sec^2/in^4
Aluminum density: 0.2539×10^{-3} lb-sec2/in^4
Dynamic pressure: $q = 5.375$ psi
Mass/unit span of box: $m = 0.1484 \times 10^{-3}$ lb-sec^2/in^2
Mass moment of inertia/unit span: $I_\alpha = 0.3083 \times 10^{-3}$ lb-sec^2/in

Three distinct configuration types were considered; they were (1) the structural box section shown in fig. 28, (2) twenty-five percent distributed mass added to the leading edge of the structural box (the front spar web) and (3) twenty-five percent distributed mass added to the trailing edge of the structural box (the rear spar web). Calculated results for the various coefficients in eq. (F-30) for the parameter values selected are presented in figs. (F-2) - (F-6). It is possible to make all of the coefficients positive -- that is, stabilize the system -- by proper choice of the ply angle. This confirms the design approach used on the X-29 aircraft to prevent torsional divergence. The coefficients a_0, a_1 and a_2 can be influenced by mass addition.

Vanishing of the coefficient a_4 coresponds to torsional divergence, the static form of instability. Vanishing of the coefficient a_2 corresponds to flutter, the dynamic form of instability. Note that fig. F-4 shows that both ply angle changes and mass addition can be used to stabilize the system against flutter, but ply angle orientation is the more powerful of the two approaches to use for design intervention.

References

F-1. Bisplinghoff, R.L. and Ashley, H., Principles of Aeroelasticity, Dover Publications, Inc., New York, 1975, pp. 189-279.

F-2. Meirovitch, L., Introduction to Dynamics and Control, John Wiley and Sons, 1985, pp. 261-265.

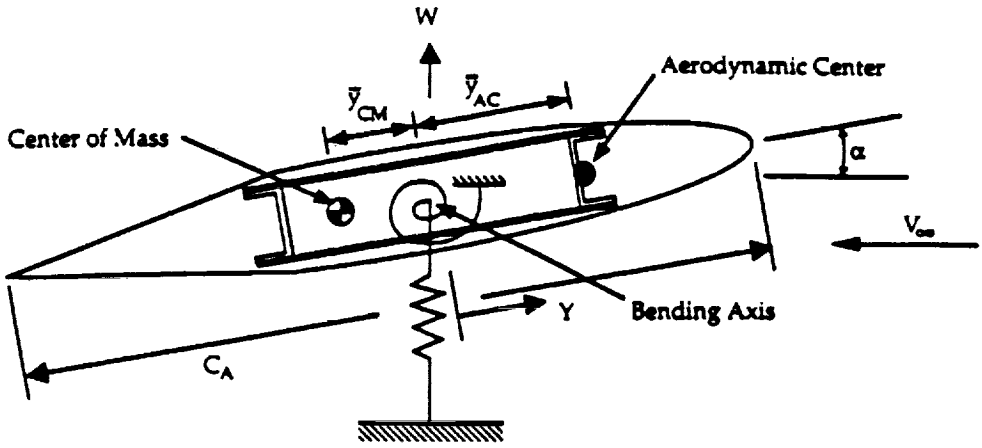

Figure F-1. - Dynamic Model

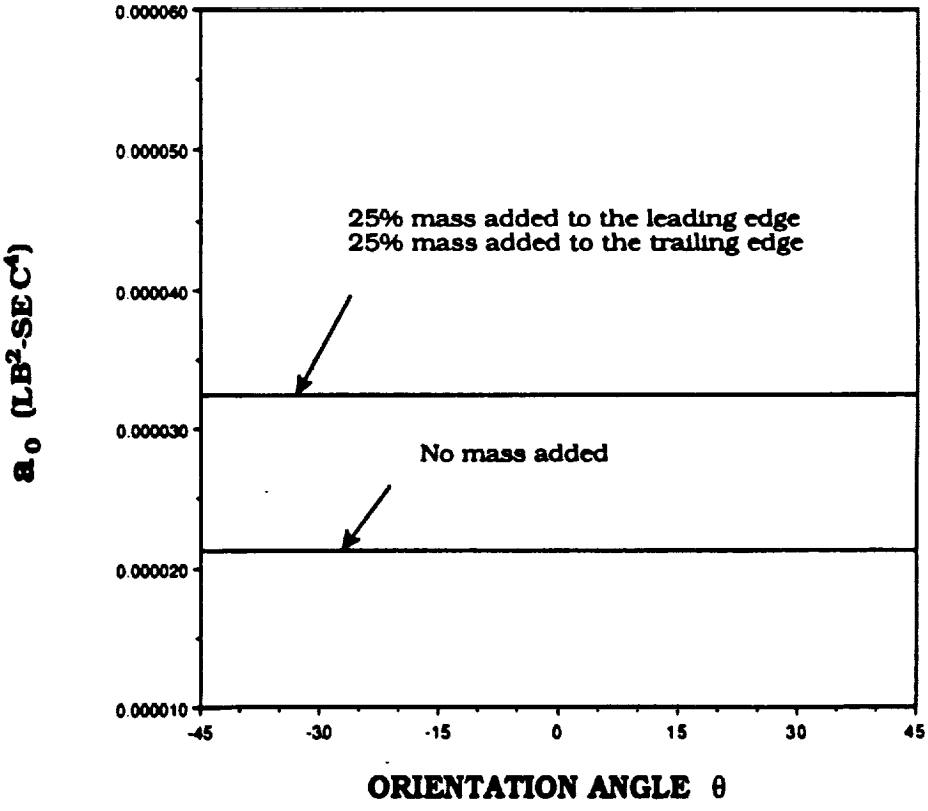

FIGURE F-2. COEFFICIENT a_0 VS. PLY ANGLE

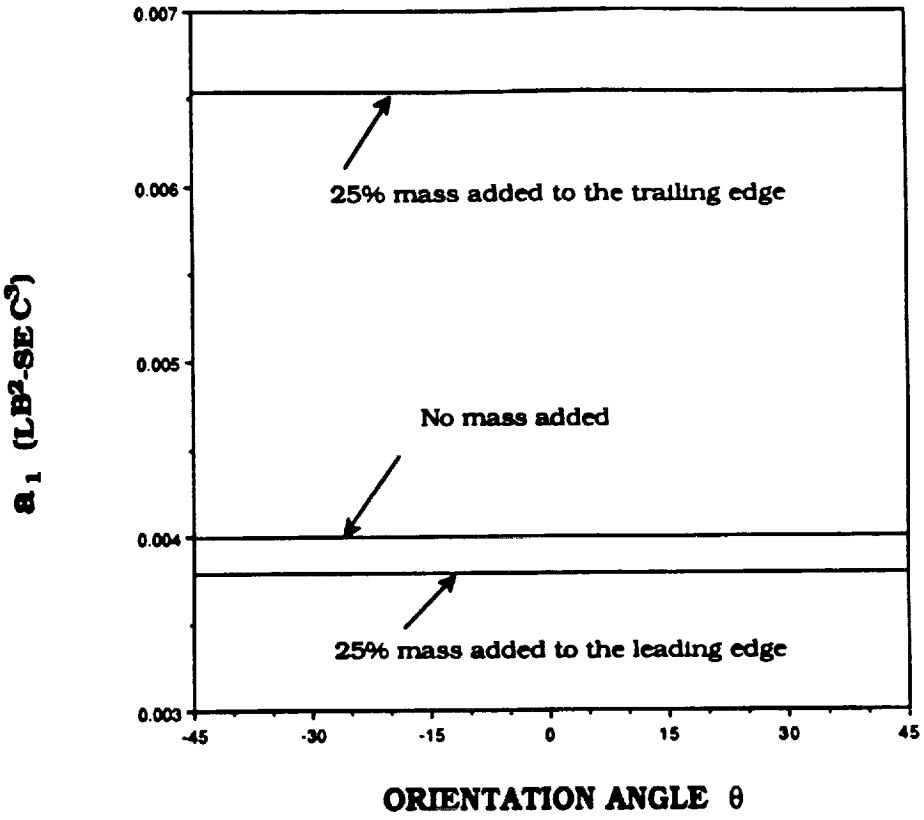

FIGURE F-3. COEFFICIENT a_1 VS. PLY ANGLE

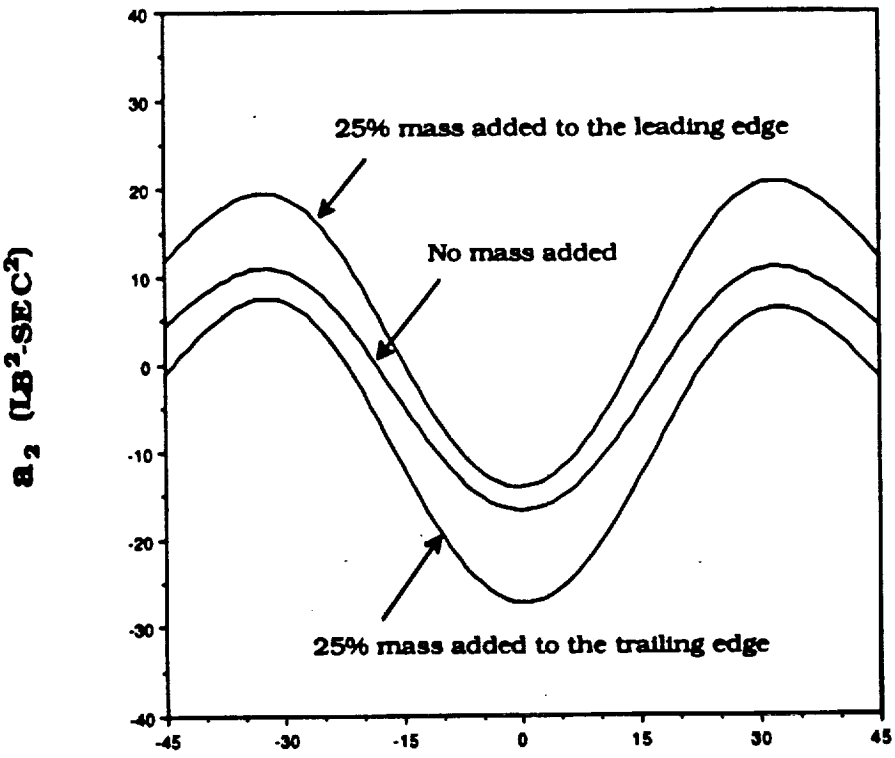

FIGURE F-4. COEFFICIENT a_2 VS. PLY ANGLE

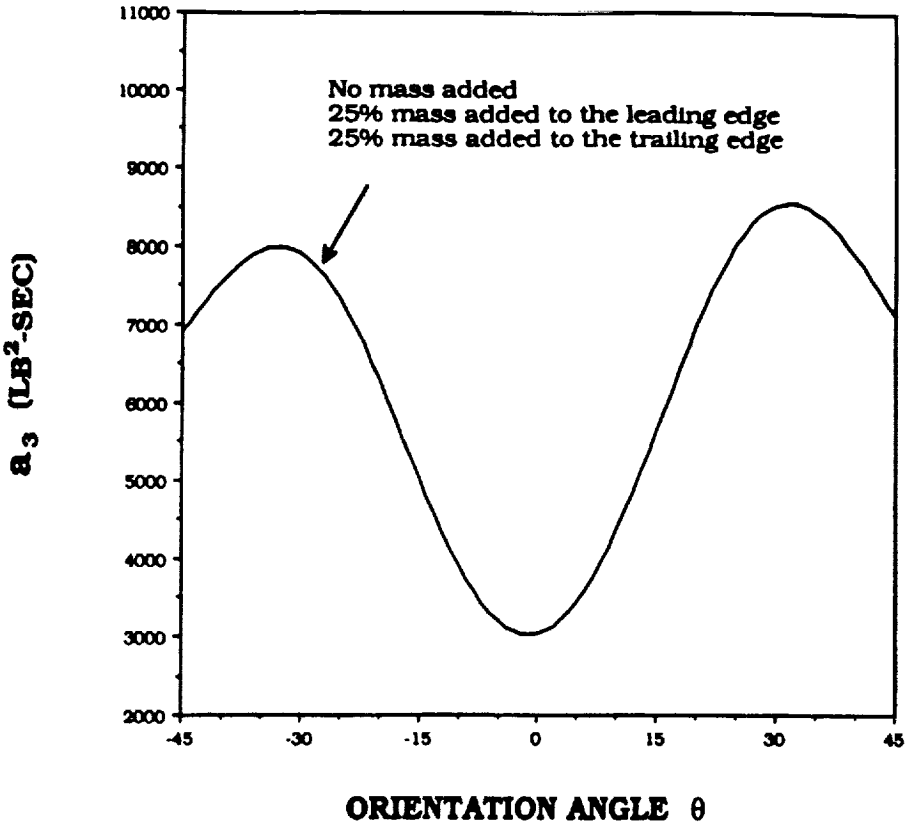

FIGURE F-5. COEFFICIENT a_3 VS. PLY ANGLE

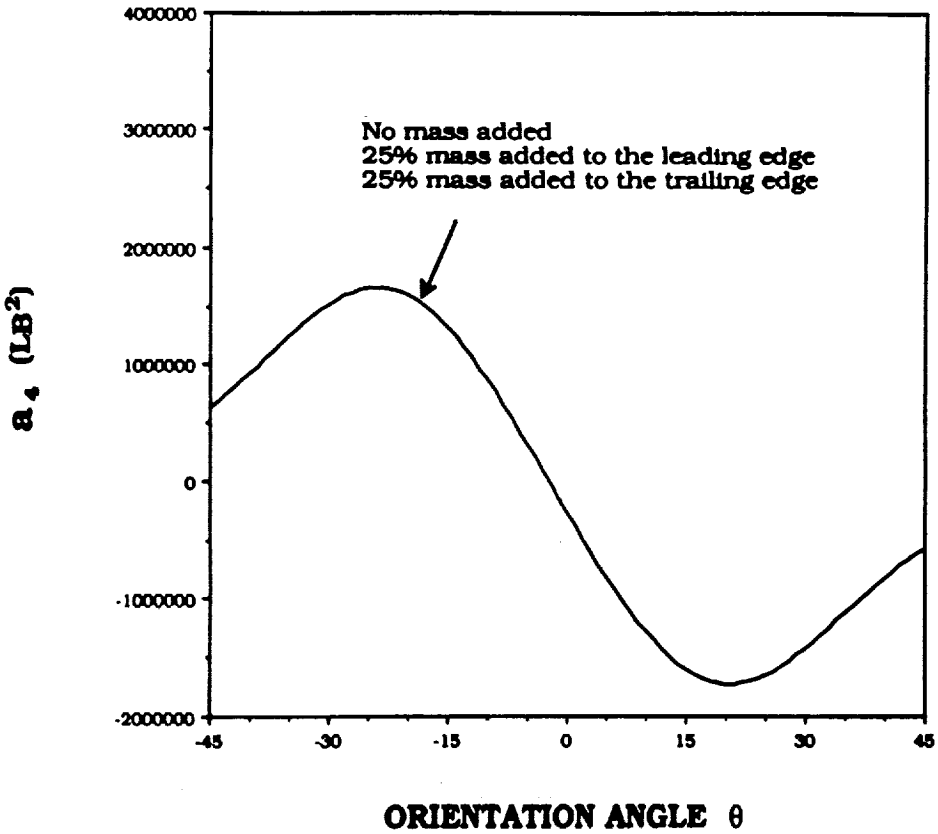

FIGURE F-6. COEFFICIENT a_4 VS. PLY ANGLE

REPORT DOCUMENTATION PAGE

Form Approved
OMB No. 0704-0188

1. AGENCY USE ONLY (Leave blank)	2. REPORT DATE	3. REPORT TYPE AND DATES COVERED
	July 1992	Contractor Report

4. TITLE AND SUBTITLE
Modeling and Analysis Methodology for Aeroelastically Tailored Chordwise Deformable Wings

5. FUNDING NUMBERS
C NAS1-18754
WU 510-02-12-08

6. AUTHOR(S)
Lawrence W. Rehfield, Stephen Chang and Peter J. Zischka

7. PERFORMING ORGANIZATION NAME(S) AND ADDRESS(ES)
Mechanical, Aeronautical and Materials Engineering
University of California
Davis, California 95616

8. PERFORMING ORGANIZATION REPORT NUMBER

9. SPONSORING / MONITORING AGENCY NAME(S) AND ADDRESS(ES)
National Aeronautics and Space Administration
Langley Research Center
Hampton, Virginia 23665-5225

10. SPONSORING / MONITORING AGENCY REPORT NUMBER
NASA CR-189620

11. SUPPLEMENTARY NOTES
Langley Technical Monitor: Damodar R. Ambur
Final Report

12a. DISTRIBUTION / AVAILABILITY STATEMENT
Unclassified - Unlimited
Subject Category 05

12b. DISTRIBUTION CODE

13. ABSTRACT (Maximum 200 words)

Structural concepts have been created which produce chordwise camber deformation that results in enhanced lift. A wing box can be tailored to utilize each of these with composites. In attempting to optimize the aerodynamic benefits, we have found that there are two optimum designs that are of interest. There is a "weight" optimum which corresponds to the maximum lift per unit structural weight. There is also a "lift" optimum that corresponds to maximum absolute lift.

New structural models, the basic deformation mechanisms that are utilized and typical analytical results are presented. It appears that lift enhancements of sufficient magnitude can be produced to render this type of wing tailoring of practical interest. Experiments and finite element correlations are performed which confirm the validity of the theoretical models utilized.

14. SUBJECT TERMS	15. NUMBER OF PAGES
Real-time data needs; Onboard data processing; Real-time processing for EOS; EOS communication needs	80
	16. PRICE CODE

17. SECURITY CLASSIFICATION OF REPORT	18. SECURITY CLASSIFICATION OF THIS PAGE	19. SECURITY CLASSIFICATION OF ABSTRACT	20. LIMITATION OF ABSTRACT
Unclassified	Unclassified		